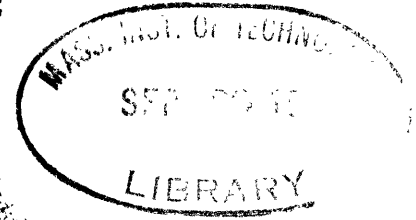


PHASE RELATIONS IN THE CONTACT AUREOLE  
OF THE ONAWA PLUTON, MAINE

by

JOHN MARSHALL MOORE, JR.  
B. Sc. University of Manitoba



SUBMITTED IN PARTIAL FULFILLMENT  
OF THE REQUIREMENTS FOR THE  
DEGREE OF DOCTOR OF  
PHILOSOPHY

at the

MASSACHUSETTS INSTITUTE OF  
TECHNOLOGY  
August, 1960

Signature of Author ..  
Department of Geology and Geophysics, August, 1960

Certified by ..  
Thesis Supervisor

Accepted by ..  
Chairman, Departmental Committee on Graduate Students

✓

PHASE RELATIONS IN THE CONTACT AUREOLE  
OF THE ONAWA PLUTON, MAINE

John Marshall Moore, Jr.

Massachusetts Institute of Technology  
Cambridge, Massachusetts

Submitted to the Department of Geology and Geophysics  
in August, 1960, in partial fulfillment of the require-  
ments for the degree of Doctor of Philosophy

ABSTRACT

The metamorphic aureole developed in low calcium slates at Onawa, Maine by an igneous body of granitic to gabbroic composition has been studied petrographically and chemically in the light of chemical thermodynamic considerations. The sequence of stable mineral assemblages from slate of the low greenschist facies to quartz-sillimanite-cordierite-biotite-potassic feldspar hornfels is deduced from petrographic and X-ray powder diffraction data. Chemical analyses of coexisting biotite and cordierite by instrumental methods show that chemical equilibrium is closely approached in the high grade assemblages. Shifts of the stability fields of the minerals can be explained in terms of the physical variables of metamorphism.

Thesis Supervisor: Professor H. W. Fairbairn  
Title: Professor of Geology

## TABLE OF CONTENTS

	<u>Page</u>
List of Figures	vi
List of Tables	viii
Acknowledgements	ix
<u>Part One</u> (Condensed for publication from Part Two)	
I. Introduction	1-1
II. Location and Topography	1-1
III. Areal Geology	1-3
IV. Petrology and Petrography	1-3
A. Slate	1-4
B. Aureole	1-5
C. Pluton	1-10
V. X-Ray Study	1-11
A. Opaque Minerals	1-11
B. Cordierite	1-12
VI. Theoretical Considerations	1-12
VII. Choice and Preparation of Samples	1-15
VIII. Chemical Analyses	1-18
IX. Graphical Analysis	1-21
X. Summary of Conclusions	1-29
<u>Part Two</u>	
I. INTRODUCTION	1
II. A. Location and Access	3
B. Topography	5

## TABLE OF CONTENTS (Cont.)

	<u>Page</u>
III. FIELD OBSERVATIONS	6
A. Previous Investigations	6
B. Areal Geology	8
C. Geology in the Vicinity of the Onawa Pluton	10
1) Slate	11
2) Aureole	11
3) Intrusive	16
IV. PETROGRAPHY	17
A. Onawa Aureole	17
1) Slate	17
2) Aureole	21
3) Intrusive	33
4) Inclusions	36
B. Other Aureoles in the Vicinity	36
V. MINERALOGICAL STUDIES BY X-RAY DIFFRACTION	39
A. Mineralogy of the Slates	39
B. Mineralogy of the Hornfelses	43
1) Non-opaque minerals	43
2) Opaque minerals	45
C. Structural State of Cordierite	50
VI. THEORY	53
A. The Phase Rule	53
B. Graphical Representation	61
C. Graphical Treatment of Pelitic Rocks	67
D. Distribution of a Minor Component Between Two Phases	73
E. External Variables in Contact Metamorphism	74

TABLE OF CONTENTS (Cont.)

	<u>Page</u>
VII. INTERPRETATION OF PETROGRAPHIC AND X-RAY DATA IN THE LIGHT OF THE PHASE RULE	79
VIII. CHEMICAL ANALYSES	83
A. Introduction	83
B. Choice of Samples	84
C. Preparation of Samples	86
D. Purity of Samples	90
E. Analytical Methods	94
F. Discussion of Analytical Procedures	97
G. Analytical Results	102
IX. DISCUSSION OF RESULTS	125
A. Precision and Accuracy of Chemical Analyses	125
1) Precision	125
2) Accuracy	129
B. Graphical Presentation of Data	136
1) A-F-M Plots	136
2) Distribution of manganese	147
C. Metamorphic Reactions in the Onawa Aureole	147
1) Prograde reactions	147
2) Retrograde reactions	163
3) Comparison with other localities	165
D. Correlation With Experimental Data	176
E. Suggestions for Further Research	180
BIOGRAPHY	182
BIBLIOGRAPHY	183

## LIST OF FIGURES

<u>Part One</u>	Page
1-1. Index map of Maine	1-2
 <u>Part Two</u>	
1. Geological map of the Moosehead Lake area	4
2(a). Geological map of the Onawa pluton and its aureole	12
2(b). Structural map of the western end of the Onawa pluton (from Philbrick (1933))	13
3. Geologic and sample location map of the vicinity of Lake Onawa	18, 19
4. X-ray powder diffraction patterns of slate 0-3, Big Wilson Cliffs, illustrating the effects of heat treatment	41
5. Hypothetical one-component pressure-temperature diagram	59
6(a) Isograd maps based on hypothetical one-component (b) system	59
7. Hypothetical three-component composition diagram	62
8. Projection through a mobile component	62
9. Projection through a pure substance	62
10. The $\text{Al}_2\text{O}_3\text{-FeO-MgO-K}_2\text{O}$ tetrahedron	71
11(a) Projections of the A-F-M-K tetrahedron on to the (b) plane $\text{Al}_2\text{O}_3\text{-FeO-MgO}$ (a) Projection through mus- covite (b) Projection through K feldspar	71
12. Mineral separation flow chart	88
13. X-ray powder diffraction intensity data for the deter- mination of quartz impurity in cordierite	93
14. Biotite-cordierite tie lines in the A-F-M triangle, projected through quartz, K-feldspar and ilmenite (a) All iron plotted as FeO (b) Analyzed FeO only plotted	137 138

## LIST OF FIGURES (Cont.)

	Page
15. Oxidation state of iron in coexisting biotite and cordierite	142
16. Compositions of biotite, cordierite, chlorite and slate in the A-F-M triangle, projected through quartz, muscovite, and ilmenite, all iron plotted as FeO	145
17. Distribution of manganese between coexisting biotite and cordierite	148
18. Suggested prograde assemblages in pelitic hornfels	150
19. Mica-feldspar assemblages across the K feldspar isograd	157
20. Reactions involving almandite garnet (=alm) in hornfels	157
21. Comparison of Onawa assemblages with those of other localities	172

LIST OF TABLES Part 2

<u>Table</u>		<u>Page</u>
1.	Table of Formations in the Moosehead Lake Area	9
2.	X-ray Powder Data for Opaque Minerals	47
3.	Distortion Index of Cordierite from the Onawa Aureole	51
4.	Scheme of Replicate Analyses	98
5.	Analyses of Standard Rocks W-1 and G-1	104
6.	Chemical Analyses	105
7.	Corrections to Chemical Analyses	113
8.	Sample Calculation of Mean Corrected Chemical Analysis	121
9.	Correction of Analysis of Chlorite Ch-65	122
10.	Calculation of Mode of Slate 0-65	124
11.	Precision of Analytical Results	126
12.	Structural Formulas of Biotite and Cordierite	131



## ACKNOWLEDGEMENTS

I am indebted to Professor H. W. Fairbairn, my thesis supervisor, for suggesting the problem and for providing wise counsel throughout the investigation. To Professor J. B. Thompson Jr. I owe my interest in metamorphic petrology; he suggested the Onawa pluton as a thesis locality and made many valuable suggestions about the metamorphism of pelitic sediments. Dr. S. S. Philbrick was most generous with his thin sections, field data, and personal interest, which enabled me to greatly expand my limited concept of the area. Dr. G. H. Espenshade of the U.S.G.S. also kindly loaned thin sections of Maine hornfels, and went out of his way to provide location data. I appreciate the interest of Mr. G. A. Chinner and Dr. W. Schreyer of the Geophysical Laboratory in my problem; discussions with them provided many new ideas about contact metamorphism. Fellow graduate students at M.I.T. who particularly contributed to the investigation are Dr. W. C. Phinney and Dr. A. H. Brownlow, who took time from their own thesis work to instruct me in instrumental analysis, and Mr. S. R. Hart, who was always willing to discuss matters petrologic. Profs. W. H. Pinson and J. W. Winchester, Mr. J. H. Crocket and Mr. C. C. Schnetzler all gave useful advice on analytical problems.

My greatest debt is to my wife, who deserves joint authorship for her part in the thesis. She contributed time, effort, and love at every stage of the project from climbing mountains through sieving rock and calculating results to typing seemingly endless tables of figures.

In the preparation of the final draft, I owe thanks to Mrs. Edith

Nicholson, the typist, for her skill and patience, and again to Charles Schnetzler for consenting to proofread and collate the final portion in my absence.

The support of this research by a grant from the National Science Foundation and by scholarship aid from the M. I. T. Canadian Trust Fund is gratefully acknowledged.

Part One

(Condensed for publication from Part Two)

## I. INTRODUCTION

This study is one of several completed in the last few years at M. I. T., all of which were aimed at quantitatively evaluating the extent to which chemical equilibrium is attained in various metamorphic processes. The methods adopted were primarily petrographic study and chemical analysis of coexisting ferromagnesian minerals by means of instrumental procedures developed by Shapiro and Brannock (1956). The contact aureole of the Onawa pluton in Maine proved suitable for such a study because previous field and petrographic work (Philbrick, 1933, 1936) showed it to be well exposed, intruded into low calcium pelites, relatively free of polymetamorphic effects and not so fine grained as to prohibit mineral separations. It thus appeared that the contact metamorphic mineral assemblages would be amenable to graphical treatment according to the methods of Thompson (1957) as a means of interpreting them in the light of chemical thermodynamic theory.

## II. LOCATION AND TOPOGRAPHY

The Onawa pluton is located in central Maine (index map, Figure 1), in Piscataquis county, in the Sebec Lake and Sebec topographic quadrangles. A map of the intrusive and its aureole, taken from Philbrick (1933), is reproduced in Figure 2(a) (Part Two, p. 12). The resistant hornfelses crop out on the peaks and slopes of the mountains which surround a swampy basin occupied by the pluton. The aureole is accessible by road at the western end. The Canadian Pacific Railway intersects the aureole and the pluton, and access to the north

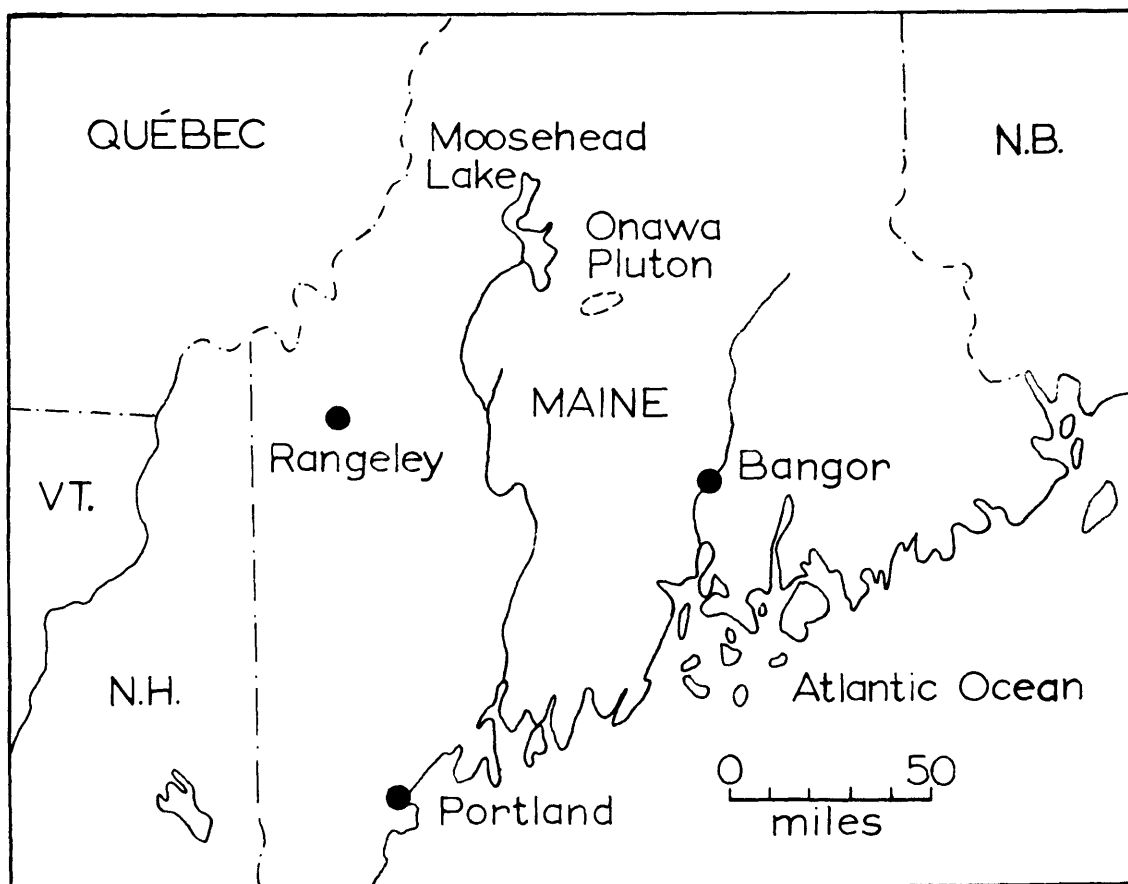


Figure 1-1. Index Map of Maine.

contact is provided by the Appalachian Trail along the Barren-Chairback range. The best exposures of the aureole are found in the vicinity of Boarstone mountain, and the bulk of the writer's work was confined to that area. The intrusive is exposed primarily along the contacts, and no detailed study is possible in the interior.

### III. AREAL GEOLOGY

The sedimentary rocks in the Moosehead Lake area trend northeast-southwest. The Onawa pluton is one of a belt of intrusives roughly concordant with the structure, most of which have developed contact aureoles in the intruded rocks. The largest of these is the Katahdin batholith, of over 500 square miles area, immediately to the north. At the north end of Moosehead Lake the stratigraphic relations are established and are reproduced in Table 1 (Part Two, p. 9). The Onawa pluton is intrusive into slates tentatively correlated with the Seboomook on the basis of lithologic similarity, but diagnostic fossils are lacking. A number of K-Ar and Rb-Sr age measurements have been made on intrusives, slate and hornfels in the area, and all are concordant at about 360 million years showing that the regional metamorphism and igneous activity are of post Lower or Middle Devonian (Acadian) age (Hurley et al (1957, 1958, 1959)).

### IV. PETROLOGY AND PETROGRAPHY

In addition to thin sections of the author's samples, slides kindly loaned by Dr. S. S. Philbrick and Dr. G. H. Espenshade were examined. Figure 3 (Part Two, pp. 18, 19) shows geology and sample locations in the Onawa area.

## A. Slate

Figure 2(b) (Part Two, p. 13), reproduced from Philbrick (1933), shows that the intrusive is discordant at the west end and that the sediments are complexly deformed. Dark grey very fine grained fissile slate and light grey massive fine quartzite are interbedded in layers varying from thin laminae to the width of an outcrop. All gradations between the two types occur, and graded bedding is common. Petrographic and X-ray study shows that the dominant assemblage is: quartz-chlorite-( $\pm$ kaolinite?)-muscovite-( $\pm$ biotite)-albite. The micas are  $10\mu$  shreds in parallel orientation enclosing light mineral grains which are often angular to subangular and up to 1 mm. Albite is untwinned and cannot be distinguished from quartz in thin section. Chlorite is pleochroic from very pale yellow-green ( $\parallel$  x) to light green ( $\parallel$  y and z). It occasionally forms stubby prisms up to 0.2 mm, often intergrown with muscovite; these increase in abundance as the intrusive is approached. Quartzitic layers have the same mineralogy as the pelitic beds. A few grains of pale brown pleochroic biotite are present only in 0-4 and in quartzitic lamellae in 0-6. Biotite is also reported by Dale (1906) in slate from quarries at nearby Monson. Accessories are platy opaque, sharp and well formed in section but ragged in plan, graphite(?), tourmaline, iron sulphide, and calcite (as flat inclusion-crowded rhombs 0.5-1 mm in 0-6, which weather to pits). No rutile was identified. X-ray powder patterns of 0-3, 0-4, -6, -65, -66, -67, -69, and -70 are virtually identical except for the presence of an andalusite pattern in 0-67. The value of  $\Delta 2\theta$  (albite  $\bar{2}01$  - quartz  $10\bar{1}0$ ) is  $1.18 \pm 0.1^\circ$ ,

which agrees within measurement error with that of the Amelia albite, indicating essentially potassium-free plagioclase. It was not possible to determine the calcium content, but this is probably negligible at the grade of metamorphism of the slate (Zen, 1960). No paragonite or phylophyllite was detected in the slate.

## B. Aureole

In the area of Bodfish at the west end of the pluton the mineralogical changes marking the outer edge of the aureole are the successive appearance, in random orientation, of andalusite as "chiastolite" prisms up to 1 cm, pleochroic reddish-brown biotite, and "spots" in the slate. In the outer 500 feet of the aureole andalusite is progressively replaced toward the country rock by chlorite and muscovite, less fine than the matrix minerals. Similar chlorite is associated with the spots, which are ovoid features .25-.5 mm with less graphite and more muscovite than the matrix. The habit and size of the spots is identical with that of cordierite nearer the contact. In 0-76, prominent cordierite first appears with minor chlorite associated, and nearer the contact no chlorite is found. Minor cordierite is definitely present in many spots nearer the edge of the aureole (e.g., Philbrick slide 1). The evidence is thus strong that the spots are retrograde after cordierite, probably the result of rehydration of the outer, more permeable part of the aureole with falling temperature at the close of metamorphism. The term "spotted slate" has been applied to contact metamorphosed slates exhibiting a variety of textural features, but it is probable that spots composed of yellow isotropic material (Harker (1950, p. 15)) and chlorite-muscovite aggregates (Ussher et al



(1909), Tilley (1924)) have formed on the sites of prograde cordierite, indicating that cordierite is common at the lowest grade of contact metamorphism. Assemblages deduced to be stable in the outer part of the aureole are thus:

quartz-andalusite-chlorite-muscovite-albite (a few chiastolite pseudomorphs in 0-65)

quartz-andalusite-biotite-chlorite-muscovite-albite (0-69, -70 contain stubby chlorite prisms but no spots)

quartz-andalusite-biotite-cordierite-muscovite-albite (0-67, -87; characteristic pelitic assemblage in the outer part of the aureole).

No assemblage indicating stable coexistence of chlorite and cordierite was observed. The grain size of the matrix of these assemblages does not exceed .15 mm. Muscovite forms tiny prisms showing no sign of incompatibility with cordierite, which contains myriad inclusions of quartz, biotite, and opaque. Accessory opaque and tourmaline similar to that in the slate, plus apatite and zircon, are present. The biotite is pleochroic from almost clear || x to medium brown || y, z in the spotted slates and lowest-grade cordierite-bearing rocks, becoming progressively redder toward the contact. The most marked color change occurs over a short range, as between 0-87 and 0-85, and is coincident with a change in the habit of the opaque to rounded stubby plates which occasionally have hexagonal outline. In 0-79 a few wisps of fibrolite were observed; this mineral occurs sporadically, commonly associated with andalusite-quartz or biotite-quartz boundaries in most hornfelses nearer the contact than 0-79. Its X-ray powder pattern shows it to be sillimanite (or mullite, for the two cannot

be distinguished except by precise measurement of cell dimensions, impossible because of dilution of the sample by quartz). Grid microcline microperthite appears in the same assemblage with andalusite (plus fibrolite) and fine muscovite only over a short interval (see Figure 3, Part Two, p. 18, 19). Toward the contact muscovite is irregularly distributed, forms poikilitic laths up to 3 mm often in obvious replacement relation to biotite, and is deduced to be unstable in the prograde assemblage. Stable associations are thus:

quartz-sillimanite-biotite-cordierite-muscovite-potassic feldspar  
(limited occurrence; 0-32, 0-43)

quartz-sillimanite-biotite-cordierite-potassic feldspar

(0-82, 0-56; characteristic pelitic assemblage in the inner part of the aureole)

As microcline and albite are intergrown in the perthite, it is impossible to differentiate discrete albite grains by X-ray, and these are not visible in thin section, except as albite-twinned and normally zoned individuals in a few hornfelses near the contact. Untwinned albite may be present with microperthite in some assemblages. The identity of the potassic feldspar modification stable during metamorphism is not obvious, as the microcline may have inverted from another form upon cooling and exsolution of albite.

Textural changes as the contact is approached include general increase in matrix grain size to an average of .1-.2 mm in potassic feldspar hornfelses, loss of foliation, disappearance of inclusions from potassic feldspar and cordierite beginning at the edges of the grains, reduction of cordierite grain size to that of the matrix, and change of andalusite habit from idiomorphic chiasolite to xenomorphic

grains 1-2 mm, poikilitic with quartz. The rock becomes lighter grey and attains the typical hornfels texture. Philbrick drew an arbitrary boundary at the inner limit of fissility, which approximately coincides with the outer limit of unaltered cordierite. The preservation of cordierite in rocks with hornfels texture can be ascribed to their low permeability to water. Whereas cordierite is visible as rusty spots on the weathered surface of low grade hornfels, it cannot be megascopically distinguished from the other light minerals in most of the potassic feldspar hornfelses. Bedding is well preserved in the muscovite-bearing rocks, but is discontinuous and less well defined toward the contact. In thin section, cordierite is distinguished by the presence of 6-fold cyclic twins, often complete at low grade but usually consisting of only 2-3 individuals in the smaller grains, and by a rough surface which increases the apparent relief. It is colorless, contains no pleochroic haloes and is thus easily mistaken for quartz or feldspar. Andalusite often is pleochroic from clear to pink. Fibrolite forms thick mats on grain boundaries, rimming biotite and andalusite. In the innermost part of the aureole ("injection zone" of Philbrick, Figure 3, Part Two, p. 18, 19) are many veinlets of several mm width, composed mainly of quartz and microcline microperthite a little less fine than in the host hornfels. All the other phases of the hornfels may also be present in them in smaller quantity. The veinlets are discontinuous; more than one parallel set may intersect, usually with no clear age relation. Borders are often enriched with biotite. Quartz-sillimanite and quartz-andalusite veinlets are less common. Philbrick

(1933, 1936) describes these features in detail and proposes a geometric classification. He considers that they are injections from the intrusive, but they exhibit the features of the pegmatites of regional metamorphism (Ramberg (1952, pp. 248-258)) and are more likely derived from the wallrock, perhaps by partial melting. Biotite in all potassic feldspar hornfels is approximately the same shade of rich red-brown; where rimmed by fibrolite it appears lighter apparently from thinning. Andalusite persists to the contact, though fibrolite is undoubtedly the stable phase. Within 50 feet of the contact, extensive replacement of cordierite, biotite and potassic feldspar by chlorite and sericite is observed. Accessories in the potassic feldspar hornfels are opaque (graphite not apparent), zircon, with prominent pleochroic haloes in biotite, apatite and tourmaline. The last is generally dichroic from light to dark brown, but near the contact forms skeletal crystals up to several mm, orange-brown in color.

An approach to textural equilibrium in most cordierite-bearing hornfels is indicated by a range of grain size of each phase limited to about one order of magnitude. Angular quartz in lower-grade rocks varies over two orders of magnitude and must be unrecrystallized detrital grains. Biotite is concentrated in the vicinity of cordierite in cordierite-muscovite parageneses, and around poikilitic andalusite metacrysts.

The stable assemblages listed describe all observed mineral associations; simpler parageneses occur, e. g., quartz-biotite-muscovite-feldspar in the quartzite, but are all consistent with the

maximum stable associations described. The arrangement of these parageneses in Figure 3 (Part Two, p. 18, 19) shows that the sequence is toward less hydrous assemblages diagnostic of increasing temperature of metamorphism as the intrusive contact is approached. The appearance of potassic feldspar marks an isograd which divides the aureole approximately in half.

### C. Pluton

The intrusive is light to dark grey, medium grained and massive. Petrographic data are from Philbrick (1933), supplemented by the author's examination of some of Dr. Philbrick's slides. All variations from granite to quartz norite and gabbro are present, the more salic varieties predominating in the poorly exposed interior. In general, microcline (sometimes perthitic) and plagioclase coexist. Two generations of plagioclase are usually present: small prismatic grains with strong normal zoning, and larger irregular more uniform crystals. Mafics are hypersthene, augite, green hornblende and biotite, often all present in the same specimen in textural relations indicating reaction in the order named from earliest to latest. Red-brown biotite is the dominant ferromagnesian in all but the most mafic varieties, and quartz and microcline are almost invariably present. Tonalite is the most common species along the contact. In the vicinity of Onawa Station mafic rocks predominate, but granitic types are dominant at the contact at Barren and Boarstone Mountains. A quartz monzonite dike occurs on the latter mountain. Biotite is usually partially chloritized, and feldspars altered to sericite and clays. An inclusion in diorite near the contact on the C. P. R. between

the Greenwood Ponds contains the assemblage: (andesine-labradorite)-hypersthene-green spinel-biotite-potassic feldspar-opaque, and thus requires that at least calcium be introduced from the melt. Angular inclusions in quartz diorite at the contact of an apophysis on the western end are of quartz-muscovite-biotite-opaque and have the texture of low-grade contact slate.

Thin sections of hornfels from the aureoles around similar intrusives at Shirley Mills-Blanchard and Squaw Mountain to the west are similar to those of Onawa, except that some calcic types are included. For more detailed petrographic description, the reader is referred to Part Two.

## V. X-RAY STUDY

### A. Opaque Minerals

Table 2 (Part Two, p. 47) presents X-ray powder data on opaque minerals concentrated from the hornfels by fine grinding in an agate mortar and centrifuging in methylene iodide. Diffractometer traces were made on a Norelco unit using FeK $\alpha$  radiation, unfiltered; photographs were taken with a 114.6 mm Debye-Scherrer camera using Fe radiation and a Mn filter. All patterns are identical within measurement error with that of ilmenite, and are distinct from those of hematite, magnetite, and rutile. The only lines which cannot be assigned to either ilmenite or impurity biotite are those in 0-75, which match the three principal features in the pattern of pyrrhotite. In addition to the patterns presented, one or more principal ilmenite

peaks are present in the records of less pure concentrates from 0-32, -38, -45, -69, -83. Qualitative tests with a magnet and concentrated HCl verify the absence of magnetite in all the assemblages studied, and verify the presence of pyrrhotite. The data show that opaque of both habits observed is ilmenite, although a change in oxidation state of some of the iron is probably not impossible.

#### B. Cordierite

On the basis of powder X-ray diffraction studies of cordierite, Miyashiro (1957) has defined the parameter "distortion index" ( $\Delta$ ), which varies from zero in "indialite" (hexagonal high temperature cordierite) to a maximum of  $.29-.31^\circ 2\theta$  in "maximum orthorhombic" cordierites. The change in symmetry is not well understood, but may be an order-disorder transformation relating to the distribution of Al and Si in the six-fold rings of the structure. It is of interest to know whether or not the intermediate structural states are stable equilibrium features, so the distortion index of all the cordierites concentrated from the hornfels (see below) was measured. Data are presented in Table 3 (Part Two, p. 51). There is no significant difference in the structural states of all cordierites above the K feldspar isograd; values of  $\Delta$  are near the maximum, indicating the low temperature modification. Values for cordierite at and below the isograd are lower, so that the trend is the opposite of that to be expected in the aureole. Possibly the lower-temperature cordierite is metastably disordered.

## VI. THEORETICAL CONSIDERATIONS

Discussions of the application of chemical thermodynamic considera-

tions to metamorphic rocks may be found in Korzhinskii (1959) and Thompson (1955, 1957) and only the essentials will be repeated here. If chemical equilibrium has been attained in the metamorphic process, the phase rule limits the number of minerals which may coexist:

$$f = c + 2 - \phi$$

Where:

$f$  = the "degrees of freedom", i. e., the number of independent intensive parameters governing the system

$c$  = the number of chemical components

$\phi$  = the number of phases (minerals)

Intensive variables may be "external" or "internal." External variables are temperature, pressure, and the chemical potentials of "perfectly mobile" components, ( $\mu_m$ ) (Korzhinskii, 1936a) which are determined by factors external to the system. Internal variables are compositional, e. g., the mole fractions of the components. "Inert" components are those which are not free to migrate in or out of the system. At arbitrary (independent) values of the external variables:

$$\phi \leq c_i \quad \text{where } c_i = \text{the number of inert components.}$$

If

$$\phi = c_i,$$

then no internal variables are possible, i. e., the compositions of coexisting solid solutions are independent of the bulk composition of the system with respect to the inert components. In such a system, these compositions are diagnostic of the external conditions. This reasoning may be applied in the study of metamorphic rocks. Thompson (1957) has detailed the considerations which enable representation



of calcium-free pelitic sediments in terms of the five components  $\text{SiO}_2$ ,  $\text{Al}_2\text{O}_3$ ,  $\text{FeO}$ ,  $\text{MgO}$ , and  $\text{K}_2\text{O}$ . Phase assemblages in this system may be illustrated graphically in a tetrahedron, provided that quartz is present in all. In Figure 10 (Part Two, p. 71), this tetrahedron is shown with the possible composition ranges of the Onawa minerals plotted. Assemblages containing muscovite may be portrayed in a triangle formed by projection through the muscovite composition; those with potassic feldspar instead by projection through the feldspar composition (Figure 11, Part Two, p. 71). These projections may be referred to as A-F-M diagrams; it is essential that  $\text{FeO}$  and  $\text{MgO}$  be separated as components in treating systems containing coexisting ferromagnesian minerals. The base of the A-F-M triangle with muscovite appears incomplete; this is only so because K feldspar projects at infinity (Thompson, 1957). The phase rule permits five phases in the system at arbitrary external conditions, of which three can be illustrated in the triangle with two understood (quartz and a potassic mineral). As an example, a schematic composition triangle is shown in Figure 7 (Part Two, p. 62). Three-phase associations occupy triangles, the corners of which are invariant at constant external conditions. Associations of fewer phases are possible if these are capable of compositional variation, and such variations in two- and one-phase assemblages are functions of bulk composition in addition to the external variables. The A-F-M projections assume that  $\text{H}_2\text{O}$  and  $\text{O}_2$  (the latter if appreciable ferric iron is represented as ferrous) are either mobile components or present as pure phases; the projective device is analogous in each case. The

presence of sodium in excess of that accommodated by muscovite and/or K feldspar permits an extra phase, such as albite, which is also understood in the projection. If minerals formed in equilibrium in a volume of rock in which temperature, pressure, and chemical potentials of mobile components are constant are plotted in the A-F-M projection, then it is a true iso- $p$ ,  $T$ ,  $\mu_m$  phase diagram. It can be shown that the shift of the tie lines, or joins, limiting fields of zero internal degrees of freedom (three-phase fields in the triangle) must be continuous with changes in external conditions (Phinney (1959) and this study, Part Two). Thus tie lines from identical assemblages formed under different external conditions may be compared on the same diagram. If equilibrium was attained and if the assumptions about the variables are correct, tie lines will not meet or intersect except in special cases.

## VII. CHOICE AND PREPARATION OF SAMPLES

None of the mineral assemblages deduced to be stable in the Onawa aureole violate the phase rule. Only one contains phases incompatible in the A-F-M diagrams, and this paragenesis (quartz-sillimanite-biotite-cordierite-muscovite-potassic feldspar) occurs in a restricted range, over which a special relation of external conditions can be proposed (i. e., the isograd represents a particular  $T$  at given  $p$  and  $\mu_{H_2O}$ ). On the other hand, assemblages with two aluminosilicates or three ferromagnesianes, which occur over a large area in the aureole, cannot be stable and thus the deduction that chlorite-cordierite-biotite and andalusite-fibrolite are not stable associations is supported by theory. It is also apparent that the stable

assemblages:

quartz-(andalusite or sillimanite)-biotite-cordierite-(muscovite  
and/or K feldspar)(±albite)

are internally invariant, so that variations in the bulk composition within the range in which these assemblages are stable will not affect the compositions of the coexisting ferromagnesian. Accordingly, it was decided to sample these assemblages at various points in the aureole and determine the compositions of the biotite and cordierite in order to determine whether equilibrium was attained in the metamorphism, and, if so, to determine the effect of changes in the external variables on the stability fields.

Assemblages could be recognized in a general way by weathering features and the hand lens. Samples of two to five pounds were collected with a small sledge hammer and cold chisel, care being taken to avoid obviously weathered material (the hornfels is extremely hard, tough, and resistant to weathering; surface alteration does not penetrate over 1 cm). All samples for study were sawn, and those which were overly inhomogeneous were not utilized. Thin sections were made of all samples and some eliminated because of the presence of prominent retrograde alteration or incorrect phase assemblage. Finally, the following samples were judged suitable for further study:

0-43, 0-45, -56, -57, -60, -75, -82, -83, -87	from Boarstone Mountain
0-38, -40	from Onawa Station
0-32	from Barren Mountain
0-65	from Bodfish

The assemblages represented are:

quartz-illimanite-biotite-cordierite-K feldspar (8 samples)

quartz-sillimanite-biotite-cordierite-muscovite-K feldspar (2)

quartz-andalusite-biotite-cordierite-muscovite-albite (1)

quartz-andalusite-biotite-(chlorite after cordierite)-muscovite-albite (1)

quartz-chlorite-muscovite-albite

The retrograde assemblage was sampled in order to determine the nature of the reaction leading to the spotted slate, and the slate from the outer edge of the aureole to determine the chlorite and bulk compositions in order to better deduce the reactions leading to the appearance of andalusite.

All the assemblages from above the K feldspar isograd contained small quantities of retrograde muscovite. In all, all minerals occurred within a radius of 1-3 mm of any point, except in 0-60, in which aluminosilicate was irregularly distributed. Both andalusite and fibrolite were present in all except 0-40, which contained only fibrolite. The inversion between these two phases does not affect the other equilibria, so that their metastable relations do not eliminate the possibility of equilibrium among the other phases. A few relict andalusites were present in 0-65, but not in such proximity that they can be considered members of the once stable assemblage.

The rocks were crushed and ground, sieved, and only the 200-325 mesh size range was suitable for mineral separation. Concentration of biotite, cordierite, and chlorite was effected by the use of the Carpc and Frantz magnetic separators, of various dilutions of bromoform and methylene iodide in the centrifuge and, in a few cases, by

sliding on paper. All "tramp iron" was removed by the magnets. It was impossible to sufficiently purify the chlorite of 0-75 and the cordierite of 0-87 for analysis. The cordierites from 0-32 and -43 were sufficiently purified for partial analysis. Small amounts of impurities remaining in the other concentrates were determined by point count where possible and are listed along with the analyses of Table 7 (Part Two, p.113). Quartz in cordierite concentrates was estimated with the X-ray diffractometer by comparing the intensity of the quartz  $10\bar{1}0$  peak with a standard curve made by preparing known mixtures of pure cordierite (from a coarse cordierite gneiss) and quartz (see Preparation of Samples, Part Two). The results are believed to be accurate to  $\pm 5\%$  (absolute). Microcline was barely detectable in two of the cordierite fractions but its presence does not correlate with alkali content and the amount is not believed to be significant. Correction for muscovite intergrown with chlorite Ch-65 was performed by reducing alkalies in the analysis to zero and correcting  $\text{Al}_2\text{O}_3$  and  $\text{SiO}_2$  accordingly.

#### VIII. CHEMICAL ANALYSES

Analytical methods used in this study are essentially those described by Shapiro and Brannock (1956).  $\text{SiO}_2$ ,  $\text{Al}_2\text{O}_3$ , total Fe, MnO,  $\text{TiO}_2$ , and  $\text{P}_2\text{O}_5$  are determined spectrophotometrically, CaO and MgO by titration with Versene, photometrically recorded,  $\text{K}_2\text{O}$  and  $\text{Na}_2\text{O}$  by the flame photometer, and FeO by the conventional dichromate titration. A modified procedure for magnesium and calcium, in which aluminum and iron are complexed with triethanola-

mine and sodium cyanide instead of being chemically separated, was used (communicated to the laboratory by Shapiro, 1958).  $H_2O^-$  was eliminated by drying at 105–115° C before weighing;  $H_2O^+$  was not analyzed as the amount of sample was limited and no method of sufficient accuracy was available. It was necessary to modify the concentrations of reagents and sample solutions in some cases as a result of high concentrations of iron and aluminum and low calcium and magnesium. Analytical results are presented in Tables 7, 9 and 10 (Part Two, pp. 113, 122, 124) corrected for estimated impurities. As these figures are the mean of two to 16 determinations (the large number of values representing individual spectrophotometer readings), it is possible to calculate estimates of precision. These are presented in Table 11 (Part Two, p. 126). Symbols are explained on the page preceding Table 11). These estimates are of the worst precision for a given element in all cases except that of aluminum in cordierite, where the precision of  $Al_2O_3$  in C-38 was disproportionately high and the next worst precision figure was utilized. It is evident that precision is entirely satisfactory except in the case of calcium and ferric iron, where low concentration results in high relative error. In the case of  $CaO$ , results were highly erratic, but the low Ca content of the minerals renders this error unimportant. A more serious precision error was observed in the  $Al_2O_3$  content of the biotites bearing over 2%  $TiO_2$ . These gave results spread by as much as 5% of the mean value, so that the mean is less certain than it appears. An improved method for the determination of Al in the presence of high iron and titanium (both of which require corrections for interference in the Alizarine-red S procedure of Shapiro and Brannock)

would be desirable.

Accuracy of the analyses may be approximately evaluated by comparing the writer's analyses of the standards G-1 and W-1 with the accepted mean values (Table 5, Part Two, p.104). W-1 more closely approximates the composition of the minerals analyzed and so was completely analyzed. The customary 100% check is not possible because of the absence of H<sub>2</sub>O values, but it is apparent that the cordierites are essentially anhydrous. One of these (C-40) exceeds 100% by an unacceptable amount. Structural formulae calculated for chlorite are presented in Table 9 (Part Two, p.122) and for biotite and cordierite in Table 12 (Part Two, p.131). Silica appears to be in excess in the chlorite formula; reducing Si so that the excess Al over the 2Al:10 O proposed by Pauling (1930) is accommodated equally in the tetrahedral and octahedral sites gives a formula in good agreement with those published by Zen (1960) from low-grade regionally metamorphosed pelites from western Vermont. It is thus possible that very fine quartz inclusions were not visible in grain mounts and obscured in the X-ray pattern by muscovite. Chlorite and biotite formulae both show considerable excess Al over the minimum required by the structure; the biotites approximate siderophyllites (Winchell and Winchell (1951)) in composition. The excess of (OH) over the ideal in most of the analyses suggests low totals, and the reciprocal variation of Al with (OH) may indicate a negative error in Al. It will be seen that this is not sufficient to affect the graphical considerations. Cordierites (including C-40) show good agreement with the ideal formula. It is of interest that the alkalies appear to

substitute for the divalent cations rather than exist "stuffed" in the channels in the structure as suggested by Folinsbee (1941b), charge balance being maintained by a slight excess of Si over the ideal. The cordierite formulae also suggest that Fe<sup>III</sup> substitutes for divalent cations rather than Al and thus may represent originally ferrous iron. The biotite formulae provide no definite information in this regard.

## IX. GRAPHICAL ANALYSIS

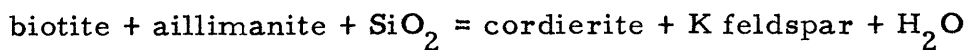
Figure 14 (Part Two, p.137) presents the analyses in graphic form, plotted on the A-F-M projection through quartz and K feldspar and, since it is a member of all assemblages, ilmenite. Each tie line represents the limiting join of the triangle sillimanite-biotite-cordierite, incomplete because of the orthogonal coordinates adopted. The entire triangle is shown schematically in the corner of Figure 14(a), incomplete because the limited range of bulk composition at Onawa prevents observation of all the assemblages in the system. Values of the "A" coordinate for the partially analyzed cordierites are arbitrary. The open boxes represent the maximum standard errors calculated for the ratios. The only join discordant within the limits of error is that of 0-32. The complete absence of other crossing joins in 14(a) indicates that the precision error is overestimated, at least for the total iron determination. 14(b) neglects Fe<sub>2</sub>O<sub>3</sub>, and inconsistencies in that plot are a reflection of variations in ferrous/ferric ratio, graphically illustrated in Figure 15 (Part Two, p.142). The standard errors of the plotted ratios are such that the scatter of



points is barely significant. As nearly as can be estimated from textural features and horizontal proximity to the contact, the order of increasing temperature of formation of the samples plotted is (beginning at the K feldspar isograd): 0-43 and -32, -45, -83, -82, -57, -56, -38, -60, -40 (on the contact). This is almost identical with the sequence of points in Figure 15, normal to the line of zero fractionation, which shows that cordierite becomes more ferrous with respect to coexisting biotite as the contact is approached. The random scatter of points along the line of zero fractionation shows that there is no over-all change in the oxidation state of iron in the ferromagnesian.

The general absence of crossing joins in Figure 14 shows that equilibrium was closely approached in metamorphism with respect to all significant compositional variables in the system, at least at metamorphic grade above the K feldspar isograd. These variables are the substitution of Fe and Mg in cordierite, and of Fe, Mg and Al in biotite. As Figure 14(a); in which the compositions are in effect projected through oxygen (all iron expressed as FeO), presents the most consistent picture, it is suggested that oxygen is best regarded as a mobile component. The absence of a phase containing essential ferric iron (such as magnetite) lends weight to this suggestion, as such an extra phase would require that oxygen be treated as an inert component. 14(a) would be the more consistent also if all iron was reduced during metamorphism and subsequently oxidized, but the systematic distribution of ferrous/ferric ratios argues against this hypothesis.

The discordance of the 0-32 tie line is interpreted as an indication of disequilibrium in that assemblage, as variations in the external variables cannot produce such an effect. Changes in these variables are reflected in shifts of the stability field, but these are not simply related to temperature. In Figure 14(a), the five most iron-rich joins represent higher-temperature assemblages than the other four, but inconsistencies are present within these groups, and assemblages sampled in close proximity, e. g., 0-82 and -83, are significantly different. Movement of the stability field necessitates the reaction:



A shift to the right results in more iron-rich compositions of the ferromagnesian. The reaction may be expected to go to the right with increasing temperature, as the dehydration suggests a positive entropy change. In common with all dehydration reactions, it goes to the left with increasing chemical potential of water. Increasing total pressure favours the denser assemblage of the left hand side, as does increasing oxygen pressure, as cordierite has a higher ferrous/ferric ratio than biotite in all except the lowest-temperature pairs. Thus, even if total (load) pressure is constant throughout the aureole as may be expected, temperature gradient is continuous, and the distribution of assemblages is as supposed, the stability field may be shifted in either direction by variations in chemical potential of water or oxygen. If the system were open to these components, local changes in chemical potential gradients as a result of permeability variations would affect the reaction; if the system were closed to all

components, bulk variations in  $H_2O$  and  $O_2$  in the "intergranular phase" would move the stability field. The over-all shift toward more iron-rich compositions indicates that the temperature effect is not annulled by other variables.

This reaction illustrates the importance of taking the mineral assemblage into account when interpreting compositional changes of minerals in terms of metamorphic grade. If biotite is coexistent only with a more iron-rich mineral, it will become more magnesian with increasing temperature, other variables being constant. Such is the case for biotite coexisting with magnetite and potassic feldspar (Wones and Eugster (1959)).

In Figure 16 (Part Two, p.145) the other analyses are presented in the A-F-M triangle projected through quartz, muscovite, and ilmenite. The position of the slate in the plot is misleading, as sodium is not taken into account. The calculated mode of Table 10 (Part Two, p.124) shows that all of the Al is accommodated in the chlorite, muscovite, and albite, so that the slate composition, projected through the opaque phase, is essentially coincident with the chlorite composition in the A-F-M plot. This would be unusual if Al, in addition to Mg and Fe, were not a compositional variable in chlorite. It is concluded that a one-phase chlorite field of considerable extent occupies this portion of the diagram at low metamorphic grade. The presence of relict andalusite in the slate shows that the solubility limit of Al in chlorite was exceeded. Either local variations in composition toward higher Al than the bulk value promoted formation of andalusite, or the retrograde reaction which destroyed the

andalusite involved the total rock and formed a more aluminous chlorite. In the latter event, the Al content of the analyzed chlorite is higher than the prograde equilibrium value.

The tie lines from 0-32 and 0-43 may be plotted also on the A-F-M projection through quartz, muscovite, and ilmenite, since both muscovite and K feldspar are members of the assemblage. These joins represent the approximate limits of compositional variation of all the pairs analyzed. If equilibrium was attained, the bulk composition of the assemblage must fall within the stability field of the coexisting phases. It is thus of interest to note that the bulk composition of slate 0-65 in Figure 16 (best indicated by the position of the chlorite composition) is nearly within all the three-phase triangles determined. As a consequence, no significant compositional changes are required to produce the potassic feldspar-bearing hornfelses from slate of the same composition as that one analyzed.

The compositions of the biotites from below the K feldspar isograd plot nearer the A apex because of lower potassium, rather than higher aluminum, contents. These lower-grade biotites are lower in  $\text{TiO}_2$  and Fe, so that the points of projection are not significantly different from those above the isograd. The change in potassium content of biotite across the K feldspar isograd is evidence that the reaction leading to the appearance of K feldspar is not the relatively simple: muscovite + quartz (+albite) = K (Na) feldspar + Al silicate +  $\text{H}_2\text{O}$  often proposed (Harker (1950), Francis (1956)) but may involve the ferromagnesian minerals also. It seems certain that the change in Ti content accompanies the change in biotite color observed petro-

graphically (Hall (1941) correlates an orange-red color with high Ti content), and a reaction involving the opaque is suggested. The lack of evidence of any phase change in the opaque requires that this be only an extension of the solubility limit of Ti (and Fe, unless the change in Fe is correlated with the K feldspar isograd rather than the Ti reaction).

Figure 17 (Part Two, p.148) is a distribution diagram illustrating the substitution of manganese for total iron as FeO in coexisting biotite and cordierite. Mn undoubtedly substitutes for Fe<sup>2+</sup> and Mg, because of similar size and valence; since the composition of the host mineral with respect to these elements varies over only a small range, the diagram has the same appearance whether Mn only, Mn/FeO, or Mn/FeO + MgO is plotted. The Mn content of the phases is a function of the bulk Mn composition of the rock, since the system is not controlled with respect to Mn variations. Unfortunately, the range of concentrations is not sufficient to indicate to what extent the solution is ideal; variations of the distribution are significant, as indicated by the size of the error box, but are small except in the case of 0-32. This variation is related neither to grade nor concentration, nor does it correlate with the position of the tie lines of Figure 14. The conclusion is that a significant, but small departure from an equilibrium distribution is present, reflected in a relative error in the average distribution coefficient (not including 0-32) of about 5 1/2%. This deviation from equilibrium is much larger than that of the Fe/Mg distribution. The marked anomaly in the case of 0-32 is more evidence that this assemblage was never close to chemical equilibrium.

Figure 21 (Part Two, p.172) compares the phase relations at Onawa with some of those determined elsewhere.

The symbols refer to the following sources of data:

01 — Onawa, Maine. Specimen 0-56

quartz-sillimanite-biotite-cordierite-K-feldspar hornfels

02 — Onawa, Maine. Specimen 0-43

quartz-sillimanite-biotite-cordierite-muscovite-potassic feldspar hornfels

C — Chinner (1959, p. 113) Glen Doll, Scotland.

garnet-cordierite-biotite-feldspar-quartz(?) hornfels

T1 — Tsuboi (1938) Kaziyabara, Japan.

sillimanite-biotite-cordierite-orthoclase-plagioclase-quartz hornfels

T2 — Tsuboi (1938) Tenryukyo, Japan.

biotite-cordierite-orthoclase-plagioclase-quartz hornfels

M — Mathias (1952) Upington, South Africa

sillimanite-biotite-cordierite-K feldspar-plagioclase-quartz rock

F — Folinsbee (1941a) Great Slave Lake, Canada

sillimanite-garnet-biotite-cordierite-spinel-microcline-plagioclase-  
quartz gneiss (biotite composition estimated from optics,  
not reliable)

Hi — Hietanen (1956) Idaho, U. S. A.

garnet-biotite-cordierite-corundum-plagioclase-quartz schist

He — Heald (1950) New Hampshire, U. S. A.

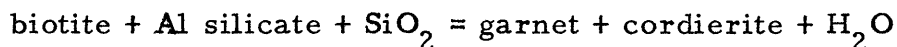
garnet-biotite-cordierite-microcline-quartz "quartz monzonite"

(analyzed phases not all from same location, but all three,  
with same optics as those analyzed, coexist).

The crossing joins are not necessarily evidence of disequilibrium,

for the composition of biotite F is uncertain (based on optics) and biotite may coexist with a different oxide assemblage than the Onawa biotites. The Onawa cordierites are as iron-rich as any in the diagram; of 62 cordierite analyses compiled by Leake, only three are more iron-rich than C-56, and these were collected from pegmatites. The most iron-rich assemblages are from contact aureoles, indicating maximum temperature and minimum pressure, but the more magnesian joins are from regional metamorphic environments. The relatively large spread of composition between environments with respect to that observed in a single aureole suggests that total pressure is the variable more strongly affecting the join than temperature, and the direction of movement, in accord with the reaction proposed, indicates higher pressures for regional metamorphism. The extremely magnesian Hietanen assemblage contains kyanite along with andalusite and sillimanite so must have formed at high pressure.

The stable coexistence of garnet with Al silicate-cordierite-biotite as in the Folinsbee assemblage requires an extra component, very likely manganese. However, the overlapping of the above field with a garnet-biotite-cordierite field (without aluminosilicate) requires a reaction:



which goes to the right with increasing temperature or pressure and is represented in the A-F-M diagrams of Figure 20 (Part Two, p.157). Chinner (1959) calls attention to the shift of cordierite-garnet joins in the same direction with increased pressure as the biotite-cordierite joins presented here. Those he plots are not necessarily the limiting

tie lines, but if the two-phase field cordierite-almandite in Figure 20(b) is not wide, the variation with bulk composition is small with respect to the variation with external conditions.

## X. SUMMARY OF CONCLUSIONS

On the basis of the petrographic and analytical data, it is concluded:

- a) Mineral assemblages in the aureole of the Onawa pluton obey the phase rule, and are arranged in a logical sequence with respect to a temperature gradient falling away from the intrusive.
- b) No hydrous aluminosilicate is required in the slate to produce andalusite at the lowest grade of contact metamorphism.
- c) Spotted slates in the outer part of the aureole are interpreted as retrograde after cordierite-bearing assemblages.
- d) Chemical analyses of coexisting biotite and cordierite in assemblages in which the mineral compositions are independent of bulk composition show that chemical equilibrium was closely approached in metamorphism with respect to Fe, Mg, and Al in all samples studied except one.
- e) The same specimen (0-32) also shows a much larger deviation from an equilibrium distribution of manganese between ferromagnesian than the others.
- f) The shift of the stability field sillimanite-biotite-cordierite with quartz, feldspar and ilmenite is toward more iron-rich compositions with increasing temperature.



- g) The shift is opposite with increasing pressure, and evidence from regional metamorphic assemblages shows that the pressure effect may be more pronounced and that the pressure of regional metamorphism is higher than contact metamorphism.
- h) The extremely iron-rich compositions at Onawa thus indicate low pressure (and high temperature).
- i) Irregularities in the movement of the above stability field in the Onawa aureole may be ascribed to variations in the chemical potentials of water and oxygen; evidence is presented that the latter is a mobile component in the inner part of the aureole.

Part Two

## I. INTRODUCTION

This project was undertaken as part of a program at M. I. T., extending over four years, to evaluate quantitatively the extent of chemical equilibrium in processes of rock metamorphism. Prior to the writer's work, two cases of regional metamorphism and one of contact metasomatism were studied, through a combination of field and petrographic observations, and chemical analysis of co-existing mineral phases in selected samples (Kranck, 1959; Phinney, 1959; Brownlow, 1960). While petrographic data permit a qualitative evaluation of the extent of equilibrium among phases in a metamorphic assemblage, quantitative data can be obtained only through analyses of individual phases. Theoretical considerations relating to this technique are described in a later section of this thesis.

At Prof. H. W. Fairbairn's suggestion, the writer decided to pursue a study of a contact metamorphic occurrence. A suitable aureole (zone of contact metamorphism surrounding a body of intrusive rock) should be:

- a) easily accessible, to permit removal of large samples
- b) well exposed
- c) previously well mapped so that field work could be kept to a minimum
- d) free from retrograde alteration, polymetamorphism, and weathering
- e) sufficiently coarse grained to permit mineral separation.

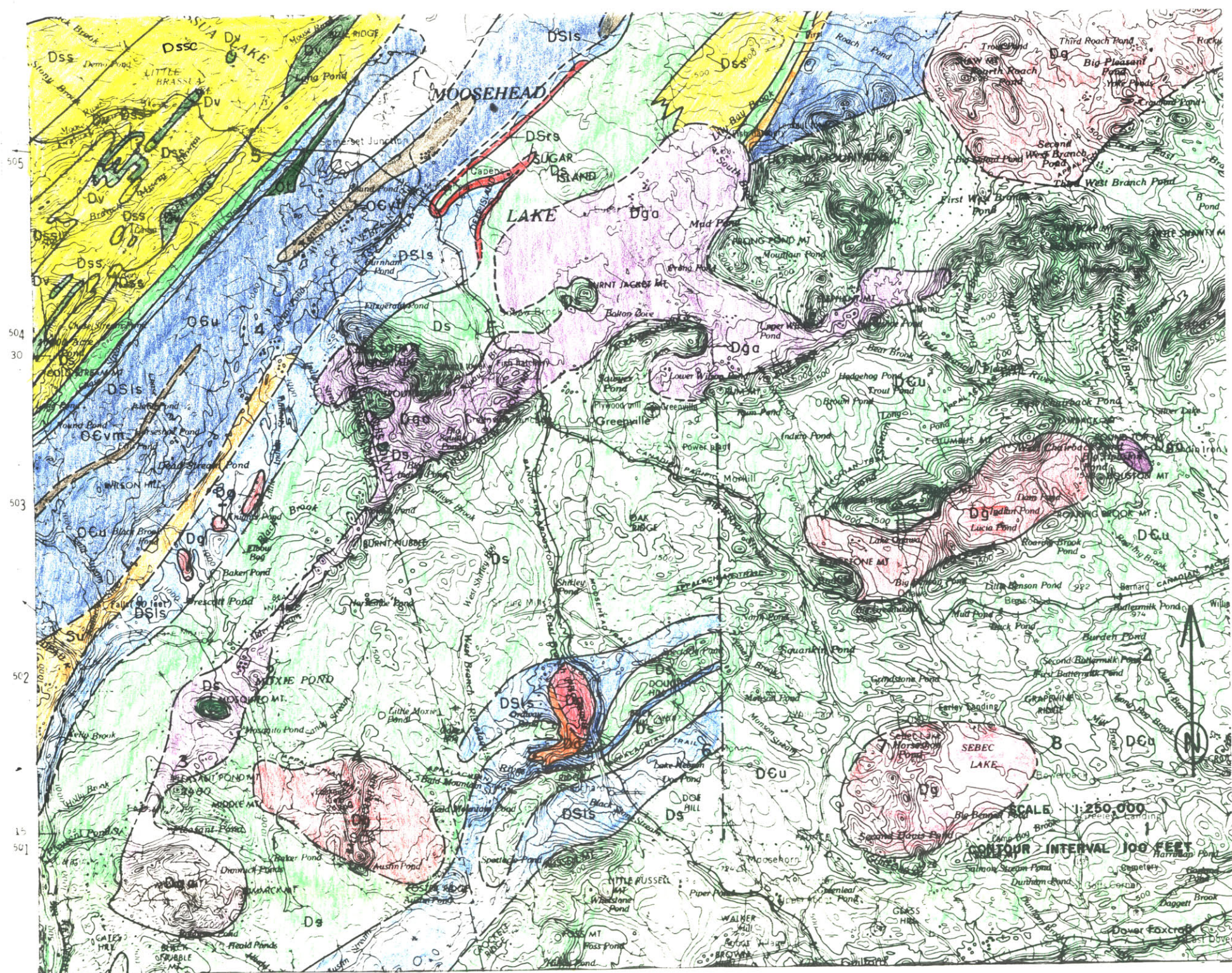
Prof. J. B. Thompson, Jr. of Harvard University suggested the

"Onawa pluton" which proved to come close to satisfying all the above requirements. This intrusive and its contact aureole have been mapped by Dr. S. S. Philbrick as a doctoral dissertation at the Johns Hopkins University (Philbrick, 1933, 1936). After studying Dr. Philbrick's work, the writer decided to use the area as a basis for his investigation.

## II. A. Location and Access

The contact metamorphic aureole which is the subject of this study surrounds an intrusive mass in Piscataquis County, Maine, lying within the Sebec Lake and Sebec topographic quadrangles. The area studied by the writer is entirely within the Sebec Lake quadrangle in the vicinity of Lake Onawa, where the rocks of the aureole are exposed chiefly in Barren, Boarstone, and Greenwood Mountains. The Onawa pluton is the boot-shaped body at right centre on the geological map, Figure 1.

The location is accessible from the south via Maine Route 15, a medium-duty asphalt road passing through Monson and Greenville. On the north side of Monson, a light-duty road, part asphalt and part gravel, provides access to the Canadian Pacific Railway at Bodfish Junction on the western outer edge of the Onawa aureole. This road continues across the intrusive contact as far as the lumber camp at Long Pond Stream. From there, a dirt road extends to Long Pond, north of the aureole. The Canadian Pacific Railway cuts across the contact zone between Bodfish and Onawa station, at the southeast corner of Lake Onawa, then turns south across the aureole again and continues east. The intrusive and contact metamorphic rocks are well exposed in a number of rail cuts. The Appalachian Trail, from Bodfish, follows the chain of mountains along the north rim of the intrusive as far east as Chairback Mountain. A gravel automobile road ascends Boarstone Mountain, much of which is private property, two-thirds of the way to the peak, and a trail



Taken from GEOLOGIC AND AEROMAGNETIC MAP OF NORTHERN MAINE  
 By Arthur J. Boucot, Andrew Griscom, John W. Allingham, and William M. Dempsey

<p>Devonian</p> <p>Middle(?) Devonian</p> <p>Lower Devonian</p> <p>Silurian or Devonian</p> <p>Silurian</p>	<p><b>Dg</b> <b>Dga</b> <b>Dd</b></p> <p>Plutonic rocks          Dg, light-colored granitic rocks          Dga, gabbro          Dd, diorite</p> <p><b>Dv</b></p> <p>Felsic igneous rocks          Dv, volcanic rocks</p> <p><b>Dss</b> <b>Ds</b></p> <p>Sandstone, slate and greenstone          Dss, dark-colored ss and sl, cgl          Ds, dark-colored, often cyclicly layered sl,          includes Seboomook formation</p> <p><b>DSrs</b></p> <p>Red slate          Contains some green slate and quartzite</p> <p><b>DSis</b></p> <p>Calcareous sedimentary rocks          Calc sl, calc ss, ls, and ls cgl</p> <p><b>Su</b></p> <p>Sedimentary rocks          Undifferentiated ls, calc sl, and calc ss,          some cgl and tuff locally</p>	<p>Ordovician</p> <p>Cambrian or Ordovician</p> <p>Cambrian, Ordovician, or Silurian or Devonian</p>	<p><b>Ot</b></p> <p>Volcanic rocks, sandstone and slate          Ot, felsic tuff</p> <p><b>Oeu</b> <b>Oevm</b> <b>Oeuf</b></p> <p>Sedimentary and volcanic rocks          Oeu, undifferentiated sed. rocks, may include          some igneous rocks locally          Oevm, mafic volc. rocks          Oeuf, felsic "</p> <p><b>Dcu</b> <b>Ddu</b> <b>Ddv</b></p> <p>Sedimentary and volcanic rocks          Dcu, undifferentiated sed. and volc. rocks          Ddu, felsic and mafic volc. rocks</p> <p>—</p> <p>Contact</p> <p>- - - -</p> <p>Inferred contact</p> <p>~~~~~</p> <p>Schematic contact showing facies change          of interfingering sedimentary rocks</p> <p>- - - -</p> <p>Approximate boundary between map units</p> <p>☒</p> <p>Contact metamorphosed rocks</p>
---	--	--	--

Figure 1. Geological Map of the Moosehead Lake Area.

extends to the peak. Streams in the area are not navigable, but numerous trails connect all the lakes and ponds. In addition, the area is cut by myriad old logging trails, which often have no particular destination.

The east end of the intrusive is attained by dirt road from Maine Route 11, at Prairie, about five miles north of Brownville Junction. This road passes by the Katahdin Iron Works, and crosses the aureole, terminating at Arnold Camps on Houston Pond.

#### B. Topography

The sediments surrounding the intrusive form an irregular topography of low (less than 300 feet) relief. The extent to which the country rock topography is controlled by structure is not known, since only the intrusive and aureole have been mapped. Where they have been metamorphosed by the intrusive, the sediments stand as high mountains, up to 2100 feet above the surrounding country. The peaks generally lie within the aureole, and the site of the intrusive is a basin, much of which is low and swampy, and occupied by lakes and ponds. The rocks of the aureole are thus well exposed, while the intrusive can be studied in detail only locally, along the contact; exposures in the interior are rare.

### III. FIELD OBSERVATIONS

#### A. Previous Investigations

The earliest geologic map including the Onawa area was produced by C. H. Hitchcock (1886), who indicated a belt of slate 15–20 miles wide in Piscataquis County, central Maine. Quarries in this slate belt at Monson, Blanchard, and Brownville Junction were described by T. N. Dale (1906). E. H. Perkins carried out reconnaissance mapping of the "Moose River sandstones" to the north, and observed that "A few miles south of the foot of the (Moosehead) lake the Monson slates appear and extend for a score or more miles to the south" (Perkins, 1925, p. 373). E. S. C. Smith (1929) collected Monograptus-like remains from a quarry dump at Brownville Junction, and suggested that the slates of the Brownville–Monson belt are Silurian. In 1931–32, S. S. Philbrick and H. E. Stocking mapped the topography and geology of the intrusive at Onawa and its wallrocks (Philbrick, 1933, 1936). A base map was compiled from U. S. G. S. and U. S. C. G. S. level and triangulation data, plane table triangulation data, barometer survey, and aerial photographs. Geologic features were located by reference to topographic features, barometer elevations, and pace and compass traverse. Field and petrographic work showed that the mass is surrounded by an aureole of hornfels produced by contact metamorphism of the slates. A. Keith (1933) mapped the slate as Silurian and also indicated a ring of Cambro-Ordovician arenaceous rocks surrounding the pluton. Since this unit coincides with the aureole, it is apparent that he mistook the hornfels



for quartzitic rocks. Philbrick's structural data (1936, p. 38) clearly indicate that the slate passes into hornfels. Philbrick (1940) published the results of reconnaissance traverses across a number of other aureoles near the south end of Moosehead Lake, which showed that they have petrographic and megascopic similarities to that of the Onawa pluton. R. L. Miller (1945) published a geological report on the Katahdin pyrrhotite deposit, which occurs in the "Ore Mountain Diorite" body at the east end of the Onawa intrusive. The gossan capping the massive pyrrhotite body within the small gabbro mass was developed as an iron mine. Hurley and Thompson (1950) published a map of the Moosehead Lake area but provided no new data on the rocks south of the lake, except that they suggested a structural break between them and the Moose River sandstones. Balsley and Kaiser (1954) published geologic and aeromagnetic reconnaissance data which include parts of the Onawa area. Magnetic data showed that the gabbro at Ore Mountain is probably larger than its exposure indicates, and that several small anomalies are present on the contact of the Onawa pluton. Geological reconnaissance data in these areas show "phyllite" or "phyllite-quartzite" in the aureole and gabbro, diorite or monzonite for the intrusive. Hurley et al (1959) showed that the age of the regional metamorphism of the Devonian Seboomook Slate to the northwest of the Moose River sandstones is similar to the age of the intrusives. Mapping is currently in progress by U. S. G. S. geologists in several quadrangles to the west of the Sebec Lake sheet, including the Greenville quadrangle (G. H. Espenshade) which borders it on the west.

## B. Areal Geology

The accompanying map (Figure 1) shows the geological units so far defined in the Moosehead Lake area. The structural trend of the sedimentary rocks is northeast-southwest, and the Onawa intrusive is one of a large number of plutonic bodies which form a belt, roughly concordant with the structure, extending across most of the width of the state. Also included in this group are the Katahdin batholith, of over 500 sq. mi. area, the gabbro extending from Moxie Mountain to Squaw Mountain, and numerous smaller bodies. The intruded rocks are dominantly slates, underlain by limestone, probably of Lower Devonian and Silurian age. At the north end of Moosehead Lake, the stratigraphic relations are established, and are reproduced in Table 1. This sequence is bordered on the south along a probable fault (Hurley and Thompson, 1950) by a sequence of Cambro-Ordovician sediments as yet undivided, followed by the "Monson slates" (Dale, 1906), which include slate, quartzite, calcareous slate and limestone. On the basis of lithologic similarities, the slate and limestone of the Monson area are tentative correlated with the Seboomook slate and Silurian-Devonian limestone to the north, but no confirmation of this suggestion has been made, since diagnostic fossils have not yet been discovered in the Monson area. Poorly preserved graptolites from Brownville Junction, 10 miles southeast of the Onawa intrusive, were termed Silurian (Smith, 1929).

The plutonic rocks of the area have intruded and contact metamorphosed most of the units described above. The youngest slate and limestone known to be intruded is Seboomook slate near Jackman,

Table 1. Table of Formations in the Moosehead Lake Area.

Stratigraphic Unit	Lithology	Age	Authority
"Moose River sandstone"	sandstone conglomerate	L. and M. Devonian (Oriskany- Onondagan)	Williams and Gregory (1900)  Perkins (1925)
Seboomook slate	sandstone, slate	L. Devonian (Oriskany)	Perkins (1925)  Hurley et al (1959)
	limestone conglomerate calcareous shale and sandstone	Devonian and Silurian	Hurley et al (1959)
- - - - - unconformity - - - - -			
	granitic rocks	pre Silurian	Hurley and Thompson (1950)

Maine (Hurley et al., 1959), where Oriskany fossils occur in a cordierite hornfels formed by contact metamorphism of slate around a quartz monzonite body. Since a number of the intrusives of the area, all of which show no evidence of metamorphism subsequent to emplacement, have similar potassium-argon and rubidium-strontium ages of about 360 million years, (Hurley et al., 1957, 1958), it is apparent that they were all emplaced during the same orogenic event and are post Lower or Middle Devonian in age. This age is similar to the age of granitic rocks of Nova Scotia (Fairbairn et al., 1950), and represents the time of the Acadian orogeny. That regional and contact metamorphism of the sediments occurred during the same period is shown by the radiogenic ages of hornfels and slate near Jackman, which are similar to the age of the intrusives.

The hornfels zones rimming the intrusives have a characteristic topographic expression. Since they are fine grained and massive, they are more resistant to erosion than either the country rocks or the intrusives; hence, they stand in relief as rings of hills surrounding a swampy basin occupied by the intrusive. Philbrick (1940) pointed out this similarity in topographic expression between the aureoles of the Onawa, Squaw Mountain, and Katahdin intrusives, and also noted that all showed similar macroscopic and microscopic features (see IV. Petrography).

### C. Geology in the Vicinity of the Onawa Pluton

The intrusive at Onawa, Maine, is roughly oval in plan, trending east-west, with maximum dimensions about 11 miles by 3 1/2 miles. On all sides, the intruded rocks are slates; contact metamorphic

effects visible in the field occur in a zone from 500 feet to 1 1/2 miles wide around the intrusive. The general geological features are shown in Figure 2a on the map made by S. S. Philbrick in 1931-1932.

### 1. Slate

The slate in the area is dark grey, very fine-grained and fissile. It is interbedded with, and grades to, light grey, fine quartzite; all gradations between the slate and quartzite occur interbedded. Layers vary from less than 1 mm to several feet in thickness: slaty or quartzitic types may predominate locally, but slate is the dominant type in the area. Cross-bedding, ripple marks, graded bedding, and scour-and-fill structures are common. In some outcrops the slate is uniform and no bedding is apparent. In general, bedding and cleavage, where observed together, are more or less coincident although up to two cleavages, both at a marked angle to the bedding, have been noted. No fossils were observed; small pits weathered in some slaty layers were proven to be the sites of calcite crystals (see IV. Petrography).

Bedding and foliation attitudes in the slate and aureole at the western end of the pluton are shown in Figure 2b, a reproduction from Philbrick (1933). The intrusive is clearly discordant at the ends, where the slates are complexly deformed.

### 2. Aureole

S. S. Philbrick, in mapping the contact aureole, divided it into three zones, termed, in the order in which they are encountered as the pluton is approached:

- a) andalusite schist zone
- b) hornfels zone
- c) injection hornfels zone

Figure 2a. Geological Map of the Onawa Pluton and Aureole.

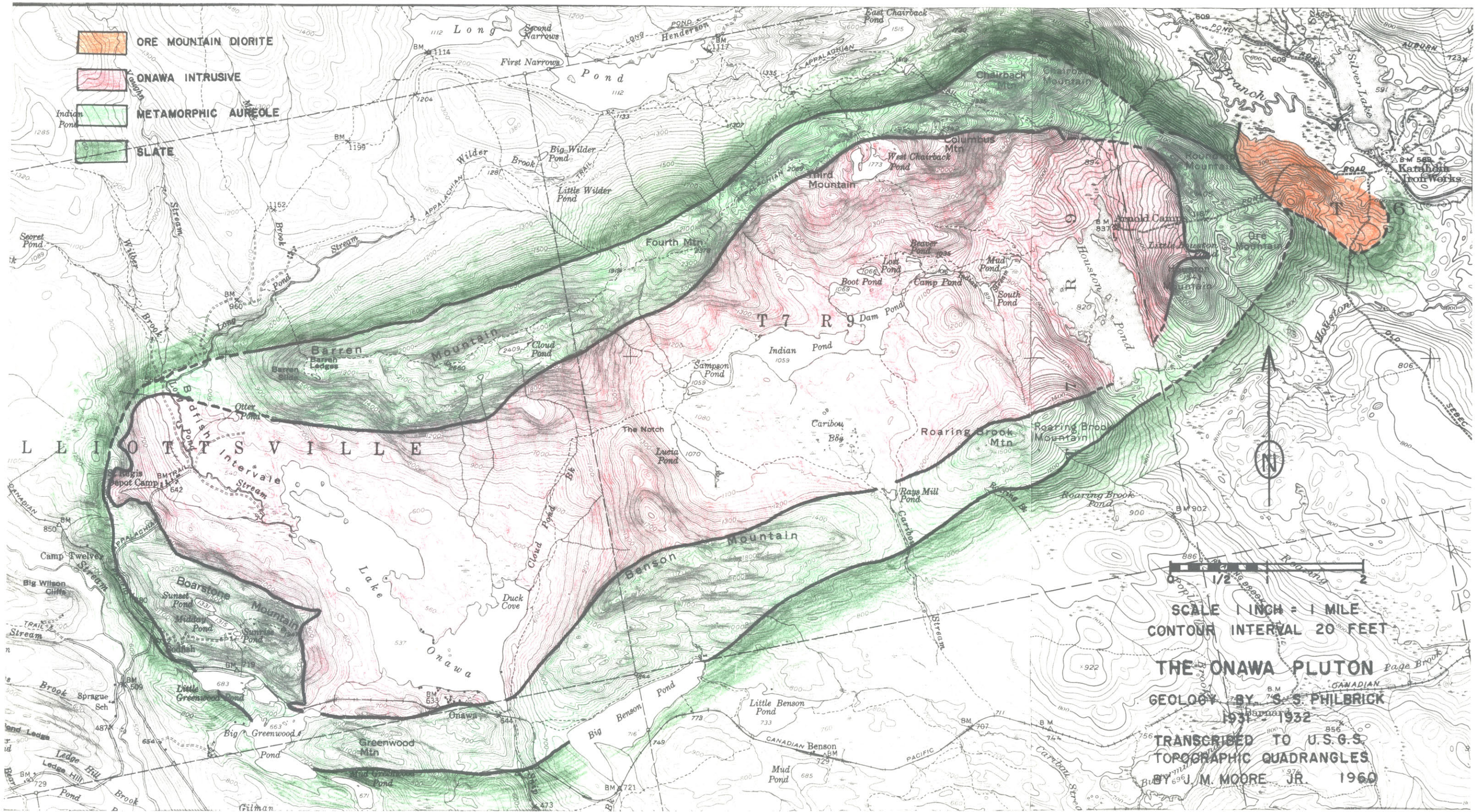
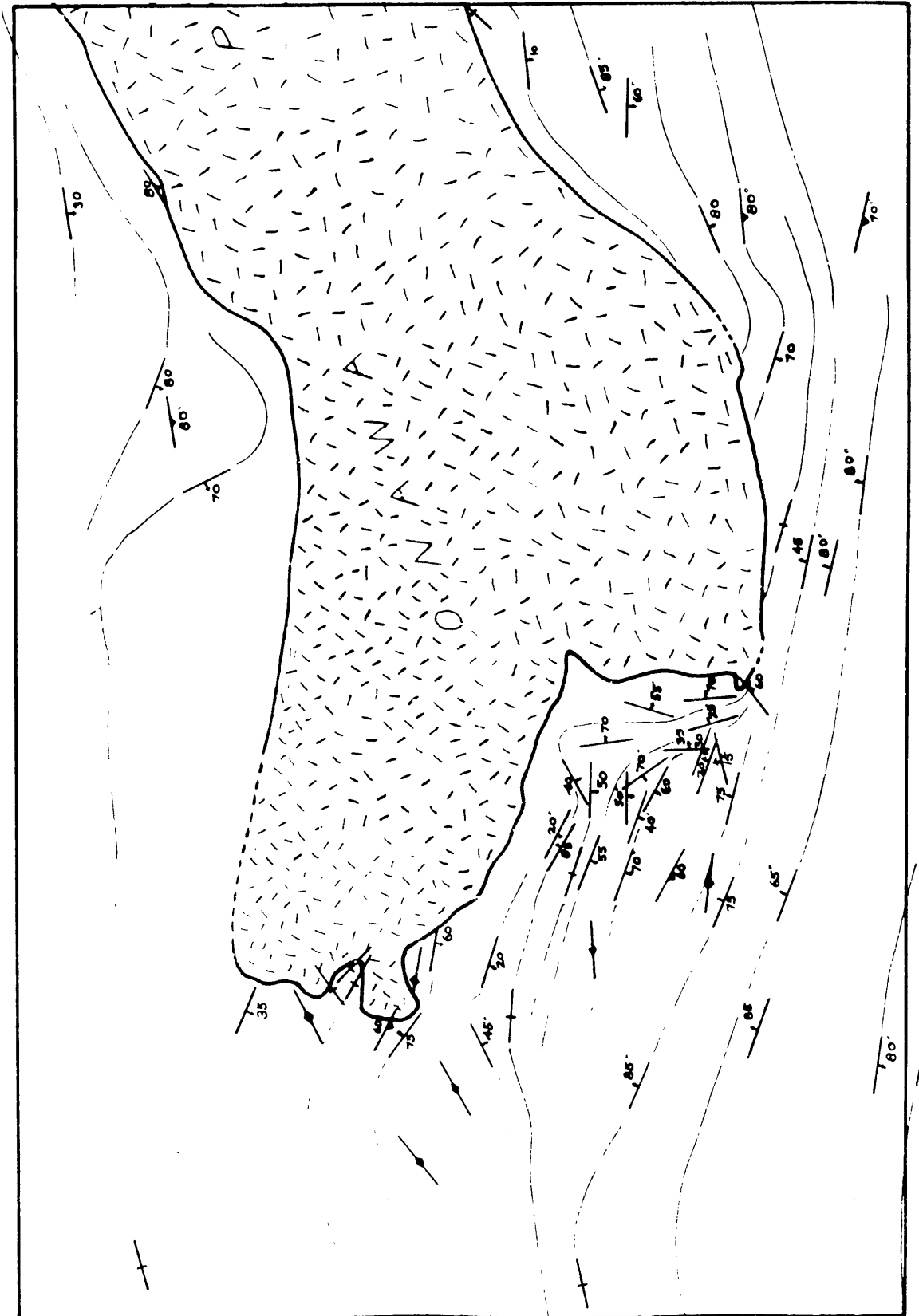


Figure 2b. Structural Map of the Western End of the Onawa Pluton, from Philbrick (1933).





These divisions have, for simplicity, been eliminated from Figure 2; however, they are reproduced on the detailed geologic map (Figure 3), from which it may be seen that they are, in part, related to the mineral assemblages of the contact metamorphosed rocks. The zones of Philbrick are based on the macroscopic appearance of the rocks and it is convenient to refer to this terminology in describing the aureole macroscopically. The "andalusite schist zone" is distinguished by the presence of rocks having some cleavage and containing andalusite prisms. In the "hornfels zone," cleavage is absent, and in the "injection hornfels zone," the rocks are traversed by many thin aplitic veinlets. The writer does not use Philbrick's term "injection" in a genetic sense.

The outer (andalusite schist) zone retains to some extent the slaty cleavage of the country rock, but contains up to 20 per cent andalusite in a very fine "spotted" matrix. The andalusite is up to 1.0cm long throughout the zone: it is randomly oriented, prismatic, with the typical "chiastolite" cross visible in sections perpendicular to the long dimension. The spots are micaceous aggregates 0.5-1.0 mm, which locally have preferred orientation parallel the slate cleavage. At Bodfish, where the writer examined the outer limit of the aureole, the andalusite appears first. A few faint spots are visible with the first andalusite, becoming prominent in 500 feet toward the intrusive.

On the weathered surface, the spots appear as pits and the andalusite prisms as elongate lumps. These features impart a characteristic appearance to the rocks of the outer part of the aureole.

Toward the pluton, the rocks become progressively less fissile and less fine-grained, attaining a "hornfelsic" texture (hornfels zone). Approximately coincident with the transition from fissile to non-fissile rocks is a change in the appearance of both spots and andalusite metacrysts. The former lose their micaceous appearance, and weather to powdery, yellow-brown material; in the fresh rock, they are darker grey and a little harder than the matrix. The andalusite occurs as irregular metacrysts rather than well-formed chiastolite prisms.

Toward the contact, the spots are less obvious, disappearing altogether approximately at the boundary of the injection hornfels zone. The rock there is light to medium grey, massive, fine-grained, equigranular except for medium-grained andalusite metacrysts. The only mineralogic distinctions possible with a hand lens are between andalusite, spots and matrix (with very fine mica) in the fissile rocks, and between andalusite, biotite, spots where present, and light minerals in the hornfels. Bedding is accentuated in the outer part of the aureole, since andalusite forms only in the slaty layers, leading to "reverse graded bedding" in graded sequences. Since quartzite beds are fine, equigranular, and non-fissile, they have a similar texture to hornfels no matter where they occur. In the hornfels bedding becomes less defined toward the intrusive. Contacts are less sharp and layers are distorted. For example, slaty layers are represented by irregular discontinuous trains of andalusite-bearing rock. Bedding is further obscured by the appearance of many prominent light-colored veinlets, generally a few millimeters wide, in planes

parallel to or intersecting it. Near the contact the rock often has the appearance of a lit-par-lit gneiss.

### 3. Intrusive

The intrusive is exposed on the inner (basinward) slopes of the mountains, at or near the contact, but poorly exposed in the interior, due to a cover of lake, swamp and glacial drift. It is grey, medium grained in general, commonly quartz-bearing, with biotite as the dominant mafic. The best exposures are found in the rail cuts of the C. P. R. along the south contact, where the intrusive is darker grey, coarser, and higher in mafics than elsewhere. The contact was not observed in outcrop by the writer: its attitude is near vertical in the few places where it could be observed by Philbrick, and it is irregular in detail. Two mappable apophyses occur, one at Bear Bluff on the western end of the intrusive, and one at Houston Mountain on the eastern end. Around both, the aureole is much narrower, and not all the macroscopic zones of Philbrick are observed. At Bear Bluff, angular inclusions of slate are present. Inclusions and autoliths are observed in the igneous rock near the contact. One was sampled and sectioned by Philbrick (see IV. Petrography).

#### IV. PETROGRAPHY

##### A. Onawa Aureole

Petrographic observations are based on the study of about fifty of the writer's thin sections, and about thirty-five thin sections of the aureole kindly loaned by Dr. S. S. Philbrick. Descriptions of individual thin sections are synthesized into a general description of each characteristic assemblage, in the order in which they are encountered travelling from the slate toward the intrusive contact. All specimens described are located on the sample location map, Figure 3, and the assemblages are described under the same headings as used there. These assemblage titles denote the maximum number of phases deduced to be stable in the pelitic rocks; assemblages of fewer phases do occur in the slates and quartzite.

##### 1. Slate

quartz-chlorite-muscovite-albite

Slate specimens 0-3, 0-4, and 0-6, collected from the Little Wilson Stream and Big Wilson Cliffs, are all similar in that they consist dominantly of chlorite and white mica as very fine ( $10\mu$ ) shreds in parallel orientation, enclosing clear subangular to angular quartz grains ranging in size from  $<10\mu$  to 1 mm, mostly less than  $50\mu$ , composing 25-50 per cent. Quartzitic layers are similar except that the micas compose 10 per cent or less of the rock and are interstitial to the quartz. That some of the light mineral is a plagioclase was determined by X-ray study (see V. Mineralogical Studies by X-ray Diffraction). It is untwinned and cannot be distinguished from quartz

SCALE APPROX. 1/2 MILE = 1 INCH

CONTOUR INTERVAL 20 FEET

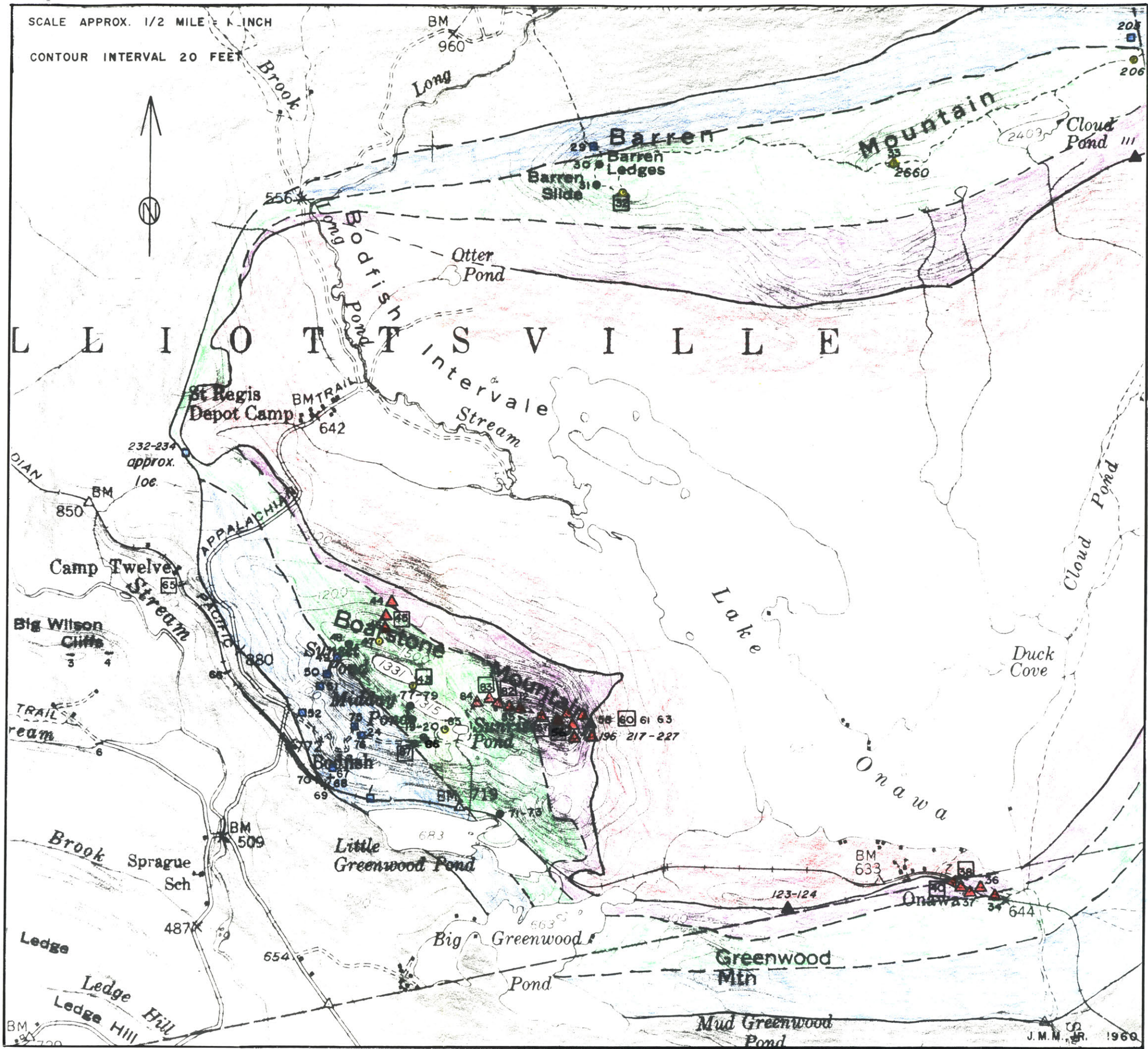








Figure 3. Geology and sample locations in the Lake Onawa area.

## LEGEND

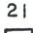

## Rock Units

	Onawa intrusive	
	"injection" zone	} Subdivisions of metamorphic aureole after S. S. Philbrick
	"hornfels" zone	
	"andalusite schist" zone	
	slate	

 limits of contact aureole

--- approximate boundaries of S. S. Philbrick subdivisions

## Specimen Locations

-  } samples examined in thin section
-  } samples from which coexisting minerals were analyzed
- 113* S. S. Philbrick thin sections examined

## Mineral Assemblages

- + quartz-chlorite-muscovite-albite
- quartz-(andalusite→chlorite-muscovite)-chlorite-biotite-muscovite-albite
- quartz-andalusite-biotite-(cordierite→chlorite-muscovite)-muscovite-albite
- quartz-andalusite-biotite-cordierite-muscovite-albite
- quartz-andalusite(±sillimanite)-biotite-cordierite-muscovite-microcline microperthite
- ▲ quartz-andalusite and/or sillimanite-biotite-cordierite-microcline microperthite
- ▲ sericite-chlorite + ▲

Enlarged from Sebec Lake Topographic Quadrangle (U. S. G. S.)

in thin section. The chlorite is pleochroic from very pale greenish-yellow to light green: some is recrystallized to stubby grains averaging  $50\mu$ , up to 0.2 mm, in random orientation, which are often intergrown with white mica parallel to the basal cleavage. A few grains of pale brown pleochroic biotite were observed in 0-4, and in the quartzitic layers of 0-6. Up to 5 per cent of the slate is an opaque mineral, with platy form well-defined in cross section, but ragged in plan. It shows no translucency, or red color in reflected light. Some grains are white in reflected light, indicating "leucoxene" alteration of a titaniferous mineral. This opaque is  $10-20\mu$ ; much finer disseminated opaque material forms tiny ragged plates, often curved. This is probably graphite. A few irregular grains are light yellow in reflected light, with a metallic lustre, indicating pyrite, although no cube outlines are visible. A few prisms of greenish-brown tourmaline with quartz inclusions are present in all specimens. No rutile was detected. 0-3 is silty, containing a variety of angular -subangular grains, 0.1-1 mm, of quartz, chlorite and sericite aggregates, and albite-twinned plagioclase (too few grains to determine composition). 0-6 contains 0.5-1 mm idiomorphic elongate grains of a carbonate, so crowded with inclusions of matrix minerals that they are almost invisible except under crossed nicols. These grains weather to tabular pits in the hand specimen, and effervesce with cold HCl; hence, they are calcite, and appear to have grown in the solid as flat rhombs. They are restricted to slaty layers, and do not exceed about 1 per cent of a given layer. This feature is fairly common in the area of the Appalachian Trail at Little Wilson Stream.

Specimens 0-65 and 0-66, from the Canadian Pacific Railway just outside the aureole are similar except that chlorite metacrysts, 50-150 $\mu$ , are more prominent, generally set at an angle to the foliation, which is wavy in 0-66. Minor biotite is present in 0-66, intergrown with chlorite metacrysts parallel to the basal cleavage. A single chlorite pseudomorph after andalusite occurs in 0-65 (this feature is described more fully under IV. A. 2. Aureole). Some angular quartz grains are polycrystalline. When a sample of 0-65 was digested for chemical analysis (see VI. Chemical Analyses), a very fine, shiny light black residue could not be dissolved. This observation confirms the identification of similar material in thin section as graphite.

Some slates from the quarries at Monson, Blanchard, and Brownville are described petrographically by Dale (1906). As in the Bodfish-Onawa area, these are interbedded with quartzite, and are petrographically similar to the specimens described above, except that biotite is always present as grains up to 100 $\mu$ , transverse to the cleavage. The minerals observed were: quartz (20 $\mu$ ), sericite, chlorite, biotite and accessories (not all present in all sections), tourmaline, pyrite ("distorted cubes"), graphite, rutile, hematite, magnetite (not in same slide with hematite). No carbonate was detected with cold HCl.

## 2. Aureole

- a) quartz-(andalusite  $\rightarrow$  chlorite + muscovite)-chlorite-biotite-muscovite-albite

This assemblage is characterized by the association in the matrix of biotite with chlorite similar to that in the slates, and by the



replacement of andalusite by white mica and chlorite. It is represented by three specimens, 0-68, 0-69, and 0-70, from the outer limit of the aureole near Bodfish. A fourth specimen, 0-67, represents the next higher-grade assemblage, to be described below. In 0-67 and other specimens of the same assemblage, andalusite occurs as subidiomorphic to idiomorphic "chiastolite" prisms, up to 8 mm long, exhibiting the characteristic cross-shaped trains of inclusions. These inclusions consist of all the matrix minerals, and are neither more nor less graphitic than the matrix. A concentration of dark material, probably graphite, is observed along the prism faces, rimming the crystal. In 0-68, a thin rim of chlorite  $10\mu$  wide, oriented parallel to the prism faces, occurs within the graphite border. The grains composing the rim are up to  $50\mu$  long. In 0-69, the rim is  $100\mu$  wide (0.1 mm), and consists of an outer rim of chlorite and an inner rim of muscovite, intergrown along the contact of the two. In 0-70, the andalusite is completely replaced, consisting of a random white mica aggregate of prisms about  $5 \times 50\mu$  with a rim of  $50\mu - 100\mu$  chlorite prisms, rudely oriented parallel the outline of the pseudomorph. The identity of the replaced mineral is obvious from the nearly square, sharp outline, rimmed by graphite. 0-69 and 0-70 have a similar matrix, consisting of about 60 per cent micas. Muscovite and chlorite occur as ragged oriented flakes  $10-20\mu$ . Chlorite occurs also as stubby oval prisms in random orientation, up to  $100\mu$  in size. Biotite, less abundant than the other micas, is  $20-50\mu$  in size, pleochroic from almost clear to light reddish-brown, and irregular in outline. Both biotite and muscovite are occasionally

intergrown with chlorite prisms, parallel the cleavage. Light minerals (quartz and albite — see V. Mineralogical Studies by X-ray Diffraction) are clear, mostly angular grains averaging  $40\mu$ , up to  $150\mu$ . The opaque, composing up to 4 per cent, is the ragged, platy type observed in the slates, and averages about  $10\mu$ . Much very fine graphite is disseminated throughout. Quartz aggregates up to 1 cm, with angular outlines, may be disrupted quartzite beds. Biotite is more prominent with respect to the other micas in these areas, which consist of 80 per cent or more light minerals. Faint spots occur in the matrix of all the specimens. These are round areas 0.25–0.5 mm in diameter with less graphite than the matrix. In 0–70, they represent a concentration of white mica, less fine than in the matrix. In 0–68 and 0–69, chlorite laths  $50\text{--}100\mu$  are also present in the spots, composing 10–15 per cent of these features. This chlorite is similar in color and habit to that replacing andalusite, being pleochroic from pale greenish-yellow to light green. In the spots of these specimens, a clear mineral, distinct from quartz, is also present, but could not be identified. Biotite is more prominent in the matrix of 0–68 than in 0–69 or 0–70, and much is intergrown with chlorite.

b) quartz-andalusite-(cordierite → chlorite + muscovite)-muscovite-biotite-albite

This assemblage is characteristic of the bulk of the "andalusite schist zone," being represented by 0–67, 0–52, 0–75, and others. It is defined by "chiastolite" prisms and by "spots," composing 5–10 per cent of the rock. These are less graphitic than the matrix, and

contain rudely prismatic light green pleochroic chlorite, 50-150 $\mu$ , free of inclusions except for a little very fine, dusty opaque. In addition, all matrix minerals are present in the spots, the white mica being a little less fine than in the matrix proper. Orientation of the minerals of the spots is either random or approximately parallel that of the matrix, but less well defined. Spots are round or oval in section and show no preferred orientation with respect to the matrix. In hand specimen, the pits formed by the weathering of spots are ovoid and in random orientation. A light mineral, distinct from quartz, is present in many spots, often in preferred optic orientation so that the spots have a position of maximum extinction. In most spots, this material cannot be identified: the observation of biaxial interference figure, index of refraction greater than the quartz, and six-fold cyclic twinning (in S. S. Philbrick slide no. 1) identifies it as cordierite, at least in some specimens. Specimen 0-75 contains cordierite, exhibiting cyclic twinning, of the same size and habit as the spots, intersected by flakes of chlorite identical to those of the spots. Specimens nearer the intrusive contain only cordierite, of similar habit, free of chlorite. Biotite rims the cordierite of 0-76, and forms similar rims about spots in 0-75 in which cordierite is absent. The chlorite is not always intimately associated with the spots. It may be absent from the spots of some specimens, e. g., 0-50, scattered throughout the matrix, but of the same appearance as that in the spots of other specimens. Similar chlorite also is intergrown to a minor extent in optic orientation with matrix biotite.

Andalusite forms chialstolite prisms as described above, generally

not over 1 cm, composing 0-20 per cent and averaging less than 5 per cent of the rock. Irregular areas in the crystal may be composed of a spongy intergrowth of andalusite and matrix, dominantly andalusite and quartz. In some cases these areas are portions in which the planes of the "cross" are parallel the section; in other cases the intergrowth clearly occupies a volume larger than that of the cross.

The matrix of the spotted assemblage is generally foliated, with parallel orientation of biotite, white mica, opaque, and light minerals (where elongate). Biotite is rudely prismatic, composes 15-25 per cent, is pleochroic light to medium brown, 30-150 $\mu$  long. It is in part poikilitic with fine quartz inclusions. White mica occurs as well-formed prisms 10-30 $\mu$ , or is occasionally intergrown with biotite. Light minerals have angular to xenomorphic outlines, are free of inclusions, average about 50 $\mu$ . The opaques are similar to those described above. A few zircon grains and apatite grains are included in biotite. A few idiomorphic tourmaline prisms, pleochroic from light yellowish-brown to dark bluish-brown, are present in most specimens.

At the Bear Bluff apophysis, this assemblage occurs no more than 100 feet from the intrusive contact.

c) quartz-andalusite-cordierite-biotite-muscovite-albite

0-75 is an assemblage transitional between this group and the assemblage described above, in that both chlorite and cordierite are prominent. 0-31 and 0-87 are typical of assemblages characterized by the presence of unaltered cordierite coexisting with white

mica. Foliation is present in some specimens, but orientation is generally random. Light mineral grains lack angular outlines, and are more uniform in size, averaging about 20 $\mu$ . The micas are similar in size and habit to those of the preceding assemblage, but instead of being interstitial to the light minerals, penetrate them randomly. Cordierite occurs as rounded metacrysts 0.25–1.0 mm, often exhibiting six-fold cyclic twinning (the pits formed by cordierite weathering are ovoid, identical to the pits formed by weathering of spots). It is elongate parallel the twin axis (c). The cordierite is crowded with rounded inclusions of all matrix minerals, particularly quartz and opaque. The borders of the cordierite merge with the groundmass. Sharp muscovite prisms in the matrix penetrate the cordierite and are included in it, but show no change in habit or concentration in the vicinity, with this exception: in several slides, e. g. 0–77, muscovite prisms intersect the cordierite in random orientation. These prisms are less fine than the matrix white mica, and usually more ragged. Cordierite consists partly of yellow isotropic material in some of these specimens.

Andalusite is smaller than in the spotted slate, not usually exceeding 1 mm. It is irregular in outline, and almost invariably forms a spongy intergrowth with quartz. It composes 0–15 per cent, averaging 2–3 per cent. Only in 0–77 was chiastolite observed. This rock is highly graphitic, and the cordierite is altered as described above.

Biotite has a reddish tint, which increases abruptly in intensity coincident with a change in the habit of the opaque minerals, as the

intrusive is approached. This change is apparent in comparing specimen 0-87 with 0-85 (which contains the next assemblage to be described), or 0-30 with 0-32. Toward the intrusive, the opaque changes from ragged platy to rounded thick plates with occasional rude hexagonal outlines. All specimens observed to contain this opaque together with red-brown biotite contain a potassic feldspar also, with the exception of specimens 0-19 and 0-20. Graphite (?) is also present in small amounts.

Quartzite beds are of simpler mineralogy, containing dominantly quartz, with muscovite, biotite and opaque. Textural features are similar to those of the pelitic members, insofar as they involve the minerals of the quartzite. 0-78, interbedded with pelitic assemblages not containing a potassic feldspar, contains a few grains of microcline microperthite. Pelitic members which grade to quartzite do so by the loss first of andalusite, then of cordierite, accompanied by a decrease in the content of mica and an increase in quartz.

d) quartz-andalusite ( $\pm$ sillimanite)-cordierite-biotite-muscovite-  
microcline microperthite

This assemblage is the same as that described above, except that the opaque is always rounded, the biotite strongly orange-red-brown, and small grains of microcline microperthite are present. 0-32 and 0-85 are typical. Grain size is less fine: quartz and feldspar average about 0.1 mm. Microcline is recognized by its low refractive index and grid twinning, not obvious in small grains, and contains numerous perthitic lamellae. It forms subidiomorphic elongate grains with abundant rounded inclusions of quartz and opaque.

It contacts and includes matrix muscovite. In one specimen, 0-46, two habits of muscovite are observed. One is as described above, the other is as larger irregular laths interfingering with biotite parallel the cleavage and including small areas of biotite, which are in optic orientation with the adjacent biotite grain.

A few "fibrolite" wisps are present in most specimens of this assemblage. They are hairlike fibres up to  $50\mu$  long, often curved and in radiating clusters, with high relief. Most commonly they are observed within quartz grains, adjacent to andalusite or biotite. X-ray data (see V Mineralogical Studies by X-ray Diffraction) shows that this mineral is sillimanite or mullite.

e) quartz-andalusite (and/or sillimanite)-cordierite-biotite-  
microcline microperthite

Although muscovite is not included in the title of this assemblage, it is invariably present in thin section as ragged poikilitic laths up to 3 mm, associated with and interfingering with biotite. It is not interpreted as being a member of the stable mineral assemblage, for reasons outlined below (VII. Interpretation of Petrographic Data). Andalusite prisms are irregular and poikilitic with quartz in some specimens and idiomorphic and clear of inclusions in others. They are pleochroic in patches from clear to pink, and range in size from 0.5-2 mm, averaging 1 mm. Fibrolite is common, but varies markedly in abundance from slide to slide. This variation is not correlated with proximity to the contact, insofar as is apparent from the surface geology. For example, specimen 0-56, from the peak of Boarstone Mountain, contains abundant fibrolite, rimming biotite grains and rounded andalusite metacrysts, and extending into adjacent

quartz grains. It occurs also with biotite in veinlike streaks, which have a milky appearance in hand specimen. These "veinlets" are localized on grain boundaries. In them, small irregular grains of biotite, pale on the edges due to thinning (although a few grains seem to be bleached on the edges), are surrounded by dense stringers of fibrolite, mainly oriented parallel to the boundary, with random fibres on the edges which penetrate quartz, potassic feldspar, and cordierite in the adjacent rock. In 0-60 and 0-61, nearer the contact, only traces of fibrolite are present. In a few specimens of this assemblage, i. e., 0-57, fibrolite is not detectable, but careful examination under high power reveals a little in most assemblages containing a potassic feldspar, generally associated with andalusite-quartz or biotite-quartz boundaries. In only one specimen, 0-77, was fibrolite observed in a hornfels not containing potassic feldspar.

With the exception of andalusite and muscovite, and the accessory minerals, the assemblage is approximately equigranular, averaging 0.1-0.2 mm, although the biotite is generally a little larger than the light minerals. Grains are for the most part xenomorphic, and orientation is random except in a few specimens exhibiting some parallelism of biotite. Biotite is orange-brown or red-brown, the deeper color being apparent in thicker sections. It contains many zircons with prominent pleochroic haloes, in contrast to the biotite of lower grade assemblages. Cordierite is larger than biotite or quartz in specimens collected near those of the preceding assemblage, but decreases in both grain size and inclusion content as the intrusive is approached, so that it is difficult to distinguish from quartz in hornfels from the peak of Boarstone Mountain. It is distinguished by a



slightly rougher surface in thin section, resulting in an apparent higher relief, by its biaxial optical character (negative with large axial angle,  $70^{\circ}$ - $80^{\circ}$  in 0-61), and by the presence of incomplete six-fold cyclic twins in conjunction with some polysynthetic twinning on (110). On the flat stage, single grains of cordierite appear complex under crossed nicols; on the universal stage, setting the c-axis vertical resolves this complexity into the twinning described. Quartz is clear, unstrained or with slightly undulatory extinction. Potassic feldspar is microcline microperthite as previously described: its texture changes in the same manner as cordierite, so that both are essentially free of inclusions near the intrusive. The grains are first cleared of inclusions on the margins: cordierite is inclusion-free in specimens in which the microcline has quartz and opaque inclusions in the centers of the grains. The degree of inclusion liberation varies greatly for a given phase in a single thin section; some grains may be perfectly clear while others are crowded. The opaque is the same sort previously described, forming thick rounded hexagonal plates or xenomorphic grains averaging about  $10\mu$ . Graphitic material is not apparent. Micas compose 5-25 per cent, averaging 10-15 per cent. Of this, 0-10 per cent may be muscovite, the abundance of which is apparently in reciprocal relation to the biotite content. Some specimens apparently exhibit concentration of opaque in the vicinity of muscovite; precise modal data would be required to verify this suggestion, since the muscovite is associated with biotite, and the opaque shows some preferential association with the ferromagnesian minerals. Andalusite composes 0-5 per cent, averaging 2-3 per cent: potassic feldspar

averages about 5 per cent, opaques 1-3 per cent. The remainder of the rock is quartz and cordierite, usually in about equal proportions, i. e., 30-45 per cent.

Other accessories observed are tourmaline, apatite, and an iron sulphide (?). Tourmaline forms small prisms, dichroic from light to dark brown. In a few hornfelses from near the intrusive contact, it forms large skeletal xenomorphic crystals, up to several mm, dichroic from light to dark orange-brown.

Within the "injection hornfels zone" the rock is cut by numerous aplitic veinlets, and milky veinlets as described above. Many of the aplitic veinlets are present in thin sections; they average .5-2 mm wide and consist almost entirely of quartz and microcline microperthite, in approximately equal proportions, although quartz may dominate. Grain size is a little less fine than in the hornfels, averaging 0.2-0.5 mm. The veinlets also contain minor amounts of the other minerals of the hornfels. A concentration of biotite and andalusite is often observed on the margins; the enclosing rock appears to be higher in cordierite. Intersecting veinlets of this type show no discontinuities or displacements, either in section or in hand specimen, but may swell at the junction.

Plagioclase feldspar, except as lamellae in microperthite, is observed only in a few thin sections of specimens taken from very near the contact. For example, 0-40 contains subidiomorphic grains of albite, normally zoned, with albite and Carlsbad-albite twinning. It is nearly calcium-free on the exterior, from extinction angle measurements on the twins. This specimen also contains, in addition to the typical microcline microperthite, large subidiomorphic grains,

0.5-2 mm, of non-perthitic grid microcline, with a few rounded inclusions of quartz and cordierite. 0-40 contains no andalusite, but many straight fibrolite needles, less fine than in the other specimens, showing preferential association with cordierite.

f) quartz-andalusite (+sillimanite)-(sericite-chlorite)-biotite-cordierite-microcline microperthite

This assemblage is texturally similar to the preceding one, but contains partial or complete pseudomorphs of very fine shreds of white mica (sericite) and pale grey-green or bright green chlorite after potassic feldspar, cordierite, and, to a lesser extent, biotite. This assemblage is restricted to within about 100 feet of the intrusive contact, and is best illustrated by sections such as 111 and 124 of S. S. Philbrick. Aggregates composed totally of high and low birefringent fibrous material have the same form as grains of cordierite and potassic feldspar, and all intermediate mixtures are observed. Opaque minerals are concentrated in masses of chlorite and chlorite intergrown with biotite. No andalusite or andalusite pseudomorphs are observed. Quartz grains, often penetrated by fibrolite, are clear and unaltered. In 0-63, the pseudomorphs have a light yellow color.

g) General observations of textural features

The only gross inhomogeneity in grain size of a given mineral is that exhibited by angular quartz grains in the slate and spotted chialstolite-bearing slate. In these assemblages quartz varies in size over two orders of magnitude. Grain size of xenomorphic quartz and of all other phases varies within one order of magnitude (e.g., quartz may range from 20-200 $\mu$  in a potassic feldspar bearing hornfels).

The minerals of a given assemblage are in general uniformly distributed and are all in mutual contact, with the following exceptions:

1) andalusite may have an irregular distribution, particularly in hornfelses in which it has low abundance. Many andalusite metacrysts which are poikilitic with quartz are partially surrounded by a quartz rim, so that they contact only a few grains of the other members of the assemblage. They do, however, contact all other members.

2) large, ragged laths of muscovite in potassic feldspar bearing hornfelses are invariably associated with biotite, although they do contact all other members of the assemblage.

3) fibrolite is preferentially associated with biotite, andalusite and quartz, but does occur in contact with cordierite and potassic feldspar also.

4) biotite often is concentrated around the perimeter of cordierite in cordierite-muscovite assemblages, and around andalusite in all assemblages in which the andalusite is irregular in outline.

### 3. Intrusive

Petrography of the intrusive is based largely on data from S. S. Philbrick (1933), supplemented by the writer's study of some of Philbrick's slides. No thin sections of the pluton were made by the writer.

The petrographic classification of the pluton rocks varies from granite to gabbro and quartz norite. The most salic varieties are sparsely exposed in the center only, with the exception of a quartz monzonite dike on Boarstone Mountain. They are two-feldspar granites and quartz monzonites containing non-perthitic microcline and zoned

oligoclase-andesine. Two plagioclases are usually present: small prismatic grains with strong normal zoning (albite exteriors), and irregular grains less markedly zoned. The strongly zoned grains have the more calcic interiors. Biotite is the dominant ferromagnesian. It is red-brown as in the hornfels, and often has muscovite and minor chlorite associated. Minor augite is present in some quartz monzonites.

The intrusive is heterogeneous near the contact, where it is much better exposed, varying from quartz granodiorite to gabbro. A modal analysis by Philbrick gives:

quartz	57%
oligoclase (Ab <sub>80</sub> )	14%
muscovite	12%
biotite	11%
perthitic microcline	5%
opaque	2%

for a quartz granodiorite. Granodiorites contain potassic feldspar (grid twinned and untwinned, perthitic and non-perthitic, in the same specimen), and two plagioclases (oligoclase-andesine) as described above. Mafic minerals include orthopyroxene, diallagic augite, green hornblende, and red-brown biotite, often in a reaction relationship in which successive rims are present in the order listed, with orthopyroxene at the center. Tonalite is the most common species, occurring dominantly along the contact, but also in several outcrops in the interior (which Philbrick interprets as suggesting an uneven roof to the pluton). Quartz is present in small amounts, together with

two plagioclases: large, strongly-zoned andesine-labradorite prisms, and small unzoned andesine-oligoclase. The same mafics are found as in the granodiorite. Small augite crystals without reaction rims occur in the  $Ab_{70}$  zone of the plagioclase. Slides 162 and 164, from the contact at Onawa station, and 142 and 149, from the contact on Barren Mountain, were examined. The Barren specimens contain microcline and quartz, with andesine or andesine-labradorite showing normal zoning with some reversals. Biotite is the only mafic, and is locally altered to chlorite plus sphene. 162 is similar to the above specimens, but 164 is more mafic, containing labradorite, and hypersthene with hornblende and biotite as successive rims. A little quartz is present, hence 164 should be termed quartz gabbro or quartz norite. Several gabbros on the margin contain 3-10 per cent potassic feldspar and have biotite as the dominant mafic. Specimen 166 from near the contact at Onawa station, is similar to 165 except that large hypersthene have schiller inclusions of clinopyroxene on the borders. The intrusive is more mafic on the contact at Onawa station than at Boarstone Mountain, judging by the samples collected by Philbrick and by the macroscopic appearance of the rocks. No specimen more mafic than tonalite is described from the Boarstone vicinity. Specimen 195, from the foot of the eastern cliff of Boarstone, is a granite with quartz, grid microcline, albite-oligoclase and only a little biotite.

Texturally, the intrusive is medium grained, less commonly coarse, massive, hypidiomorphic granular or slightly porphyritic, except at the Bear Bluff apophysis on the western end, where it contains microphenocrysts of oligoclase in a fine grained matrix. In general,

sericite and clay alteration of feldspars is present in varying degrees, and biotite is partially chloritized, the chlorite resembling that of the sericitic hornfels along the contact.

#### 4. Inclusions

No inclusions of the pluton were sampled by the writer, but two thin sections of S. S. Philbrick's, containing inclusions, were examined. One is of an inclusion taken from an outcrop of diorite on the C. P. R. between the two Greenwood Ponds. It consists of about 60 per cent andesine-labradorite with albite, Carlsbad-albite, and pericline twinning. Hypersthene composes 20 per cent, dark green spinel 5 per cent, intensely red-brown biotite 5 per cent, potassic feldspar 5 per cent and opaque 3 per cent. Some of the biotite is intimately associated with hypersthene and opaque. Grain size is fine to medium. Angular inclusions in fine-grained porphyritic quartz diorite at the contact of the Bear Bluff apophysis resemble a slate in texture, and consist of about 40 per cent fine quartz, some of which has angular outlines, 40 per cent very fine white mica, 15 per cent yellow-brown biotite, a platy opaque mineral, some of which from its red-brown translucent color, is hematite, and a little pyrite.

#### B. Other Aureoles in the Vicinity

Through the courtesy of Dr. G. H. Espenshade, the writer had the opportunity to examine thin sections of hornfels from the aureole of a granodiorite-diorite mass between Shirley Mills and Blanchard, 15 miles southwest of the Onawa pluton along the strike of the slates, and from the aureole of the gabbro of Squaw Mountain, at the southwest

corner of Moosehead Lake. These rocks are very similar in textural and mineralogical features to the Onawa hornfels, and only those features of particular interest are described here.

#### 1. Shirley Mills-Blanchard

Several of the specimens are of lime-silicate hornfels, not observed in the Onawa area. These were not studied in detail, but assemblages observed are:

quartz(?) - tremolite-clinozoisite-potassic feldspar

quartz-tremolite-biotite

quartz-calcite-tremolite-clinozoisite

quartz-calcite-biotite

These assemblages are not in general complete, since several phases were not identified. The quartz-calcite association persists to within 500 feet of the contact; the aureole is at least one-half mile wide.

The lime silicate assemblages are approximately the same distance from the intrusive as pelitic hornfels bearing prominent fibrolite, and largely sericitized. At the north end of the intrusive, a spotted chiastolite slate contains a few small garnets. Andalusite in this slate is cross-cut by low-birefringent masses with a very fine cross-fibre structure, perhaps a clay mineral. A spotted chiastolite slate from the west side of the intrusive, high in biotite, contains andalusite prisms up to 2 cm long, with thin sericite rims. Poikilitic laths of muscovite in the matrix are up to .5 mm long, and have a concentration of graphite on their borders. This muscovite is similar to that found in higher grade rocks in the Onawa aureole. Fine, well-formed white mica prisms occur in the matrix also.



## 2. Squaw Mountain

One lime silicate assemblage observed is: quartz-calcite-tremolite-diopside, about 1000 feet from the contact near Greenville. The distribution of pelitic assemblages is not so regular as at Onawa. A number of high grade hornfels bearing sillimanite (fibrolite and better-formed prisms), red-brown biotite, and potassic feldspar occur around the peak of Big Squaw Mountain, up to 1/4 mile from the contact. Northeast, along the contact, similar hornfels occurs immediately adjacent to chiastolite slate containing brown biotite, very fine muscovite, graphite and irregular platy opaque. Both specimens come from less than 500 feet from the contact. Espenshade suggests that the gabbro contact dips shallowly beneath Big Squaw Mountain, hence the apparent width of the aureole may be much greater than the actual width. Northeast of Greenville, spotted slate and cordierite-muscovite assemblages occur up to 1/2 mile from the gabbro contact. One slate contains ellipsoidal cordierite metacrysts, crowded with inclusions, up to 2 mm × 4 mm, in a matrix of biotite, muscovite and quartz, all less than 50 $\mu$ . No aluminosilicate is present.

Two specimens of hornfels from Burnt Jacket Mountain, collected by S. S. Philbrick, in the aureole of the same gabbro mass as at Squaw Mountain, are similar to the assemblages of the peaks of Boarstone and Big Squaw Mountains.

## V. MINERALOGICAL STUDIES BY X-RAY DIFFRACTION

The fine grain of the rocks of the aureole makes determination of the mineralogy difficult, and powder X-ray diffraction methods were required in a number of instances. For this work, a Norelco Wide Range Goniometer with a Geiger counter head was utilized. Mounts were made by dry-grinding the sample to a fine powder in an agate mortar, grinding for a short period in amyl acetate to produce a suspension, and transferring the suspension to a glass microscope slide by means of an eye dropper. By allowing the suspension to settle for a few seconds in the dropper, and discarding the first few drops, a uniformly fine "smear" was obtained on the slide, which dried with a smooth surface. Both iron and copper targets were used, with various scanning and chart speeds, as required. No internal standard was added: quartz provided a "built-in" standard in many cases.

### A. Mineralogy of the Slates

Diffraction patterns were made of slates 0-3, 0-4, 0-6, and 0-66 from outside the limit of andalusite, and 0-65, 0-70, 0-69, and 0-67 from the outermost part of the aureole. Mounts made as described above were scanned with  $\text{CuK}\alpha$  radiation, Ni-filtered, in the range  $5^\circ$ - $38^\circ$   $2\theta$  at  $1/4^\circ$  per minute, and recorded on a scale of  $2^\circ$  per inch. Scale factor, multiplier, and time constant settings were 2, 1.0, and 16 respectively. All patterns are very similar, and diffraction peaks characteristic of the following minerals were observed:

Chlorite (+kaolinite?)

muscovite-biotite

andalusite (0-67 only)

quartz

plagioclase (probably  $\text{NaAlSi}_3\text{O}_8$ )

The data clearly indicate that no other phases are present in sufficient amount to register on the diffraction trace. In an attempt to resolve the patterns of chlorite and kaolinite, should the two be present, two mounts, those of 0-3 and 0-66, were heated in an electric furnace. Heating to 400°C for one-half hour produced no significant change in the pattern. Heating to 500°C and 800°C produced essentially identical effects in each specimen. The patterns of 0-3 are presented in Figure 4 traced free-hand from the chart record. The pattern of the unheated mount is typical of all the Onawa slates. The indices assigned to the muscovite reflections are taken from Yoder and Eugster (1955); the pattern matches that of a synthetic or natural 2M muscovite, rather than that of a 1M or 3T polytype. The albite indices are taken from Smith (1956); not all of the albite pattern in the range 22.1°-24.3° 2θ is recorded in all specimens, but all the major reflections are present in positions not significantly different from those of the Amelia, Va. albite. For example, the value

$$\Delta 2\theta = 2\theta (\text{albite } \bar{2}01) - 2\theta (\text{quartz } 10\bar{1}0)$$

was measured off the records of 0-3, 0-65, and 0-70. The values are 1.15° to 1.20°, averaging  $1.18 \pm 0.1^\circ$ , which matches the value of 1.18° for the Amelia albite from the data of Smith (1956). Tuttle and Bowen (1958) have shown that the position of the  $\bar{2}01$  peak of high temperature alkali feldspars is very sensitive to composition, and that the data for 2θ vs. composition can be approximately applied to the low-temperature

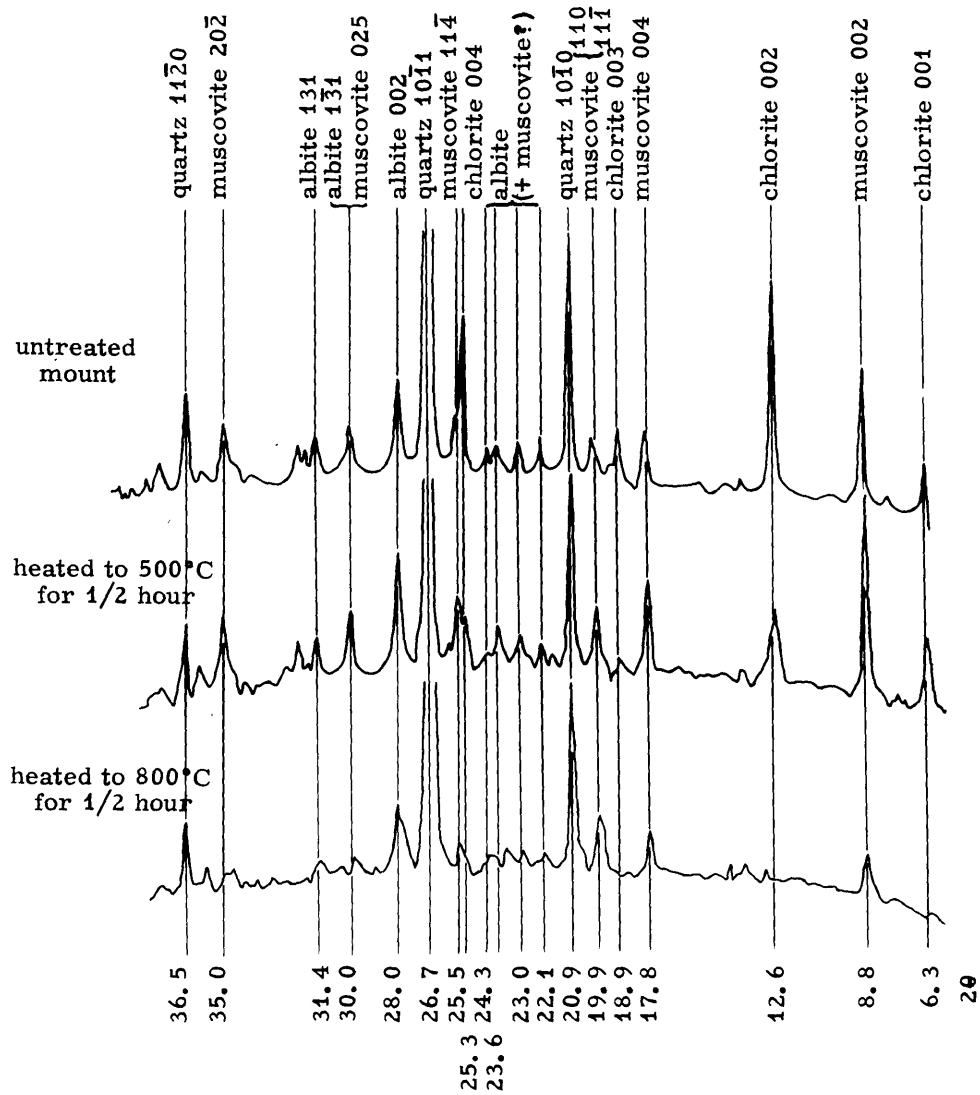


Fig. 4. X-ray Powder Diffraction Patterns of Slate 0-3, Big Wilson Cliffs, Illustrating Effects of Heat Treatment.

modifications. The  $\Delta 2\theta$  value for a pure high albite is 1.14 ; the slightly larger value obtained for the feldspar in the Onawa slates, which agrees closely with that of the Amelia feldspar, a potassium-free low albite, shows that the feldspar of the slates is also an essentially potassium-free low albite. The calcium content of this feldspar could not be measured by means of the powder data as the significant reflections are too weak or obscured by the patterns of the other phases. It is probable that the calcium content is very low in a plagioclase formed at a low grade of regional metamorphism, hence the term "albite" is tentatively applied. Zen (1960) determined by means of extinction angle, refractive index, and powder X-ray measurements, that the feldspar in slates and phyllites of Western Vermont is nearly pure  $\text{NaAlSi}_3\text{O}_8$ .

The chlorite peaks are indexed assuming a 14 Å c-axis dimension. No measurable variation in basal spacing was observed from one slate to another, the mean value of  $d_{001}$  being  $14.10 \pm .03$ , on the basis of  $2\theta$  (chlorite 004) measurements relative to quartz  $10\bar{1}1$ . Bradley (1953) observed a shift of the chlorite 002 peak toward a lower angle, and a shift of the 004 toward a higher angle, relative to kaolinite, upon heating to  $400^\circ\text{C}$  and higher. No significant shift is noted for these specimens, and no kaolinite peaks are resolved. The attenuation of chlorite 002 and higher-order basal reflections with respect to 001 upon heating is apparently a characteristic of chlorite and does not indicate that 002 and 004 are reinforced by a kaolinite pattern. A sample of chlorite separated from slate 0-69, pure except for minor biotite and muscovite, exhibited the same effect upon similar heat treatment. Chemical data

bearing on the possibility of a hydrous aluminosilicate in the slate are presented later in the thesis. The heating experiments verify, however, that:

1) The asymmetry of the chlorite 004 peak toward the high-angle side is due to reinforcement by the muscovite  $11\bar{4}$  reflection, which remains after the chlorite structure is destroyed.

2) The pattern ascribed to albite is not significantly affected by heating (lower intensities in the pattern after heating to 800°C can be ascribed to warping and flow of the glass slide mount). Probably the albite 002 peak at  $28^\circ 2\theta$  is reinforced by muscovite 114.

It is concluded on the basis of petrographic and X-ray data that the non-opaque mineral assemblage of the slates is:

quartz

chlorite

muscovite (+biotite in some specimens)

albite

## B. Mineralogy of the Hornfelses

Although most of the minerals of the hornfelses could be determined in thin section, X-ray diffraction patterns were made of representative samples, chiefly in order to determine the identity of the white micas and feldspars, and of the opaque minerals.

### 1. Non-opaque minerals

Mounts were made of non-magnetic fractions from the Frantz magnetic separator (see VI D. Preparation of Samples) of 0-75, 0-87, 0-43, 0-82, 0-56, and 0-40. The only characteristic peaks observed

were those of:

biotite-muscovite

andalusite

quartz

microcline ( $27.5^\circ 2\theta$ ) (not in 0-75 or 0-87)

plagioclase

The two feldspars, where observed, are believed to be intergrown in the perthite, since no discrete plagioclase was visible in any of the specimens X-rayed except 0-40. The petrographic identification of cordierite was verified by X-ray in 0-87 and in all specimens from which cordierite was separated and analyzed. A pink veinlet about 2 mm wide in specimen 0-55 was sampled and examined by X-ray and found to consist of quartz and andalusite, rather than garnet as had been suspected. This identification was subsequently verified petrographically. To ascertain the identity of the "fibrolite" observed in thin section, a typical milky-white, quartz-fibrolite veinlet was examined by X-ray and found to consist of quartz and simmilanite or mullite. The two aluminosilicates can be distinguished only by precise cell dimension measurements (Agrell and Smith, 1960). Attempts to record the high-angle pattern required to perform this measurement failed due to high dilution of the aluminosilicate by quartz. The term "sillimanite" is thus used tentatively, and is probably the more reasonable choice, since natural mullite has been positively identified only in metamorphic rocks formed under extremely high temperature-low pressure conditions.

## 2. Opaque minerals

Since no positive identification of opaque phases could be made in thin section, X-ray identification was required. Opaque concentrates of two sorts were utilized:

a) Mineral concentrates obtained in heavy liquid sink fractions in the course of biotite and chlorite separations, heavier than the pure ferromagnesian phases due to abundant opaque inclusions.

b) Nearly pure opaque concentrates obtained in the following way: A relatively coarse screen fraction of the ground sample (generally 100-140 mesh) was cleaned of tramp iron with an Alnico magnet covered with paper. Very few rock particles were picked up, and those removed were easily dislodged by tapping and returned to the sample. (This behaviour did not necessarily indicate the absence of magnetite, since the opaques are about one-tenth the particle size of the rock fragments, and would form only a minor portion of most grains.) About fifty grams of each sample, free of iron, was mechanically ground one-half hour in an agate mortar, and centrifuged in full-strength methylene iodide in a separatory funnel, at 1000 rpm for 5 minutes. Most samples produced a small sink fraction consisting almost entirely of opaque minerals, which was mounted in the usual way and its X-ray pattern recorded. These patterns were compared with the ASTM standard patterns, and with data obtained by the writer from known minerals, in order to identify the heavy minerals present. Heavy minerals to be expected in hornfelses can be differentiated by the following X-ray data, in the range  $30^{\circ}$ - $56^{\circ}$   $2\theta$  (FeK $\alpha$ ):



Mineral	°2θ of Characteristic peaks, Fe Kα radiation			
magnetite		38.1	45.0	55.2
ilmenite	30.1	41.4	44.8	51.5
hematite	30.5	42.2	45.4	
rutile			45.8	

These values are taken from ASTM data and were verified by running a number of known hematite, ilmenite, and magnetite samples. Additional peaks at 34.8°, 37.5° and 40.5° 2θ were observed in the pattern of an ilmenite sample from Roseland, Va. No internal standard was used, since other work on the same diffractometer shows that calibration errors do not exceed 0.2° 2θ, an amount insufficient to confuse the pertinent patterns. Unfiltered Fe Kα radiation was used. Samples were scanned at 1° per minute, recorded at 2° 2θ per inch. Scale factor-multiplier-time constant settings were 4-1.0-4. In addition to the diffractometer measurements, powder photographs were taken of two samples, 0-40 and 0-43, with a Phillips 114.6 mm Debye-Scherrer type camera, using Fe Kα radiation and a Mn filter. The observed 2θ and intensity values (relative to a maximum of 10, estimated by eye from the photographs) are reproduced in Table 2, for the concentrates consisting dominantly of opaque minerals.

The data in Table 2 clearly indicate that ilmenite, or a mineral with a virtually identical powder pattern, is the only detectable opaque phase present in all specimens examined except 0-75. These data are in accord with the observation of rude hexagonal outlines and "leucoxene" coatings in thin section, but conflict with the petrographic observation of a change in opaque habit between specimens 0-43 and 0-87, which

Table 2. X-ray Powder Data for Opaque Minerals.

ASTM Ilmenite		Ilmenite Roseland Va.		0-40 <sup>†</sup>		0-40		0-57		0-43 <sup>†</sup>		0-87		0-75		ASTM <sup>+</sup> Biotite	
2θ	I	2θ	I	2θ	I	2θ	I	2θ	I	2θ	I	2θ	I	2θ	I	2θ	I
						11.2	3							11.2	7	11.2	10
				27.2	1									26.5	2		
30.1	5	30.3	4	30.2	2	30.2	3			30.2	2	30.3	3	30.6	2		
				33.8	1	33.8	2			33.8	4	33.9	2	33.8	10	34.0	10
												34.1	1				
		34.8	2														
		37.5	3	37.4	1	37.4	2	37.4	2	37.4	1	37.5	2	37.4	6		
														38.0	6		
		40.5	1	40.6	1							40.6	1				
41.4	10	41.5	10	41.4	10	41.4	10	41.4	10	41.3	10	41.4	10	41.4	7		
										43.3	1			43.1	8		
44.8	8	45.0	5	44.9	7	45.0	5	45.0	5	45.0	7	45.0	4	45.0	3	44.5	10
				46.0	1												
														50.3	3		
51.5	7	51.6	2	51.4	4	51.5	3			51.2	2	51.5	3	51.5	1		
				56.3	1					56.2	1			56.0	10		
										57.4	1						
		61.5	1	61.2	1	61.2	1	61.2	1	60.9	1						
62.8	8	62.8	3			62.6	2	62.6	2	62.6	3						
				67.4	5												
68.5	10	68.7	4	68.3	8	68.4	4	68.4	4	68.2	7						
				71.6	1					71.6	1						
72.9	5			72.9	1					72.9	1						
				73.5	1												
80.4	8			80.0	7					80.0	4						
82.4	8			82.5	7					82.6	3						

<sup>†</sup> photograph

<sup>+</sup> principal reflections

— limits of observation

coincides with a change in the color of the biotite. A reaction is suggested involving titanium. No phases bearing significant titanium are present other than biotite and the opaque. Since the opaques in each specimen have identical X-ray patterns, the logical conclusion is that ilmenite is present in both. The only other possibility is that ilmenohematite is the lower grade phase, appearing in 0-87 and 0-75. Since hematite and ilmenite have the same structure, identical patterns could result if solid solution of Ti in hematite causes an expansion of the structure. The platy, ragged habit of the opaque of 0-87 is the same as the habit of the opaque in all slates and low-grade hornfelses observed, up to about the appearance of potassic feldspar, where the rounded type of 0-43 and higher-grade rocks appears. This platy opaque shows no transparency on thin edges, nor does the powder have a red color, but extensive solid solution of Ti may change these physical properties of titanium-free hematite. The analyses of chlorite Ch-65 and the total rock from which it was separated show that the iron of the opaque mineral is ferric rather than ferrous. In order to positively determine the identity of the opaque minerals, either chemical analyses or cell dimension vs. composition data are required.

The only major reflections which cannot be attributed to either ilmenite or biotite are the prominent peaks at  $38.0^\circ$ ,  $43.1^\circ$  and  $56.0^\circ 2\theta$  in the pattern of the 0-75 opaque. These features are identical with the three principal lines in the pattern of the ASTM pyrrhotite. The strongest line in the pyrrhotite pattern is that at  $56^\circ 2\theta$ , weak lines at this position suggest that pyrrhotite is a minor member of the

opaque assemblage in other specimens. This observation is in accord with the presence of a few opaque grains in most thin sections which have a yellowish cast in reflected light. The opaque concentrate of 0-75 generates  $H_2S$ , detectable by its odor, when treated with 6N HCl, verifying the presence of pyrrhotite.

In addition to the data presented for dominantly opaque concentrates, data was obtained from ferromagnesian concentrates of high opaque mineral content. One or more principal ilmenite peaks were observed in 0-32, 0-38, 0-45, 0-69, and 0-83. These data are less certain than that for the purer concentrates, since the patterns are more complicated.

Since the absence of magnetite, particularly in the higher-grade hornfelses, is surprising, further tests for this mineral were applied. Some of the hornfelses contain two sizes of opaque, the finer occurring mostly as inclusions in cordierite. It was suspected that this finer opaque might not be concentrated in the M. I. sink fraction. Samples of 0-40 and 0-57 were finely ground in a hand mortar and a magnetized needle passed through the powder. Most of the material adhering was identified as tramp iron in shiny flat flakes from the grinder; a small amount of very fine black powder adhered also. However, the opaque powder from 0-40 behaves similarly, and no magnetite was detected even in the powder photograph. Magnetite decomposes in concentrated HCl, rapidly coloring the solution yellow. No reaction was observed when a drop of acid was placed on uncovered thin sections of 0-61, 0-43, and 0-56, except a gradual, faint yellowing which was probably due to solution of iron from biotite and cordierite. No reaction was

observed in the vicinity of opaque grains, even after 1 1/2 hours in the case of 0-56, although the section was slightly etched.

On the basis of these investigations, the entire opaque assemblage is termed ilmenite ( $\pm$ pyrrhotite) in all the hornfelses.

### C. Structural State of Cordierite

Recently, Miyashiro (et al, 1955; 1957) and Iiyama (1958) have published the results of X-ray diffraction and optical studies of cordierite in which two polymorphs have been discovered: indialite, the high temperature form which is hexagonal, and cordierite, which is orthorhombic. On the basis of powder X-ray data, it is apparent that both have closely similar structures (cordierite was found by Gossner and Mussgnug (1928) to be a structural analogue of beryl). A difference in powder pattern is apparent in the vicinity of  $2\theta$  (Cu K ) =  $29^\circ$  where the  $12\bar{3}1$  peak of indialite is split in cordierite into 131, 421, and probably 511 (Miyashiro, 1957). Miyashiro has found a complete variation in the parameter:

$$\text{"Distortion Index" } \Delta = 2\theta_{131} - \frac{2\theta_{511} + 2\theta_{421}}{2}$$

from zero (indialite) to a maximum of  $0.29\text{--}0.31^\circ 2\theta$  in cordierite. Miyashiro proposes an order-disorder relationship between indialite and cordierite, relating to the manner in which Al substitutes for Si in the rings of Si(Al)-O tetrahedra which form the framework of the structure. If the substitution of one Al per five Si in the rings is random, then hexagonal symmetry results. If it is ordered, the unit cell is orthorhombic. Intermediate states, possibly metastable, are indicated by the range of  $\Delta$  values observed in natural cordierites. Since

it is of interest to know whether  $\Delta$  shows a systematic variation with temperature of formation, measurements were made on the available cordierite concentrates, using the same X-ray mounts made to determine purity of the samples (see VI. D, Preparation of Samples).

Unfiltered Cu  $K\alpha$  radiation was used. The mounts were scanned at  $1/4^\circ$  per minute, data recorded at  $1/2^\circ$   $2\theta$  per inch. Scale factor-multiplier-time constant settings were 4-1.0-8. The range  $28.75^\circ$ - $29.75^\circ$   $2\theta$  was scanned at least four times for each mount, and the  $\Delta$  values averaged. Data are presented in Table 3, in order of proximity to the intrusive contact, the nearest at the top:

Table 3.

Distortion Index of Cordierite from the Onawa Aureole

Specimen No.	$\Delta$ ( $^\circ 2\theta$ )		Average $\Delta$ ( $^\circ 2\theta$ )
	Mount 1	Mount 2	
0-40	.28	.26	.27 $\pm$ .02
0-38	.25	.28	.26
0-60	.26	.28	.27
0-56	.26	.25	.26
0-57	.27	.28	.28
0-82	.27	.26	.26
0-83	.26	.27	.26
0-45	.27	.28	.28
0-43			.25
0-32			.25
0-87			.22

The data of Table 3 show that there are no significant differences in structural state among all the cordierite in potassic feldspar-bearing

hornfels, but that those in rocks bearing primary muscovite have slightly lower  $\Delta$  values. This relationship is the opposite of that to be expected if the structural state is an equilibrium property, approaching hexagonal symmetry with increasing temperature. A possible interpretation of the data is that an Si: Al-ordered cordierite is the stable modification under the conditions of metamorphism, and that the  $\Delta$  value for an ordered cordierite in the composition range of the Onawa specimens is 0.26-0.28. The lower values then must represent metastable disorder in the lower-grade specimens.

Another consequence of the data is that the uniformity of  $\Delta$  in the potassic feldspar-bearing hornfels suggests that optical properties might show good correlation with composition. Optical and compositional data have shown that refractive indices and 2V are a function of Fe/Mg ratio (Leake, 1960), water content (Iiyama, 1958), alkali content (Folinsbee, 1941b), and structural state (Miyashiro, 1957). The last variable is easily determined by powder X-ray examination, hence if any two of the compositional variables remain constant, a unique solution exists for the third, providing that regression curves are available. Leake (1960) has summarized the present state of knowledge in this connection, and it is obvious that no precise determinations of any compositional variable could be made on the basis of the data currently available. However, it might be possible, in an occurrence such as Onawa, to detect compositional variations with detailed optical studies, provided that optics are not sensitive to small ( $\pm 0.02^\circ$ ) variations in  $\Delta$ . Such a study could show whether the cordierite of assemblages such as those sampled by the writer is truly homogeneous throughout a sample as predicted (see VI. Theory).

## VI. THEORY

### A. The Phase Rule

A thermodynamic model of a rock may be proposed on the basis of the theory of heterogeneous equilibria of Gibbs (1948), provided that the assumption of chemical equilibrium among the constituent minerals is valid. The accuracy of such a model is thus a test of, among other things, the assumption of equilibrium. Applications of thermodynamic considerations to metamorphic rocks are not common in the literature; probably the earliest of these is Goldschmidt's study of the Kristiania hornfelses (1911), in which he showed that the phase rule is obeyed by mineral assemblages in these pelitic and calcareous rocks. More recent treatments show that equilibrium is at least approached in a variety of metamorphic and metasomatic processes, e. g., Thompson (1955, 1957), Korzhinskii (1959), and Zen (1960).

Applying the terminology of Gibbs to metamorphic rocks, these may be described as assemblages of phases (minerals) constituting a system, the boundaries of which are arbitrarily defined. The state of the system is a function of intensive variables, such as temperature and pressure, and extensive variables, such as the masses of the phases. If sufficient parameters are known, then the state of the system is defined. A mathematical formulation of this statement is the phase rule, which has been expressed in a number of ways.

In a heterogeneous (multiphase) system, the exact differential of the Gibbs free energy can be written for each phase ( $\alpha, \beta \dots \phi$ ). This



is a suitable expression since pressure and temperature are the important physical variables in metamorphism:

$$\begin{aligned} dG_a &= V_a dp_a - S_a dT_a + [\mu_i dn_i + \mu_j dn_j + \dots + \mu_c dn_c]_a \\ &\vdots \\ dG_\phi &= V_\phi dp_\phi - S_\phi dT_\phi + [\mu_i dn_i + \mu_j dn_j + \dots + \mu_c dn_c]_\phi \end{aligned} \quad 1)$$

Where:

$G$  = Gibbs free energy

$T$  = temperature

$p$  = pressure

$V$  = volume

$S$  = entropy

$\mu_i$  = chemical potential of component  $i$  =  $\frac{\partial G}{\partial n_i}$   $p, T, n_j, \dots, n_c = \text{const.}$

components ( $i, j, \dots, c$ ) are the minimum number of independent chemical combinations (with or without physical significance) required to form the phases of the system.

$n_i$  = number of moles of component  $i$ .

This expression arises from the first and second laws of thermodynamics, and it is a consequence of the second law that  $G^0$ , the free energy of the system as a whole, is a minimum ( $dG^0 = 0$ ) at equilibrium, i. e., in a situation in which the state of the system does not change spontaneously with time. It follows that, at equilibrium:

$$\begin{aligned} T_a &= T_\beta = \dots = T_\phi \\ P_a &= P_\beta = \dots = P_\phi \\ \mu_{ia} &= \mu_{i\beta} = \dots = \mu_{i\phi} \\ &\vdots \\ \mu_{ca} &= \mu_{c\beta} = \dots = \mu_{c\phi} \end{aligned} \quad 2)$$

If the system is closed to all components, i. e., if no material can cross the boundaries, then all  $n$ 's are constant, since material cannot migrate between phases either, as a result of equations (2).

We thus have  $\phi$  equations:

$$\begin{array}{rcl} n_{ia} + n_{ja} + \dots + n_{ca} & \approx & \text{const.} \\ \vdots & & \vdots \\ n_{i\phi} + n_{j\phi} + \dots + n_{c\phi} & \approx & \text{const.} \end{array} \quad 3)$$

Or, expressing the quantities as mole fractions  $X_i \approx \frac{n_i}{\sum n_i}$  :

$$X_{ia} + X_{ja} + \dots + X_{ca} \approx 1 \quad \text{etc.}$$

Thus, in a closed system at equilibrium, there are  $\phi(c+2)$  independent intensive variables ( $p, T, \mu_1 \dots \mu_c$ ) related by  $[(c+2)(\phi-1) + \phi]$  independent equations (2) and 3)). The number of unspecified intensive parameters  $f$  (degrees of freedom) is thus:

$$f \approx \phi(c+2) - [(c+2)(\phi-1) + \phi]$$

$$\approx c + 2 - \phi$$

which is the familiar Gibbs Phase Rule.

Korzhinskii has introduced a modification to this formula by considering "perfectly mobile" components, to which the system is "open" (Korzhinskii, 1936a). Such components have chemical potentials defined by conditions external to the system, and are free to move in or out in response to changes, either inside or outside the system, of the determining parameters. An example of such a component would be water in a system separated from a reservoir of pure water by a rigid, perfectly insulating membrane permeable only

tò water. The chemical potential of water in the system would then be determined by the physical conditions of the reservoir, not the system. The components to which the system is closed are referred to as "inert."

The derivation of the Gibbs phase rule is not different for open than for closed systems, since the system is stationary at equilibrium and all restrictions apply equally to inert and mobile components (Korzhinskii, 1959, p. 11). However, it is convenient to make the following distinctions (after Korzhinskii, 1959):

$$c = c_i + c_m \quad \text{where } c_i \approx \text{no. of inert components}$$

$$c_m \approx \text{no. of mobile components}$$

$$f \approx f_{\text{ext}} + f_{\text{int}}$$

where:

$f$   $\approx$  the maximum number of independent intensive variables (degrees of freedom)

$f_{\text{ext}}$   $\approx$  the number of "external" degrees of freedom, i. e., the maximum number of independent external variables. The external variables are  $p$ ,  $T$  and the chemical potentials of mobile components ( $\mu_m$ ), which are those parameters determined by conditions external to the system

$$= c_m + 2$$

$f_{\text{int}}$   $\approx$  the number of internal degrees of freedom, i. e., the maximum number of independent intensive variables which exist at constant values of the external variables. Such variables are compositional (i. e.,  $X_{i\alpha}$  etc.)

Thus:

$$f_{\text{ext}} + f_{\text{int}} = (c_i + c_m) + 2 - \phi$$

$$f_{\text{int}} = c_i + (c_m + 2) - \phi - (c_m + 2) = c_i - \phi$$

Since:  $f_{\text{int}} \geq 0$ ,

$$\phi \leq c_i$$

This formula is equivalent to Goldschmidt's (1911) phase rule, and shows that the number of phases in the system is independent of the number of mobile components. When the number of phases is equal to the number of inert components,  $f_{\text{int}} = 0$ . Consider a system of three inert components and no mobile components. If three phases are present in equilibrium, the state of the system is determined at given T, p. However, if only two phases are present, then one independent internal intensive variable is possible, for example a variation in the mole fraction of a component in a phase, the other mole fractions varying dependently. In a closed system, such a variation is meaningful in comparing two or more systems of the same components, but with different bulk compositions, under identical external conditions. If three phases are present in each, then the compositions of the phases cannot change with bulk composition. However, if less than three phases are present, one or more independent compositional variables with bulk composition may exist.

If less than two degrees of freedom exist, more phases may coexist. For example, temperature may be dependent, so that  $f_{\text{ext}} = 1$ . In the three component system, four phases may then coexist along a line in p, T space (univariant equilibrium). At some unique value

of both  $T$  and  $p$ , five phases may coexist (invariant point). These relations are illustrated in the schematic pressure-temperature diagram of Figure 5. This represents a system of one inert component. Under divariant conditions, one phase only is stable; the maximum possible is three. The univariant line in this system corresponds to the "isograd" of metamorphic petrology (line of constant metamorphic grade in the field). In a volume of rock over which gradients of  $T$  and  $p$  are present, an infinity of surfaces exist relating these two variables. Depending upon the composition of the system and the values of  $p$  and  $T$ , some of these surfaces may correspond to univariant equilibria (in the absence of mobile components). For example, suppose that a volume of rock has the composition of the system in Figure 5, and assume that the section through the volume represented by the land surface is one of constant pressure  $p_1$ . The "geologic map" of Figure 6a is this section. The line  $T = T_1$  is an isograd, along which  $\alpha$  reacts to form  $\gamma$ ,  $\alpha$  and  $\gamma$  being stably coexistent along the line only. On the low temperature (low grade) side of the isograd, the rock consists only of  $\alpha$ ; on the high temperature side, it consists of  $\gamma$ . If the section were to represent  $p = p_2$ , then three phases:  $\alpha$ ,  $\beta$ , and  $\gamma$  would coexist along the line  $T = T_2$ . The probability of this occurrence in the field is very low. The configuration of isograds around an invariant point would generally be the same as that of the univariant lines in Figure 5, since the land surface does not represent exactly a constant  $p$  section. A map in which gradients of both  $p$  and  $T$  exist is shown in Figure 6b.

Of course, these maps are simplifications of the geologic situation. In actual rocks, complications occur since these systems are multi-

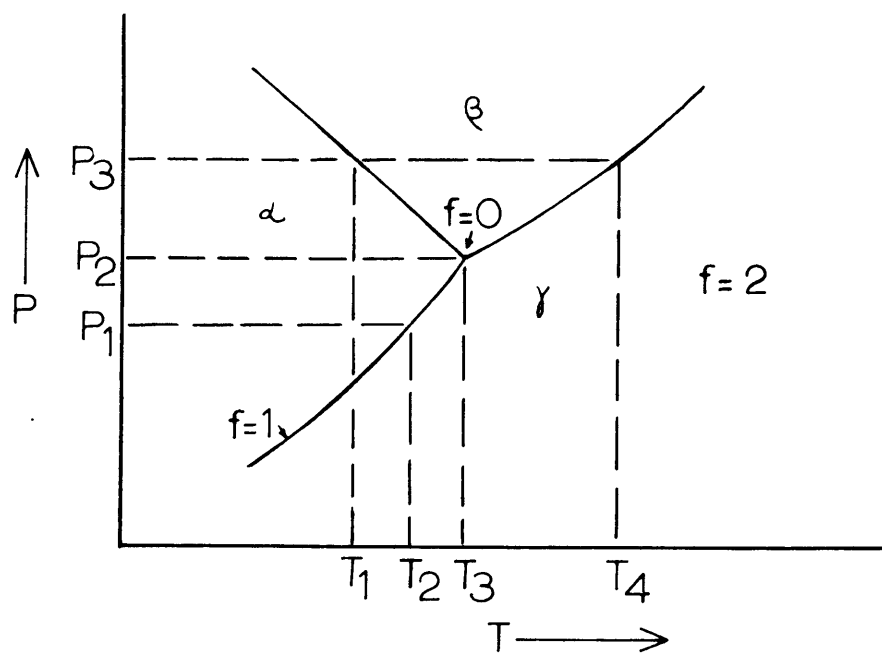


Figure 5. Hypothetical one-component pressure-temperature diagram.

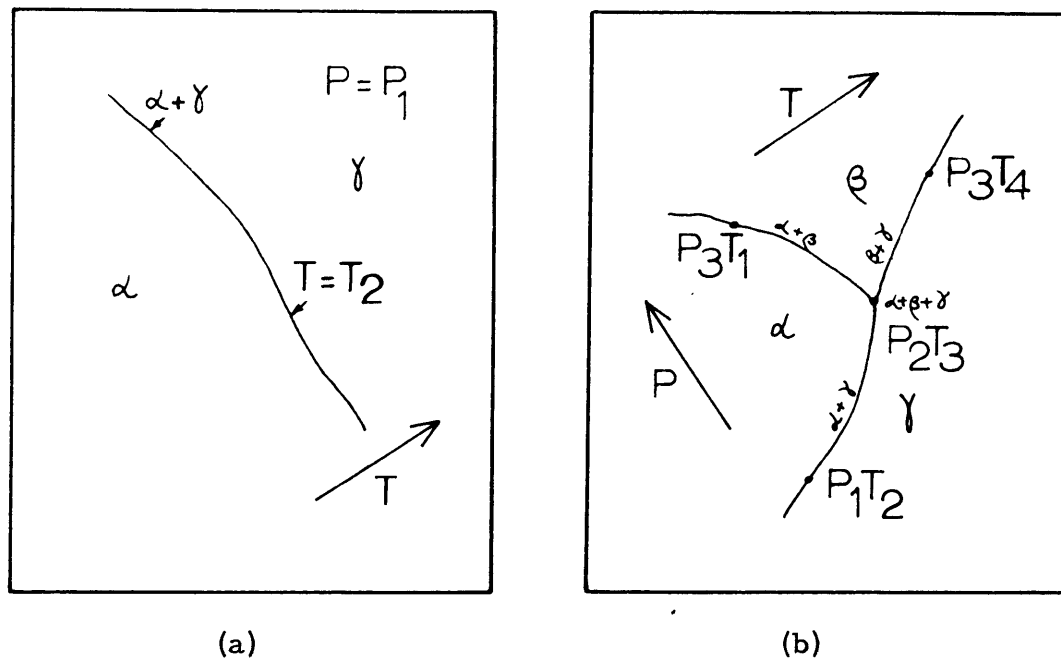


Figure 6. Isograd maps based on hypothetical one-component system.

component, may include mobile components, and usually contain solid solution phases. If  $f_{\text{int}} = 0$ , the position of the isograd is independent of bulk composition, and is a true indicator of a change in external conditions. The presence of mobile components increases  $f$ ; the isograd is then represented by a surface in  $p, T, \mu_m$  space. As the topographic surface represents a section through this surface, the isograd is always a line no matter how many mobile components are present, provided that special relationships between topography and the external variables do not exist.

If  $f_{\text{int}} > 0$  or if solid solutions occur, reactions marking isograds may not be abrupt, but will take place over bands rather than lines on the topographic surface. This statement will be illustrated in dealing with reactions in the Onawa aureole in a section to follow.

Application of the thermodynamic model to metamorphic rocks requires that equilibrium be attained or at least closely approached in the coexistent phases. Weathering effects are proof that these assemblages are not in chemical equilibrium at the earth's surface. However, weathering is limited to the immediate surface, and the persistence of assemblages other than the weathering products shows that metastable relicts survive, often essentially unchanged, from previous processes at different external conditions.

Phase rule considerations must be applied only to phase assemblages which are formed under a single set of external variables. The determination of the stable phase assemblage depends in general upon the interpretation of textural relations. If textural features indicate absence of reaction among the phases, compositional analysis

may be utilized to determine whether stable chemical equilibrium was once attained and preserved metastably after the process ceased.

## B. Graphical Representation

If mineral assemblages represent phases in equilibrium, they should be governed by the phase rule, and their occurrence should be regular, i. e., the least energy state for a given system of given bulk composition should always result in the same assemblage under a given set of external conditions. Such relationships are best illustrated by graphical representations of composition, such as that shown in Figure 7. This is a hypothetical system of three inert components, A, B, and C. The vertices of the triangle represent the extremes of composition; e. g., point A is 100% A, and any bulk composition is represented by a point in the triangle. If the general case of two degrees of freedom is represented, i. e., if the diagram is an isothermal, isobaric representation, the maximum number of phases possible is three; hence the diagram is composed of one, two, and three-phase areas. Several different types of compositional variation of the single phases are illustrated, limited by the structures of the phases.  $\alpha$  is a pure substance, exhibiting no compositional variation.  $\gamma$  and  $\delta$  are capable of only one independent variation,  $\beta$  and  $\epsilon$  of two. Tie lines, or "joins", connect the compositions of coexisting phases. The edges of these groups, or "bundles", of tie lines define triangular fields in which three phases are coexistent. The plot is a graphical analogue of the phase rule in that the corners of these fields are fixed at fixed external conditions, hence the compositions of the coexisting phases are independent of bulk composition



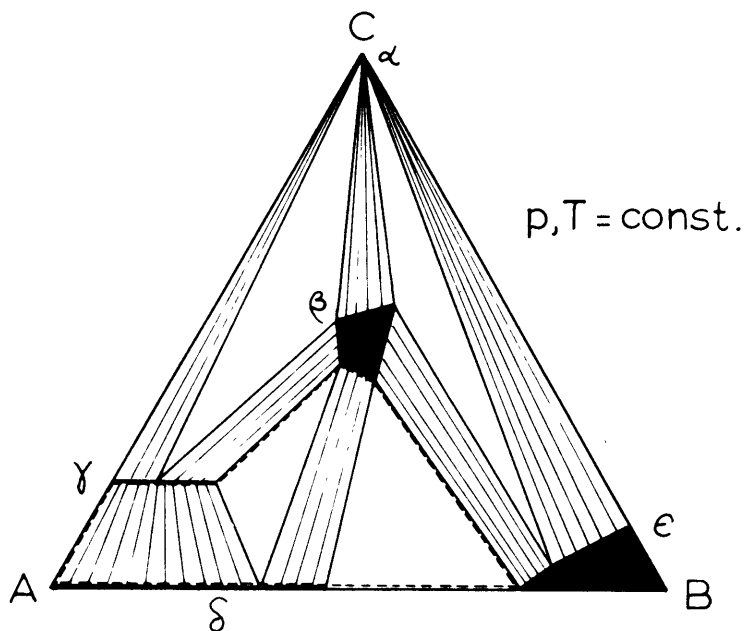


Figure 7. Hypothetical three-component composition diagram.

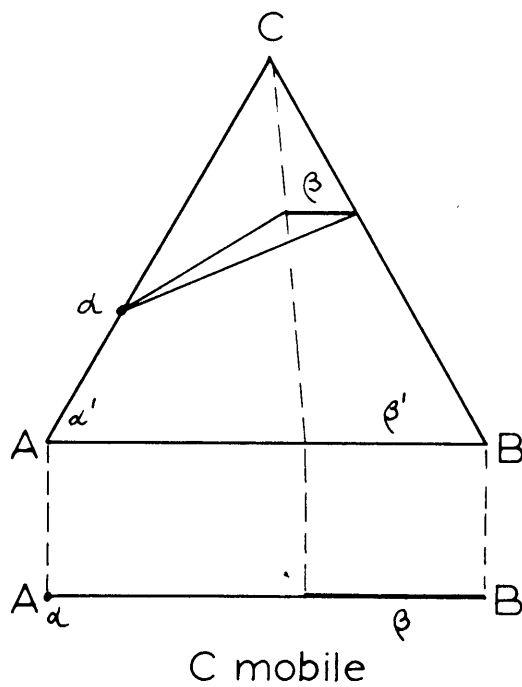


Figure 8. Projection through a mobile component.

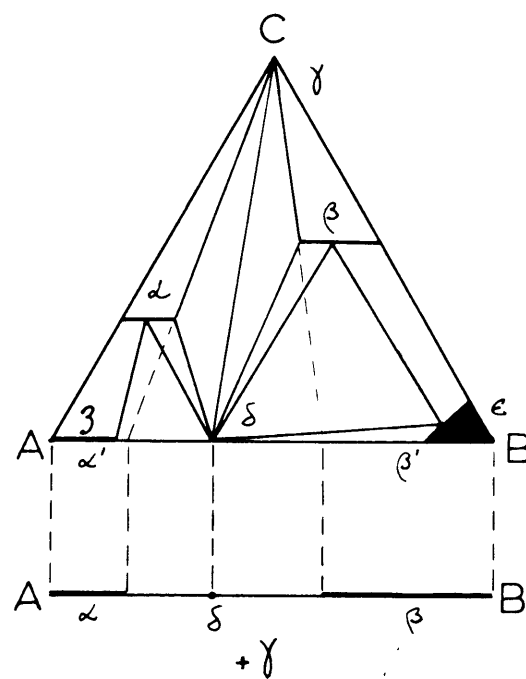


Figure 9. Projection through a pure substance.

variations, while the compositions of coexisting phases in a two-phase field or one-phase field vary with bulk composition. A bulk compositional change results in a change in the chemical potentials, which are continuous functions of the mole fractions. Since the compositions of the coexisting phases in a two-phase field are a reflection of the chemical potentials, tie lines must exhibit continuous variation with composition, i. e., must not intersect or meet at a point except in the limiting case of a pure substance, or at phase changes, where discontinuities in the mole fractions occur.

It can also be shown that, for a divariant system such as is represented by the three-phase fields of Figure 7, the mole fraction of any component in any phase is a continuous function of  $p$  and  $T$  also. Phinney (1959) has derived this relation for a two-phase, two-component system, the calculation being more complex for systems of more components. The following relations are obtained for two phases  $\alpha$  and  $\beta$  with components  $i$  and  $j$ :

$$dX_{j\alpha} = \frac{X_{j\beta}[(X_{j\beta} \Delta \bar{V}_j + X_{j\beta} \Delta \bar{V}_i) dp - (X_{j\beta} \Delta \bar{S}_j + X_{j\beta} \Delta \bar{S}_i) dT]}{(X_{i\alpha} - X_{i\beta}) \frac{\partial \mu_{i\alpha}}{\partial X_{i\alpha}}_{p, T}}$$

$$dX_{j\beta} = \frac{[X_{j\beta}(X_{j\alpha} \Delta \bar{V}_j + X_{i\alpha} \Delta \bar{V}_i) dp - (X_{j\alpha} \Delta \bar{S}_j + X_{i\alpha} \Delta \bar{S}_i) dT]}{(X_{i\alpha} - X_{i\beta}) \frac{\partial \mu_{i\beta}}{\partial X_{i\beta}}_{p, T}}$$

where symbols are as previously defined, plus:

$\Delta \bar{V}_j$  = The difference between the partial molar volume of component  $j$  in phase  $\alpha$  and the partial molar volume of component  $j$  in phase  $\beta$

$\Delta \bar{S}_j$  = The difference between the partial molar entropy of component  $j$  etc.

It is obvious that the sign of each expression must be the same, since the  $X$ 's are all positive, and the other terms are identical in each. Thus, the ends of a tie line must each move in the same direction in response to changing  $p$  and/or  $T$ . Thus no intersections will result if limiting tie lines from different locations are plotted on the same diagram, provided that the phase assemblage and components are the same. This relation was derived assuming inert components ( $\mu_{i\alpha} = f(p, T, n_{i\alpha}, n_{j\alpha})$ ), but is perfectly general at equilibrium, hence assemblages may be compared between which  $\mu_m$  varies also. The above relations, it should be stressed, apply only to limiting tie lines, i. e., divariant or less (at constant  $\mu_m$ ) assemblages in which the compositions of the phases are independent of bulk composition. It is apparent in Figure 7 that tie lines in two-phase (trivariant) fields must always contain the point representing the bulk composition, hence any changes in slope will result in intersection of the two tie lines representing successive states.

The arrangement of fields of coexisting phases determines their stability with respect to changes in bulk chemical composition of the system. For example, in Figure 7, at constant  $p, T$ , phase  $\delta$  is not stable at bulk compositions outside the dashed line. Such relationships of phase assemblage to bulk composition are the basis of the mineral facies principle first proposed by Eskola (1915); rocks formed at

equilibrium under the same conditions of  $T$  and  $p$  show similar changes of mineral assemblage with changes in bulk composition. The observation of such regularities in the mineral associations of metamorphic rocks is in itself good evidence for at least approximate attainment of equilibrium in natural occurrences.

Mobile components in the system do not appear in the composition plot, since they do not change the value of  $f_{int}$ . Phases containing the mobile components are plotted with respect to the inert components only. This device is equivalent to projecting through an apex representing the mobile component; for example, Figure 8 shows a hypothetical three component system in which two,  $A$  and  $B$ , are inert, while the third,  $C$ , is mobile. Since, under trivariant ( $(2+c_m)$  variant) conditions, only two phases can coexist stably, the system can be represented by projecting phases  $\alpha$  and  $\beta$  to  $\alpha'$  and  $\beta'$  on the line  $AB$ , specifying  $C$  as a mobile component. A completely analogous projective device can be employed if one of the phases of the assemblage is a pure substance, coexistent with all the other phases. Figure 9 illustrates this situation in a three-inert-component system. Since  $\gamma$ , with fixed composition  $C$ , coexists with all other phases, their compositions may be projected through  $C$  on to the base  $AB$ ,  $\gamma$  being specified as an additional member of the assemblage. This projection reduces by one the number of dimensions required to represent a system, hence can be useful in considering multicomponent systems. The projection point need not be an apex; projection through any point in the diagram may be utilized, provided that no inconsistencies arise. Different assemblages plotted in this manner all must contain the phase through which the other phases are projected.

Since the two graphical devices described above are topologically similar, an uncertainty in the role of a component may not always pose a problem. To cite a specific geologic case, the role of water in metamorphic rocks may be discussed. If the apex C in Figure 9 is  $H_2O$ , a projection through that composition may have one of two meanings:

- 1) Water is mobile, and only two phases may coexist in the system of two inert components A and B.
  - 2) Water is present as a discrete phase, coexistent with  $\alpha$  and  $\beta$ .
- In most cases, such an uncertainty can be resolved, since all phases should be observable. However, in the case of water, it may be present on grain boundaries where it escapes detection by ordinary methods. In either eventuality, the number of detectable phases will be the same. If, on the other hand, water is present as a component but not as a phase, one more solid phase is permitted than in either of the instances tabulated above.

Inert components may be subdivided into several types (after Korzhinskii, 1959, p. 71):

- 1) Determining inert components; those which determine the phase assemblage.
- 2) Excess components; those present in several phases of the assemblage, including a pure substance or a phase containing only the excess component and one or more mobile components, which is a member of all assemblages under consideration. Such a component may form a point of projection as described above.
- 3) Isomorphous components; those components which substitute for each other over such an interval of composition that they can be

combined into one component without violating the phase rule. For example, in Figure 7, if bulk compositions do not fall outside the two-phase field  $\alpha - \epsilon$ , the system can be represented in one dimension as  $A - (B, C)$  without violating the phase rule.

4) Accessory components; these occur in accessory phases (forming a small proportion of the system) in pure form or combined with the other components, and do not generally have significant solubility in the major phases. They do not affect the degrees of freedom of the system, since the addition of such a component results in the presence of an extra phase, leaving  $f$  unchanged.

5) Trace components; these are isomorphous with the major components, and are usually considered not to affect the state of the system appreciably. Such assumptions must always be tentative.

### C. Graphical Treatment of Pelitic Rocks

The above considerations may now be applied to the system under study. Pelitic or argillaceous sedimentary rocks (shales or mudstones) are those originally composed dominantly of quartz and clay minerals of very fine grain size, the products of weathering of terrestrial rocks. Solution of calcium in the weathering process and separate precipitation as limestones results in low calcium content; high aluminum content and potassium in excess of sodium are the dominant compositional features. The range of major element composition of pelites, based on analyses from Tilley (1926) and Guppy (1956) is:

$\text{SiO}_2$	54-63%	$\text{CaO}$	0.3-2%
$\text{Al}_2\text{O}_3$	16-25%	$\text{Na}_2\text{O}$	1-2%
$\text{Fe}_2\text{O}_3$	0.3-2.5%	$\text{K}_2\text{O}$	3-5%
$\text{FeO}$	4-9%	$\text{TiO}_2$	$\approx 1\%$
$\text{MgO}$	0.4-3%	$\text{H}_2\text{O}$	$\approx 4\%$
$\text{MnO}$	0.4-0.5%		

All other elements constitute trace or accessory components in almost all cases and need not be considered here. Since the elements listed as oxides above constitute too complex a system to be graphically treated as independent components, the following means of simplification are adopted:

- 1) In the majority of pelites,  $\text{CaO}$  and  $\text{MnO}$  are not quantitatively important, and may be tentatively eliminated from consideration.
- 2)  $\text{TiO}_2$  is principally an accessory component, and eliminating it from the system will not affect phase rule considerations.
- 3) Sodium substitutes principally in micas and feldspars; depending upon the mineral associations, it may or may not be important in graphical treatments. The system to be adopted will not include  $\text{Na}_2\text{O}$ ; the consequences of this simplification will be discussed later.
- 4) Since the metamorphic equivalents of shales have a much lower bulk  $\text{H}_2\text{O}$  content than the original sediments (for example, the potassic feldspar-bearing hornfelses described in IV. Petrography could not, from the mineral assemblage, contain in excess of about 1% water), it is apparent that large volumes of water must migrate through the rocks during metamorphism. This observation leads to the suggestion that water could be a mobile component. That the bulk

composition with respect to other major components does not change significantly during contact metamorphism is shown by studies such as that of Pitcher and Sinha (1959). The fact of water transfer in rocks does not alone justify consideration of  $H_2O$  as a perfectly mobile component in the sense of Korzhinskii; if diffusion rates are slower than the rate of attainment of equilibrium, then the chemical potential of this component will be determined by  $p$ ,  $T$  and the mole fractions. However, the general absence of coexisting phases in metamorphic rocks which differ only in water content (J. B. Thompson, Jr., lectures, 1959) supports the suggestion of mobility. The presence of a phase near pure  $H_2O$  is not ruled out, but graphical treatment as a mobile component is equivalent to consideration as a phase, as explained above. Hence,  $H_2O$  will not be included in the plot of the system.

5) Since almost all pelites are quartz-bearing, the device of projection through quartz (nearly pure  $SiO_2$ , as near a pure substance as any mineral) does not unduly restrict the application of the composition plot.

6)  $FeO$  and  $Fe_2O_3$  are equivalent to the two components  $Fe$  and  $O$ . If the system is closed to oxygen,  $Fe_2O_3$  must be treated as an independent component. If it is open to oxygen (or if  $O_2$  is present as a phase) it is valid to project through oxygen, which is graphically equivalent to expressing all iron as  $FeO$ . Another possibility is to ignore the content of ferric iron, in which case assemblages are strictly comparable only if each phase has the same ferrous/ferric ratio from one to the other.  $Fe_2O_3$  will not be included in the plot,



and the results of various treatments of iron will be apparent later.

The system is now reduced to five components:  $\text{SiO}_2$ ,  $\text{Al}_2\text{O}_3$ ,  $\text{FeO}$ ,  $\text{MgO}$  and  $\text{K}_2\text{O}$ ; all minerals commonly observed in low-calcium pelites and their metamorphic equivalents can be formed from these oxides as independent components, with the exception of essentially sodic phases (albite, paragonite), if essentially potassic minerals are considered to be the pure K end members. Assemblages of five phases are divariant at arbitrary T and p and constant  $\mu\text{H}_2\text{O}$ , thus at least five phases must be present in order for there to be no compositional variables at constant external conditions. Projection through quartz permits graphical representation as a tetrahedron, illustrated in Figure 10, with the possible compositions of minerals of the Onawa hornfels plotted. Since such a diagram is still awkward to employ in quantitative studies, further projection is desirable.

Two projections are utilized:

- 1) Muscovite is essentially a pure substance with respect to the components adopted, hence it can be used as a projection point. This device is that proposed by Thompson (1957) for muscovite-bearing pelitic schists, after making simplifications similar to those listed above.
- 2) For rocks without muscovite potassic feldspar is a suitable point of projection. Such projections are utilized by Korzhinskii (1936b) and more recently by Chinner (1959).

These two alternative projective transformations of the tetrahedron are pictured in Figure 11. In each case, phases on the  $\text{Al}_2\text{O}_3$ - $\text{K}_2\text{O}$  join plot either at the  $\text{Al}_2\text{O}_3$  apex or at infinity. Since the two phases

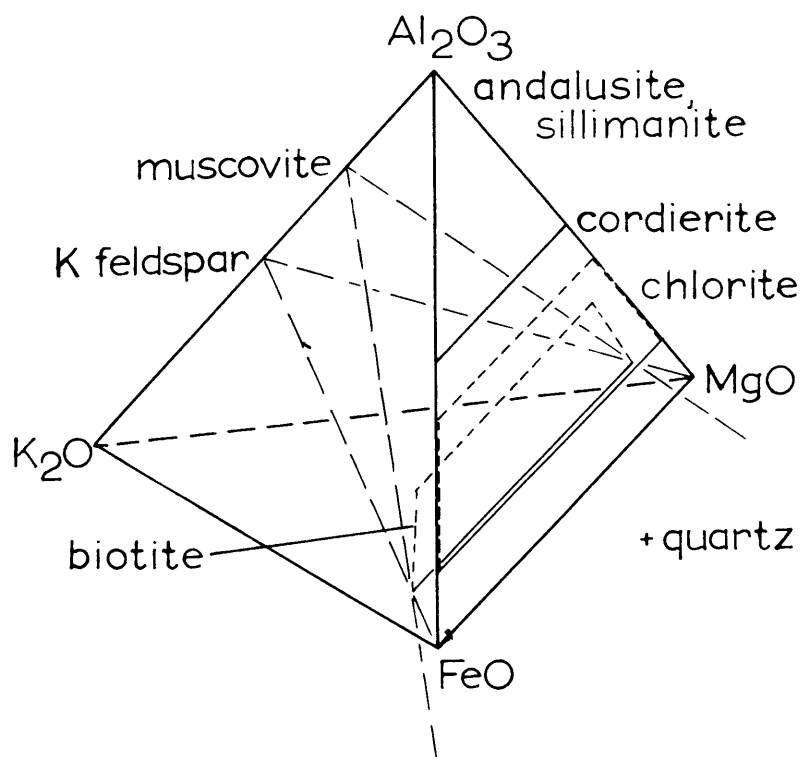


Figure 10. The  $\text{Al}_2\text{O}_3\text{-FeO-MgO-K}_2\text{O}$  tetrahedron.

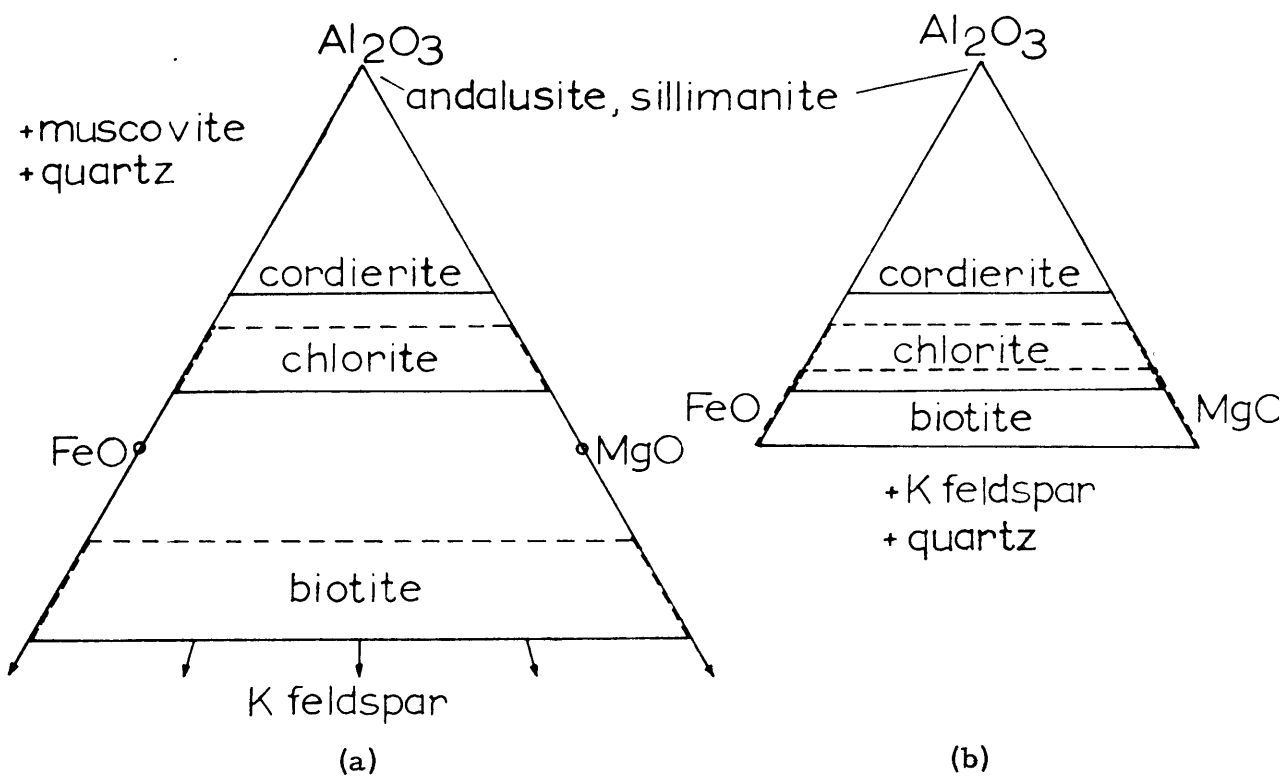


Figure 11. Projections of the A-F-M-K tetrahedron on to the plane  $\text{Al}_2\text{O}_3\text{-FeO-MgO}$ . (a) projection through muscovite  
(b) projection through K feldspar.

andalusite and sillimanite plot on the same composition point, they can be isolated as a one-component system, and only one of the two should be found in a divariant assemblage. Similarly, K feldspar-muscovite-aluminosilicate are colinear and thus define a two-component system, thus only two of the three are stable at  $f=2$ . The presence of sodium must be considered, however. If the amount of sodium does not exceed its solubility limit in muscovite and K feldspar under the external conditions, the paragenesis (phase assemblage) will not be altered; if it is present in excess, a sodic phase such as albite or paragonite will appear, leaving the degrees of freedom unchanged. In the former case, however,  $f_{int} = 3$ , and the point of projection can shift with bulk Na/K composition, possibly leading to inconsistencies in the comparison of different occurrences. In the projections illustrated, only one of muscovite and K feldspar can coexist with aluminosilicate in the general case, and the diagrams are labelled accordingly.

The projections may be used as true isothermal-isobaric phase diagrams provided that the mineral compositions plotted are those of an assemblage coexisting in equilibrium, formed at a given temperature and pressure. Further, limiting tie lines of three-phase fields (actually five-phase fields with two of the phases understood in the projection) from different occurrences may be compared on the same diagram and will shift with  $T$ ,  $p$ , and  $\mu_m$  without intersecting. An estimate of the extent of equilibrium may thus be obtained from inspection of such an array of tie lines. Given that approximate equilibrium exists, the dependence of the mineral assemblage upon bulk composition will also

be apparent, from the arrangement of stability fields in the diagram. These projections may be designated "A-F-M" diagrams, in contrast to "A-C-F" and "A-K-F" plots (Fyfe, Turner and Verhoogen, 199-239) which project FeO and MgO on to the same point, thus making quantitative treatment of coexisting ferromagnesian minerals impossible.

#### D. Distribution of a Minor Component between Two Phases

Another approach to the study of equilibrium among phases is the determination of the distribution of components in which the phases can be considered infinitely dilute. The theory applicable to dilute solutions has been well summarized and collected by McIntyre (1958). For an infinitely dilute component  $i$  distributed between two phases  $\alpha$  and  $\beta$ , in equilibrium:

$$\frac{X_{i\beta}}{X_{i\alpha}} = K_i^D \quad p, T$$

where the quantities are those already defined,  $K_i^D$  being the distribution coefficient of  $i$  between  $\alpha$  and  $\beta$ , constant at given  $p$  and  $T$ . The coefficient is not a function of the mole fractions of other dilute solutes ( $j \dots n$ ) so long as all of the mole fractions ( $X_1, X_j \dots X_n$ ) can be considered insignificant in the derivation. The values of  $X_1 \dots X_n$  at which this assumption no longer holds must be determined by experiment. For some solutions (ideal solutions) the relation holds over the entire concentration range. It is also independent of any other phases which may be present in the system. In order to compare distribution coefficients from one system with those of another, the compositions of the solvents must be identical. The distribution

can thus be written in another way:

$$\frac{\frac{X_{i\beta}}{X_{c\beta}}}{\frac{X_{i\alpha}}{X_{c\alpha}}} = (D_i)_{p, T}$$

where  $X_c$  is the mole fraction of some "carrier", conveniently a major element for which  $i$  substitutes. The variation of the distribution coefficient with external conditions is simplest if the solute forms a substitutional solid solution with the solvent(s), i. e., is an isomorphous component. If the solute is a determining inert component, its distribution between phases is significant, but can be more profitably treated by the graphical methods already described. As an example of a useful treatment of an isomorphous component, the distribution of Mn between two ferromagnesian phases, A and B, could be studied. In order for  $D_{Mn}$  to be comparable from one pair to another, A and B must each be constant in Fe/Mg ratio. If this condition is satisfied  $D_{Mn}$  will show systematic variations with T and p. If the solution is non-ideal or cannot be assumed dilute, then  $D_{Mn}$  will show systematic variation with  $X_{Mn}$ .

#### E. External Variables in Contact Metamorphism

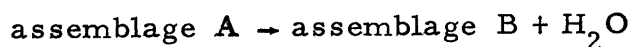
The relationship of mineral paragenesis to chemical composition and external variables and the range of composition to be expected in pelitic rocks have been discussed; it is now pertinent to consider the nature of the external variables in contact metamorphism. This process embodies only those mineralogical changes which have a distinct spatial relation to contacts of plutonic rocks; this relationship has resulted in the distinction of contact from regional meta-

morphism since the earliest studies. Other bases exist for the distinction; contact metamorphic rocks commonly are massive and fine grained ("hornfels"), in contrast to the medium-to-coarse foliated texture of regionally metamorphosed rocks. In rocks of similar bulk chemical composition there are contrasts in the mineral assemblages of the two environments; for example, andalusite and cordierite are characteristic of pelitic hornfels, whereas kyanite, garnet, and staurolite are more commonly observed in regional environments than in contact rocks. Such contrasts have led to the suggestion of contrasting physical environments, and recent experimental studies to be discussed in a later section support this theory. For the present, only contact metamorphism will be discussed.

Plutonic bodies surrounded by zones of contact metamorphism ("aureoles") commonly show features indicating crystallization from a dominantly molten "intrusive" mass, e. g., dikes, xenoliths, deformation of the walls, abrupt irregular contacts, and textural and mineralogical features duplicated in laboratory studies of melts (Tuttle and Bowen, 1958). That these intrusive rocks do not largely melt their wallrocks is shown by the preservation of original features of the unmetamorphosed rocks, such as sedimentary structures and (at sufficient distance from the contact) original mineral assemblages, even when the bulk compositions of intrusive and intruded rocks are not greatly different. It is thus valid to propose a temperature gradient falling away from the contact to a regional level some distance away. The progressive changes in the mineral paragenesis as the contact is approached support the existence of some gradient; other external

variables must be considered. Since there is usually abundant evidence of deformation without fracture in the wallrocks of an intrusive, it is unlikely that they would support a pressure gradient for long; variations in pressure with depth as a result of irregularities in the contact and surface topography are not significant with respect to the pressures supposed for contact metamorphism, to be discussed later. Thus the aureole is a zone of essentially constant pressure. The other possible external variables are the chemical potentials of mobile components. The intrusive might well act as a source or sink for these components; for example, it is known that granitic melts can dissolve at least 10% by weight water, (Tuttle and Bowen, 1958, p. 57), most of which must be expelled upon crystallization. On the other hand, it is not necessary that the melt contain so much water, and a dry melt intruded into water-rich sediments would be a sink rather than a source of water. The chemical potential gradient resulting from each of these cases, a function of temperature and concentration, could thus be opposite in sign. The same considerations apply to oxygen. A gradient in the chemical potential of a mobile component is thus possible, but the sign cannot be predicted for the general case.

Most of the metamorphic reactions observed as an intrusive contact is approached are dehydration reactions, i. e., have the form:



If  $\text{H}_2\text{O}$  is mobile, an increase in its chemical potential tends to favour the left hand side of the reaction, commonly termed the "low grade"

side. There is a positive correlation of "grade" with temperature, since dehydration reactions have a large entropy change and are thus favoured by increasing temperature. A rising  $\mu_{\text{H}_2\text{O}}$  will tend to drive a dehydration reaction to the left, and thus level the "metamorphic gradient". Thus, given a system, pressure, contact temperature and thermal gradient, the highest metamorphic grade will be attained in the presence of a  $\mu_{\text{H}_2\text{O}}$  gradient in opposition to temperature. Since the  $\mu_m$  gradients depend upon diffusion rates, discontinuities will be present at significant permeability discontinuities, such as might be present at the contacts of differing sedimentary horizons. Similarly, thermal conductivity differences between differing units in the wallrock will introduce discontinuities into the temperature gradient. Such discontinuities are not necessarily significant with respect to the over-all gradient. The external variables of contact metamorphism may thus be summarized:

- 1) Essentially constant pressure.
- 2) Negative thermal gradient away from the intrusive.
- 3) Possible chemical potential gradients, positive or negative with respect to the contact.

The width and maximum metamorphic grade of the aureole is a function of these variables and of the contact temperature and  $\mu_m$  of the intrusive. The outer limit represents the distance from the intrusive at which these variables attain the regional values.

It is interesting to consider the closing stages of contact metamorphism in the case of the intrusion of low-grade pelites as at Onawa. Dehydration of the intruded rock by the formation of less hydrous



assemblages with increasing temperature liberates a great deal of water. Depending upon the direction of the chemical potential gradient, this is either "soaked up" by the intrusive or driven out of the aureole. Recrystallization of the slaty rocks to hornfels destroys much of their permeability. As the intrusive cools, removal of the temperature gradient renders the anhydrous assemblages unstable with respect to lower-grade parageneses, but rehydration reaction reactions can take place only as water is "available". The hornfelses are less liable to this "retrograde" alteration (which is retrograde in that it represents a reversal in grade, but is part of the contact metamorphic process) than those more permeable rocks, such as the less metamorphosed slates which retain fissility, and hornfelses which are highly fractured. If the water released in the prograde process migrates outward, it is more likely that retrograde hydration reactions in the outer, fissile part of the aureole will go to completion than if the water was absorbed by the magma upon intrusion. This suggestion is applied to the Onawa aureole in discussion to follow.

## VII. INTERPRETATION OF PETROGRAPHIC AND X-RAY DATA IN THE LIGHT OF THE PHASE RULE

Examination of the petrographic and X-ray data on the Onawa aureole in the light of the phase rule lead to a number of conclusions:

- 1) All phases present can be represented in the compositional system developed above, with the limitations discussed.
- 2) The textural relations of the very fine muscovite prisms occurring in the outer part of the aureole suggest equilibrium; this muscovite occurs with potassic feldspar only in a very limited way, along a rough line encircling the intrusive. Since this line is normal to all proposed gradients of external conditions, it is postulated as an isograd. Above this isograd, muscovite also occurs but with textural peculiarities. Muscovite:

- 1) forms ragged plates larger than most of the other minerals, invariably associated with biotite.
- 2) interfingers with, and encloses portions of biotite grains.
- 3) varies from 0-~10%, in reciprocal relation to biotite.
- 4) is perhaps associated with a concentration of opaque mineral in the vicinity of biotite.

This textural relationship suggests replacement of biotite, therefore muscovite is not believed to be a stable member of the assemblage.

- 3) Andalusite and sillimanite (or mullite) cannot both coexist with quartz under general conditions (andalusite and sillimanite cannot coexist with or without quartz, since they are of identical composition) provided that they consist only of  $\text{Al}_2\text{O}_3$  and  $\text{SiO}_2$ . Since these two

minerals coexist with quartz over much of the aureole, disequilibrium is suggested in the absence of proof that they depart significantly from the  $\text{Al}_2\text{O}_3\text{-SiO}_2$  join. The presence of fibrolite as a reaction product of other phases (e. g., forming at biotite-quartz junctions) indicates that it is the stable aluminosilicate where it appears. The preservation of these reaction textures is evidence that the Al-silicate is not truly in equilibrium with the other phases, but it is considered to be a member of the stable assemblage for lack of positive evidence to the contrary.

4) The association of chlorite with spots having the form of cordierite grains and often containing cordierite remnants is strong evidence that chlorite is replacing the cordierite, probably with the production of muscovite as a reaction product. If cordierite is completely replaced, the phase rule is not violated; if both chlorite and cordierite are present, there are too many phases in the assemblage to occur over a range of temperature at constant pressure. Chlorite-bearing "spot" assemblages are present only in fissile rocks, and are deduced to represent the retrograde alteration of cordierite at the close of metamorphism. A similar interpretation is attached to chlorite-muscovite replacements of andalusite, chlorite-"sericite" assemblages along the intrusive contact, and muscovite replacement of cordierite in several hornfelses, which may have a spatial association with massive "bull" quartz veins. An exception to this generalization are the few assemblages studied from the outer edge of the aureole in which chlorite and biotite coexist without any evidence of retrograde formation after cordierite. The texture of chlorite in these specimens

is mostly similar to that of chlorite in the slate, where there is also no evidence of chemical disequilibrium. Chlorite which replaces andalusite in the same specimens has a habit similar to that of the spots, and is deduced to be retrograde. The few faint spots in these specimens could be incipient cordierite, representing an isograd, but are not identifiable as such.

5) With the exception of the disequilibrium effects noted above, all phases show evidence of stable coexistence and do not exceed the number specified by the inert components. Uniformity of grain size of each phase and obliteration of detrital textures, indicating textural equilibrium, is largely attained by the K-feldspar isograd. Presence of textural disequilibrium in lower grade assemblages does not necessarily indicate chemical disequilibrium; the consistent simple paragenesis of the slates is a strong argument for equilibrium at a low grade of regional metamorphism, even though all contain angular quartz.

6) Assemblages containing stable muscovite also contain albite; the phases are thus controlled with respect to all compositional variations including  $K_2O-Na_2O$ . The microperthite of the assemblages above the K feldspar isograd represents an exsolution of albite from an originally homogeneous microcline, hence only one feldspar is a member of the equilibrium assemblage. The phases are thus not controlled with respect to variations in bulk  $Na_2O/K_2O$  ratio, and this ratio may be expected to vary in the total feldspar and biotite with bulk composition of the rock.

A summary of stable assemblages in the Onawa aureole, representing

the maximum number of phases deduced to be stable in the system at successive increasing grades of metamorphism, is:

- 1) quartz-chlorite-muscovite-albite-(Fe-Ti) oxide
- 2) quartz-andalusite-chlorite-biotite-muscovite-albite-(Fe, Ti) oxide
- 3) quartz-andalusite (sillimanite in some assemblages?)-cordierite-biotite-muscovite-albite-(Fe, Ti) oxide
- 4) quartz-(andalusite or sillimanite)-cordierite-biotite-muscovite-microcline-ilmenite (isograd)
- 5) quartz-(andalusite or sillimanite)-cordierite-biotite-microcline-ilmenite

Assemblages 2) and 3) are the maximum number of phases permitted in the system including  $\text{Na}_2\text{O}$  if water and oxygen are mobile components, and  $p$  and  $T$  are arbitrary. 5) contains a maximum in the system less  $\text{Na}_2\text{O}$ . 4) represents an isograd separating 3) and 5). The assemblage of the slate consistently contains two less phases than permitted at arbitrary  $T$  and  $p$ . Since it is unreasonable to suggest more mobile components,  $f_{\text{int}}$  must equal 2, hence the bulk composition must fall within a mineral stability field in which two independent compositional variables are possible. Of the phases present, only chlorite could possibly exhibit such variation, and evidence will be presented below to show that this is so.

## VIII. CHEMICAL ANALYSES

### A. Introduction

Information about phase relations in metamorphic mineral assemblages can be obtained in two ways:

- 1) By descriptive textural and mineralogical studies such as those already presented.
- 2) By studies of the compositional variations of coexisting minerals exhibiting solid solution of two or more elements.

The theoretical basis for these studies has been outlined, and the descriptive data tentatively interpreted on this basis. In this section, the results of a study of the chemical compositions of minerals in the Onawa hornfels are presented. Such a study permits:

- 1) Determination of the phase relations in a part of the system represented by pelitic rocks, under the physical conditions of contact metamorphism.
- 2) Evaluation of the extent to which equilibrium was attained in the contact metamorphic process.

Many physical properties of minerals are sensitive to compositional variations, e. g., optical properties, density, and unit cell parameters. However, for biotite, chlorite, and cordierite, the important solid solutions in the aureole, composition cannot at present be determined with sufficient precision on the basis of physical properties alone. Therefore it was necessary to separate the minerals of the assemblages one from another, and analyze them by chemical methods. For most petrologic purposes, a number of analyses are

generally required; hence the analytical methods used must be not overly time-consuming. For such studies, the "rapid" instrumental procedures of Shapiro and Brannock (1956) and others are highly suitable, since they provide adequate precision and require far less time per sample than conventional gravimetric methods.

#### B. Choice of Samples

Of the assemblages deduced to have been stable, on the basis of the considerations presented above, the following have been separated into constituent minerals and coexisting biotite-cordierite pairs analyzed (the O-numbers in parentheses refer to the sample number, and the mineral fractions are designated B- or C-):

quartz-(andalusite or sillimanite)-cordierite-biotite-muscovite-  
microcline-ilmenite (0-32, 0-43)

quartz-(andalusite or sillimanite)-cordierite-biotite-microcline-ilmenite  
(0-45, 0-56, 0-57, 0-82, 0-83, 0-38, 0-40, 0-60)

Two biotite-cordierite pairs from the first assemblage, and eight from the second have been analyzed. In addition, biotite from several other assemblages, in which separation difficulties prevented recovery of pairs of adequate purity, were analyzed. These are:

quartz-andalusite-cordierite-biotite-muscovite-albite-(Fe, Ti) oxide  
(0-87)

quartz-andalusite-chlorite (retrograde after cordierite)-biotite-  
muscovite-albite-(Fe, Ti) oxide (0-75)

Chlorite from:

quartz-chlorite-muscovite-albite-(Fe, Ti) oxide (0-65) and the whole rock 0-65 were also analyzed.

All these phases can be represented in the projections developed above, and all the biotite-cordierite pairs and biotites are from assemblages in which the ferromagnesian compositions are controlled with respect to bulk composition variables in the  $\text{Al}_2\text{O}_3\text{-FeO-MgO-K}_2\text{O}$  tetrahedron.

The samples were chosen in the field on the basis of the following requirements:

- 1) Correct phase assemblage, in which bulk composition variables do not affect the ferromagnesian compositions. Phases were identified by weathering features, e. g., rusty pits are the weathered sites of cordierite grains if the cordierite is inclusion-bearing; if the cordierite is free of inclusions the rusty stain is more evenly distributed.
- 2) Absence of alteration.
- 3) Homogeneity, with close association of all the constituent phases.

In general, the depth of weathering observed in hand specimen does not exceed one centimeter. By using an eight-pound sledge hammer and a cold chisel, it was possible to obtain fresh samples of two to five pounds. Thinly bedded occurrences were avoided, as were hornfelses in which the content of andalusite is so low that the metacrysts of this mineral are widely spaced and irregularly distributed. In short, the objective was to obtain in each sample a single mineral assemblage, in which, if the assumptions described above are correct, the chemical compositions of the coexisting ferromagnesians should be uniform throughout.

Sample locations were determined from features recorded on the U. S. G. S. topographic quadrangle maps, and tied in where necessary by



pace or pace-and-compass traverse between known points. The locations of all samples studied petrographically and chemically are recorded on the large-scale map in Figure 3, with location symbols denoting the maximum mineral assemblage of the pelitic beds.

### C. Preparation of Samples

Samples under consideration for chemical study were first sliced with a diamond saw and the plane surfaces examined to ascertain that the sample was homogeneous. If so, a representative slice was taken for thin sectioning. If petrographic examination proved that the sample was suitable for further work, it was processed as below. Inhomogeneous samples, and samples not satisfying the petrographic criteria for equilibrium, were rejected, with two exceptions. 0-40 was processed, even though the sillimanite shows preferential association with cordierite, and is of low abundance, because it was the only unaltered sample of hornfels available from the igneous contact. 0-60 was somewhat less homogeneous with respect to andalusite, and had a higher muscovite content than desired, but was the most suitable sample in the general geographic location. All other samples processed contained andalusite separated by no more than 2 mm (where present in the assemblage) and muscovite not in excess of 10% of the total mica (in samples from above the potassic feldspar isograd).

Any weathered exterior was removed with a small hammer and the sample broken into small pieces on an iron plate. It was then fed through a jaw crusher, the second pass producing a product about one-quarter inch in size. This was repeatedly passed through a disc pulverizer, the product being screened between passes with an automatic

sieve shaker. In general, all material greater than 200 mesh was reground until sufficient quantity of 200-325 mesh was obtained. 200-270 and 270-325 mesh sizes were sieved until free of fines, since liberation was not achieved in coarser fractions. These size fractions were kept separated throughout the following procedure. Where sufficient mineral concentrate could be obtained from the 270-325 fraction, this alone was used; when, as in the case of cordierite, more was required than could be obtained from the finest size, both fractions were concentrated and combined after separation.

The accompanying flow chart (Figure 12) illustrates the sequence of operations. Rough separating of biotite and cordierite was performed on a Fratz isodunamic magnetic separator with standard feed; fine separations were made with an identical instrument using an asymmetric vibrator feed (Faul and Davis, 1959). Settings of field strength, feed rate and inclination were determined by trial and error. The fraction with the concentration of the desired mineral was recycled several times; after one or two passes all tramp iron was removed. Magnetic separation did not remove all impurities, such as biotite grains with opaque inclusions and quartz with cordierite; hence, heavy liquids were required. Also, the fine grain size made the use of a centrifuge necessary in order to achieve clean separations. Fractions were centrifuged in 150 ml. separatory funnels at approximately 1000 rpm for five minutes. Biotite separation was accomplished in methylene iodide, diluted by trial and error, first so that the biotite barely floated, then so that it barely sank. Cordierite was just floated in dilute bromoform. Quartz and feldspar were largely removed in the Frantz separator, both before and after heavy liquid separations.

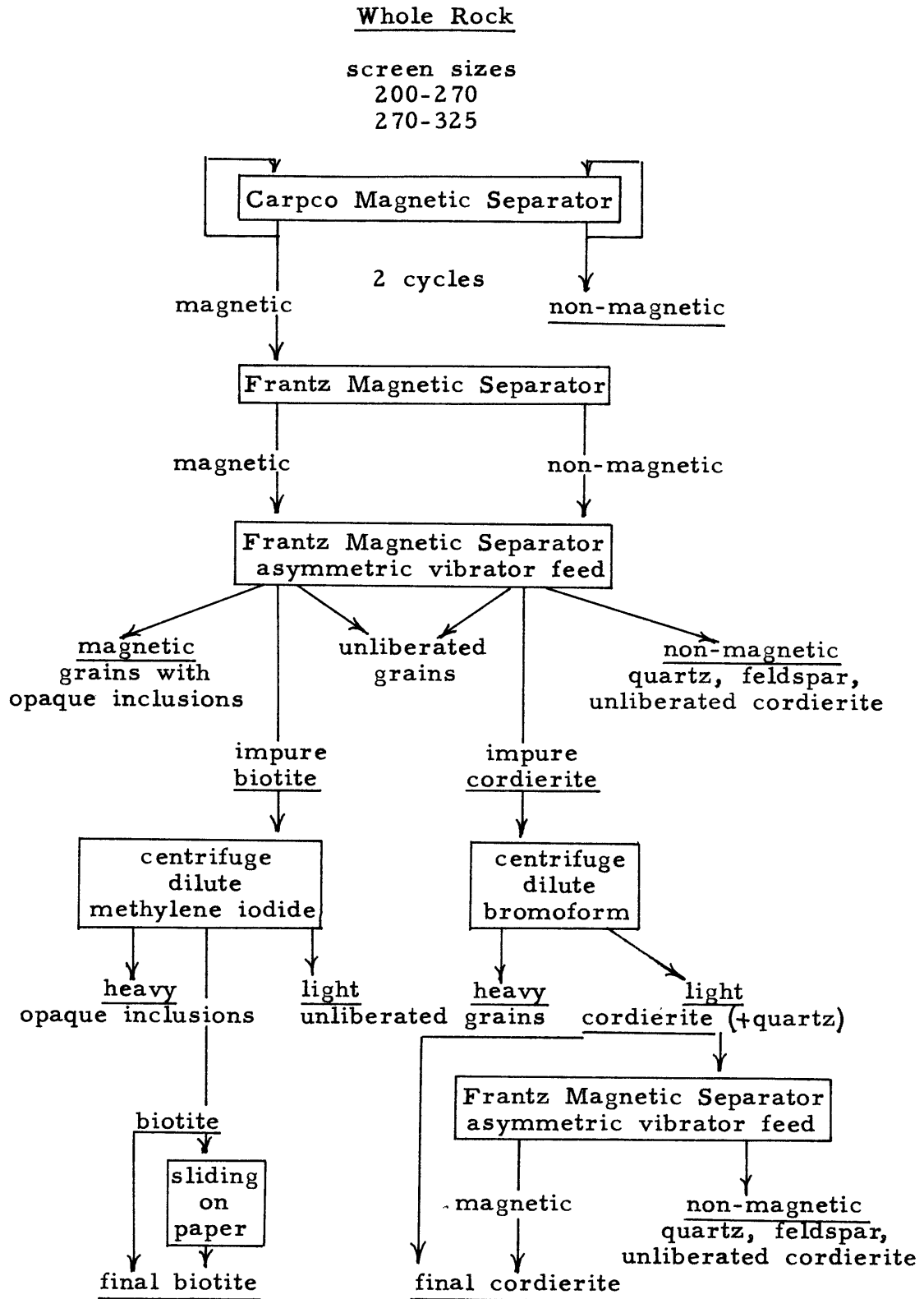


Figure 12. Mineral Separation Flow Chart.

Some biotite samples were finally purified by sliding them back and forth between sheets of paper, the fraction retained on the paper each time being the final concentrate.

Several specimens required variations of this procedure. Cordierites C-32, C-43 and C-45 were concentrated roughly on the Frantz separator, then ground in an automatic agate mortar. The fines were removed by the following method:

- 1) The powder was stirred in acetone and allowed to settle for a few seconds.
- 2) The fines were decanted.
- 3) The procedure was repeated until all fines were removed.

The remainder was purified with the Frantz separator and then ground to a powder before heavy liquid treatment. The sink-float separation was repeated several times and the final float taken for analysis.

C-38 and C-40 were also ground to a powder before final heavy liquid separation.

Sample 0-87 was hand-picked after the first crushing and only those pieces containing andalusite were processed further. The rejected material consisted of quartzite and pelite without aluminosilicate.

Chlorite Ch-65 was separated in the same manner as the biotite.

Slate 0-65 was a small piece of the same part of the hand specimen from which the thin section was made, weighing about 15 g. While such a sample carries no guarantee of being representative of the Onawa slates in general, it should approximate the composition of the larger sample from which it was taken, since the rock was megascopically uniform throughout. The chip was unweathered; it was broken with a

tungsten carbide mortar and pestle and ground in an agate mortar until all passed a 200 mesh screen. The powder was thoroughly mixed in the glass vial in which it was stored before analysis.

All mineral concentrates were thoroughly washed with acetone after heavy liquid treatment, and stored in small glass vials. 1.5-5g. of each mineral were obtained in the final concentrate from 2-5 pounds of total rock.

#### D. Purity of Samples

Purity of all analyzed mineral samples was checked in oil mounts under the petrographic microscope: 1000 points were counted for all biotites, chlorite Ch-65, and cordierites C-32, C-43, and C-45 on a stage movable in increments, only points occupied by mineral grains being counted. 500 points were counted for cordierites C-56, -57, -82, -83 and C-60. Impurity in C-38 and C-40 was estimated by comparison with the other sample mounts. By point counting, all impurities in biotite could be estimated. These were inclusions of ilmenite, quartz and zircon, and discrete grains of the other members of the assemblage, usually with ilmenite inclusions. In cordierite, only biotite and ilmenite could be counted; light minerals could not be differentiated without undue consumption of time. Inclusions were weighted  $1/2$  to  $1/4$  on the basis of approximate estimates of mean grain thickness and inclusion diameter. Impurity contents estimated in this way range from 0.3-3.1% by volume, exceeding 1.2% in only two samples, B-87 and B-75.

Cordierite purity was more difficult to ascertain, since quartz and feldspar cannot be distinguished from cordierite in crushed grains. Staining with potassium ferricyanide was attempted; the blue ferrous

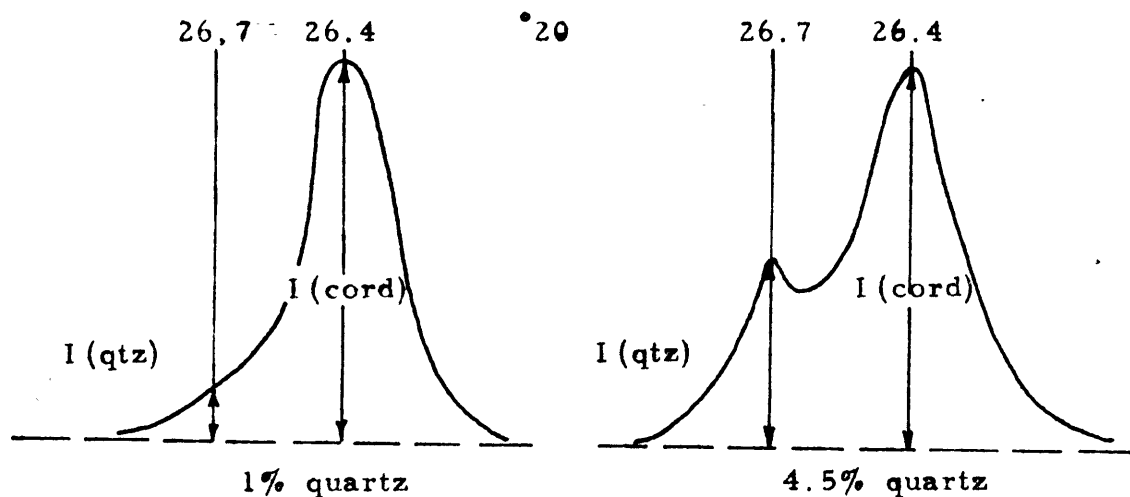
ferricyanide is formed by reaction with iron-bearing minerals. The following procedure gave the best results of all variations attempted: A small amount of sample was spread over the bottom of a small waxed paper cup and the surface decomposed for five minutes in HF fumes by the method of Chayes (1952). The sample was then removed and covered with a 0.25% aqueous solution of  $K_3Fe^{III}(CN)_6$  for five minutes, after which it was washed by gently flushing with water. This procedure permitted only a semi-quantitative estimate due to uneven staining of cordierite, peeling of stained surfaces, and partial staining of quartz. Standard mixtures of quartz and cordierite obtained by hand-picking a cordierite-biotite-garnet gneiss from New Hampshire were used as control.

A better method of determining cordierite purity involved the X-ray diffractometer. Preliminary traces of cordierite concentrates showed that the dominant impurity was quartz. Standards were prepared by mixing cordierite, separated with the Frantz separator from the above gneiss, with 0-4.5% by weight quartz. The mixtures were thoroughly ground together by hand in an agate mortar and duplicate mounts made by the procedure described in Section V. These were scanned with  $CuK\alpha$  radiation, Ni filtered, at  $\frac{1}{4}^\circ$   $2\theta$  per minute, and recorded at  $\frac{1}{2}^\circ$  per inch, scale factor 8, multiplier 1.0, time constant 8. The cordierite peak at  $26.4^\circ$   $2\theta$  and the quartz peak at  $26.7^\circ$  were recorded. At least four records were made of each duplicate, the mount being shifted in the holder between each. Some repeat runs were made on different occasions. For a given mount,  $2\theta$  values were measured at approximately half peak height, and intensity of each peak with respect to background was measured at the mean  $2\theta$  value for the peak.

Mean values of  $I(\text{qtz})$  and  $I(\text{cord})/I(\text{qtz})$  were plotted against % quartz. While the ratio defines a curve,  $I(\text{qtz})$  varies linearly with quartz content (Figure 13). Since the  $26.4^\circ 2\theta$  peak of cordierite shows marked variations in shape and intensity from specimen to specimen,  $I(\text{qtz})$  was used as an indication of the quartz content of cordierite concentrates. The line relating  $I(\text{qtz})$  and % quartz does not pass through zero; this is not due to quartz impurity in the cordierite, since Frantz-pure and hand picked cordierite give identical results. Rather, it is due to enhancement of the quartz peak by the tail of the cordierite peak. For 0% and 1% mixtures, no quartz peak was visible; peak position was determined from traces of the other standards.

Cordierite mineral fractions were mounted and scanned in exactly the same way as the standards, except that three readings of each duplicate mount were made. Standard errors  $\left( s_{\bar{x}} = \sqrt{\frac{\sum d^2}{n(n-1)}} \right)$  of the mean standard intensity values provide a measure of the precision and accuracy of the quartz estimates. Since similar standard errors are attached to both standard and sample means (e. g., C-57, with  $I(\text{qtz}) = 4.9$ , has  $S_{\bar{x}} = 0.44$ ), the error  $2S_{\bar{x}}$  is attached to the determination of quartz content. Since the line has the slope % quartz/unit  $I(\text{qtz}) \approx 0.5$ , the limits of error of the quartz determination should not exceed  $\pm 0.5\%$  quartz, since the quartz impurity determined is not greater than 3%. In this calculation, weighing error in preparing the standards is considered negligible in comparison to the other errors.

The quartz content of the cordierites is the lowest that could be attained without reducing the weight of sample below that required for analysis. Since abundant fine quartz inclusions were present in C-32



quartz in cordierite wt. %	I (qtz) chart units			$s_{\bar{x}}$ (% quartz)
	$\bar{x}$	$s_{\bar{x}}$	$2s_{\bar{x}}$	
0	2.3	.20	.40	.2
1.0	4.3	.29	.58	.3
2.9	8.0	.42	.84	.4
4.5	11.0	.74	1.5	.8

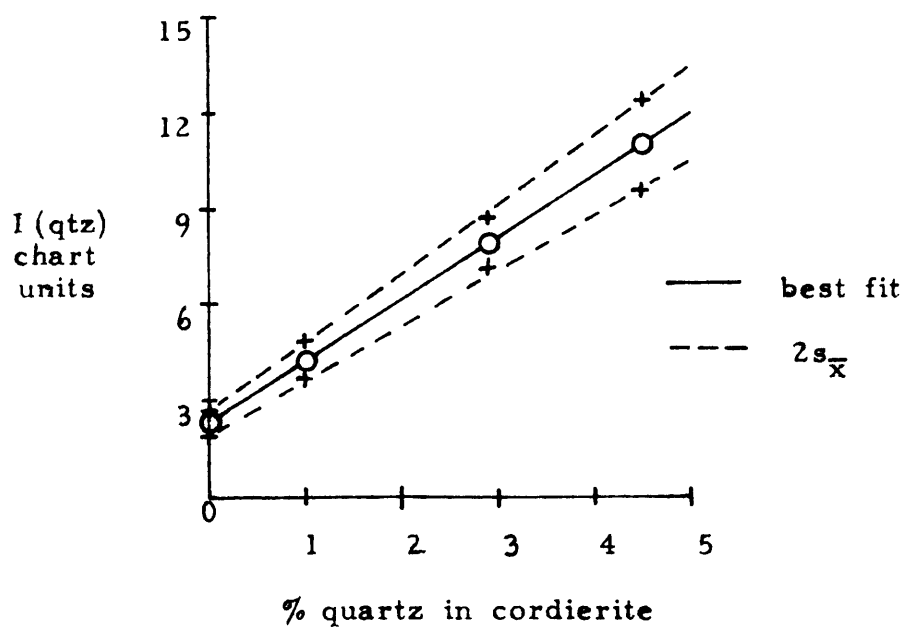


Figure 13. X-Ray Powder Diffraction Intensity Data for the Determination of Quartz Impurity in Cordierite.



and C-43, the quartz content of these samples could not be reduced below about 20%; these were only partially analyzed.

A barely detectable diffraction peak at  $27.5^\circ 2\theta$  indicated the presence of potassic feldspar in C-56 and C-38.

Ch-65 was thought to be quite pure on the basis of microscopic examination; however, alkalis in excess of 1% in the analysis (see Analytical Data) are not consistent with the structure of chlorite and suggested considerable muscovite contamination. Subsequent examination revealed white mica intergrown with the chlorite along the basal cleavage, not obvious in mounts in which the platy grains lie flat. A muscovite peak of about 3 chart units was observed at  $8.8^\circ 2\theta$  in a diffractogram of the analyzed chlorite. A mixture of 5% by weight muscovite with pure chlorite, checked with a "blank" run gave a muscovite about  $1\frac{1}{2}$  chart units, indicating that up to 10% muscovite is present in the analyzed chlorite.

Impurity estimates for which the analyses are corrected, along with total impurity, are tabulated with the analyses of Table 5.

#### E. Analytical Methods

The methods of chemical analysis used in this study are essentially those described by Shapiro and Brannock (1956), as currently practised at M. I. T.  $\text{SiO}_2$  and  $\text{Al}_2\text{O}_3$  are determined colorimetrically in a solution made by fusing 50 mg of sample with NaOH in a nickel crucible, and diluting to 1 litre with water and a little HCl.  $\text{SiO}_2$  is determined as the molybdenum blue complex,  $\text{Al}_2\text{O}_3$  as the orange complex with calcium and Alizarine red-S. Corrections for iron and titanium in solution are applied to the aluminum determination. National Bureau

of Standards soda-feldspar no. 99 is used as standard. FeO is determined by the classical dichromate titration, the sample being digested in boiling HF and  $H_2SO_4$  in a closed platinum crucible. The dichromate solution was standardized against iron wire reduced with stannous chloride, by a procedure similar to that described in Pierce and Haensch (1958). The iron equivalent of the solution was determined to be 2.030 mg. FeO/ml. (about 30° C.) for a solution of 2.7352 g. N. B. S.  $K_2Cr_2O_7$ /2 litres (20° C.). This value is higher than that given by Shapiro and Brannock (1956, p. 45) normalized to the same concentration of dichromate, hence it is suggested that the analyst should standardize his own dichromate solution to compensate individual variations in technique.

All other major elements are determined in a solution made by digesting 0.5 g of sample in HF and  $H_2SO_4$  in a platinum dish on the steam bath, and diluting to 250 ml with water. Total iron is determined colorimetrically as the orange ferrous o-phenanthroline complex;  $TiO_2$  as the yellow Tiron complex after elimination of the dark blue ferric Tiron complex by reduction with sodium dithionite.  $P_2O_5$  is determined as the yellow molybdivanadophosphoric acid complex; MnO is oxidized to permanganate with potassium periodate. CaO and (CaO + MgO) as MgO are determined by titration with Versene, photometrically recorded. Iron and aluminum are complexed with sodium cyanide and triethanolamine and do not interfere. (MgO + CaO) as MgO also includes MnO, so that the result must be corrected accordingly. Standards are ferrous ammonium sulphate for total iron, N. B. S. titanium dioxide no. 154 for  $TiO_2$ , N. B. S. phosphate rock no. 120

for  $P_2O_5$ , N. B. S. manganese ore no. 25b for MnO, N. B. S. dolomite no. 88 for CaO-MgO.

$K_2O$  and  $Na_2O$  are determined with the flame photometer with lithium as internal standard. Standards are alkali chloride solutions run concurrently with the samples. The writer plotted a standard curve to determine the slope only, and read standards close to the samples in concentration alternately with the samples. The standard reading, together with the slope, was used to determine the concentration of the sample.  $H_2O$  was not determined in this study, since insufficient sample was available in most cases to use the modified Penfield method, and since this method is proved to be highly inaccurate for hydroxyl water in silicate minerals (Groves, 1951). MgO and  $Fe_2O_3$  are calculated by difference; all other analytical results are independent except for the corrections required due to interference.

Sample solutions were prepared in duplicate from two fractions of the sample weighed to the nearest .0001 g after drying at 105-115° C. for 2-12 hours. In the case of C-32, C-43, and Ch-65, only one solution for the determination of total Fe, etc. was prepared due to shortage of sample. Temperature corrections were applied to all dilutions to volume, and solutions stored in polyethylene bottles. All pipets, the spectrophotometer cell, and the flame photometer feed funnel were coated with a silicone (Beckman "Desicote") to eliminate the necessity of rinsing between sample solutions. In preparing solutions of the complexes, the same pipet was used for both standards and samples, eliminating the necessity of calibration, and a blank reference was

prepared. Duplicate aliquots were taken from each sample solution to prepare solutions for element determinations except in the case of MnO and TiO<sub>2</sub>, where precision has proved to be sufficiently high that fewer replicate determinations are required (Phinney, 1959). Since P<sub>2</sub>O<sub>5</sub> analyses were performed only as a check on phosphate content, only one aliquot of the sample solution was taken for this procedure. Two to four spectrophotometer readings were made on each solution. FeO was determined by duplicate titrations of the sample; photometric titrations of CaO-MgO were performed on duplicate aliquots of each sample solution.

Where precision was judged to be inadequate (a discrepancy between duplicate determinations of 2% of the mean value was the maximum precision error permitted for all major constituents) sample solutions were rerun, and in one case (C-83) a new sample solution was prepared when a consistent error was obtained. Analytical results are thus mean values of at least the number of replicate determinations shown schematically in Table 4.

As a test of accuracy, the interlaboratory standard diabase W-1 and granite G-1 were analyzed by the same methods, concurrently with the samples. Since W-1 more closely approximates the composition of biotite and cordierite than G-1, it was completely analyzed. G-1 was analyzed only for those elements in concentrations in the samples more closely matching the granite than W-1.

#### F. Discussion of Analytical Procedures

The procedures of Shapiro and Brannock were developed for total rock analysis. Since minerals have higher concentrations of

Table 4. Scheme of Replicate Analyses

<u>Constituent</u>		<u>Total number of determinations</u>
1) $\text{SiO}_2$ $\text{Al}_2\text{O}_3$ total Fe $\text{Na}_2\text{O}$ $\text{K}_2\text{O}$	<p style="text-align: center;">Sample</p> <p style="text-align: center;">A                      B</p> <p style="text-align: center;">┌───┴───┐            ┌───┴───┐</p> <p style="text-align: center;">1       2              1       2</p> <p style="text-align: center;">} solutions</p> <p style="text-align: center;">┌───┴───┐</p> <p style="text-align: center;">a   b   c   d</p> <p style="text-align: center;">instrument readings</p>	16
2) $\text{MnO}$ $\text{TiO}_2$ $\text{P}_2\text{O}_5$	<p style="text-align: center;">Sample</p> <p style="text-align: center;">A                      B</p> <p style="text-align: center;">┌───┴───┐            ┌───┴───┐</p> <p style="text-align: center;">a   b   c   d            a   b</p> <p style="text-align: center;">} solutions</p> <p style="text-align: center;">┌───┴───┐</p> <p style="text-align: center;">a   b   c   d</p> <p style="text-align: center;">(MnO)</p> <p style="text-align: center;">┌───┴───┐</p> <p style="text-align: center;">a   b</p> <p style="text-align: center;">(TiO<sub>2</sub>, P<sub>2</sub>O<sub>5</sub>)</p> <p style="text-align: center;">instrument readings</p>	8(MnO) 4(P <sub>2</sub> O <sub>5</sub> , TiO <sub>2</sub> )
3) $\text{CaO}$ ( $\text{CaO} + \text{MgO}$ ) as $\text{MgO}$	<p style="text-align: center;">Sample</p> <p style="text-align: center;">A                      B</p> <p style="text-align: center;">┌───┴───┐            ┌───┴───┐</p> <p style="text-align: center;">1       2              1       2</p> <p style="text-align: center;">} solutions</p> <p style="text-align: center;">} titrations</p>	4
4) $\text{FeO}$	<p style="text-align: center;">Sample</p> <p style="text-align: center;">┌───┴───┐</p> <p style="text-align: center;">1       2</p> <p style="text-align: center;">} titrations</p>	2

certain elements than rocks, some adjustments of the procedures were required. For example, the total Fe complex for biotite samples was prepared in 200 ml instead of 100 ml volumetric flasks in order to reduce the iron concentration to the necessary range without inducing undue volumetric measurement error. Greater concentration of complexing reagent for Fe and Al was required for CaO-MgO determinations in cordierite. In order to attain optimum Al and Si concentrations, as much as 100 mg of sample was fused; e. g., about 20%  $\text{Al}_2\text{O}_3$  was expected in the biotites, and the optimum concentration of the complex is exceeded in a solution prepared in the standard way of material containing in excess of 20% apparent  $\text{Al}_2\text{O}_3$ . Since appreciable corrections for Ti and Fe were expected, it was decided to reduce sample concentration to 80% of the standard value. Since the relative error attached to a weight of 40 mg is higher than desired, 80 mg were fused and half the specified amount of sample solution was used, the remainder being made up by blank solution. That fusions of up to 100 mg are permissible is shown by the precision and accuracy of the  $\text{SiO}_2$  and  $\text{Al}_2\text{O}_3$  values for the standard diabase W-1, tabulated below, since 100 mg of these samples were fused.

High  $\text{TiO}_2$  in all biotites except B-75 and B-87 caused the formation of a red precipitate in the alizarine red-S solutions prepared for the determination of Al. This effect was noted by the authors who developed the procedure (Parker and Goddard, 1950). No precipitate was observed by the writer in solutions of Ti concentration equal to or less than that equivalent to a sample containing 1.3%  $\text{TiO}_2$ , prepared

in the standard way, but was apparent after a time in solutions containing the equivalent of 2.0% or more. Appearance of the precipitate resulted in anomalous spectrophotometer readings, but since this effect was not apparent until at least three hours after preparation of the solutions, it was possible to make absorbance measurements prior to this. In some cases, four readings of each solution were impossible, and thus some  $\text{Al}_2\text{O}_3$  figures are based on as few as 11 instrument readings per sample rather than 16. Reference blank settings for the  $\text{Al}_2\text{O}_3$  determination also behaved anomalously, in that slit width corrections were always positive, suggesting that the blank darkens with time, an effect not exhibited by the sample and standard solutions. Altogether, the  $\text{Al}_2\text{O}_3$  procedure gives the least satisfactory results of all the analytical methods used, and is the least sound due to the corrections required, instability of the solutions, and large number of additions required in preparation.

The determination of small amounts of calcium proved difficult in the presence of high concentrations of iron and aluminum. Titration curves were erratic, times for biotite titrations often being shorter than the blank time, despite the use of a "spike" of up to 70 seconds titration time. Much better precision was obtained for higher concentrations, replicate runs in the vicinity of 500 s. agreeing to the second whereas runs in the vicinity of 20-30 s. might differ by 6-8 s. Many runs were spoiled by the appearance of a white precipitate (aluminum hydroxide?) which obscured the end point. This effect was largely eliminated by reducing both acid and base concentration in the solution, maintaining the pH constant at the optimum value.

Negligible CaO is assumed for all samples which showed titration times equal to or shorter than the blank, even if replicate runs gave higher results since, for a given sample, the titration curves which gave the best defined end points were almost invariably those of least time. No result so rejected exceeded 0.42% CaO, and no mean result rejected, including all discordant values (expressing negative times as 0% CaO), exceeded 0.16% CaO. The error induced in the MgO determination is thus not great.

The first permanganate solutions prepared gave discordant results for most samples. Boiling a duplicate set for a longer period (in excess of 10 minutes) gave results of high precision, of uniformly higher MnO than the first set, hence the discordant results were rejected. In a few cases, periodate in excess of the amount specified was required to produce the permanganate color, perhaps due to oxidation of iron in the solution. Titanium solutions developed a white precipitate about 15 minutes after addition of the reducing agent, necessitating the making of consecutive duplicate readings on each solution.

Colorimetric measurements were made on groups of as many as 44 solutions including 4 standard, 2 standard rock, and 2 blank solutions, with no significant loss in precision with respect to smaller "batches." Replicate readings were made in reverse order so that instrument drifts would be compensated in the mean. Unstable solutions such as the Al complex were prepared and measured in smaller groups.



## G. Analytical Results

Table 5 presents the analytical results for the rock standards W-1 and G-1 and compares them with the interlaboratory mean values published by Fairbairn (1953). In Table 6, the values are given for the duplicates of all minerals and the slate analyzed, uncorrected for impurities. In general, agreement between replicate readings of sample solution A or B is much better than that between A and B, hence a breakdown of the results for each solution is not given except in the case of  $\text{SiO}_2$  and  $\text{Al}_2\text{O}_3$ , where some intra-solution anomalies are present.

In Table 7 the mean analysis of each sample is presented, with  $\text{Al}_2\text{O}_3$  corrected for Fe and Ti interference. In the adjacent column the analysis is corrected for the impurities listed in the table. A sample correction calculation is reproduced in Table 8. In the case of biotite, chlorite and slate, totals of complete analyses less  $\text{H}_2\text{O}$  lower than 100% are arbitrarily made up to 100.00% by the addition of  $\text{H}_2\text{O}^+$  to the analysis.  $\text{H}_2\text{O}^-$  does not enter the analysis since all samples were dried before weighing.

Mole ratios calculated from the corrected analyses are tabulated also in Table 6; their significance will be apparent in Section IX.

In Table 9, the mean analysis of chlorite Ch-65 is corrected for muscovite by reducing the alkali content to zero, correcting the values for  $\text{SiO}_2$ ,  $\text{Al}_2\text{O}_3$  and  $\text{H}_2\text{O}$  (by difference from 100.00) on the basis of the ideal muscovite formula. The corrected analysis is recalculated to 100.00%. Structural formulae to 18 O, OH are calculated for the

uncorrected and the corrected analysis; the table is also a sample calculation of a structural formula.

In Table 10, the mean analysis of slate 0-65 is presented, together with a calculation of the mode on the basis of the corrected chlorite composition, assuming the muscovite to have the same Na/K ratio as the alkalies in Ch-65.

Table 4. Analyses of Standard Rocks W-1 and G-1.

Wt. %	W-1					G-1			
	A	B	C	Mean	Interlab. <sup>1</sup> Mean	A	B	Mean	Interlab. <sup>1</sup> Mean
SiO <sub>2</sub>	53.23	53.28	—	53.26	preferred: 52.69				
Al <sub>2</sub> O <sub>3</sub> uncorr.	15.38	15.65	—	15.52	preferred: 15.55				
Al <sub>2</sub> O <sub>3</sub> corr.				14.72	preferred: 14.72				
total Fe as Fe <sub>2</sub> O <sub>3</sub>	10.74	11.09	10.86 <sup>2</sup>	10.86	11.18				
FeO	8.44	8.62	—	8.53	8.71				
Fe <sub>2</sub> O <sub>3</sub>	1.27	1.62	—	1.45	1.50				
CaO + MgO as MgO	14.28	14.64	14.56 <sup>2</sup>	14.46	14.51	1.31	1.31	1.31	1.40
CaO	10.2	—	10.6 <sup>2</sup>	10.4	10.96	1.34	1.24	1.29	1.41
MgO				6.98	6.63			0.38	0.39
TiO <sub>2</sub>	1.04	1.04	1.08 <sup>2</sup>	1.05	1.10				
MnO	—	—	.168 <sup>2</sup>	.168	.165				
K <sub>2</sub> O	0.63	0.65	—	0.64	0.63	5.50	5.50	5.50	5.42
Na <sub>2</sub> O <sup>3</sup>	2.16	2.20	—	2.18	2.00	3.47	3.51	3.49	3.25
P <sub>2</sub> O <sub>5</sub>	0.128	0.135	—	0.132	0.126				

1 - Fairbairn (1953); preferred values for SiO<sub>2</sub> and Al<sub>2</sub>O<sub>3</sub> established by analysis of the synthetic "haplogranite"

2 - Solution C gave uniformly low results, probably due to a weighing error. Values for C are corrected by the factor  $\frac{\text{total Fe (C)}}{\text{total Fe (mean of A and B)}}$

3 - The positive error in Na<sub>2</sub>O is consistent, and experienced by others in this laboratory Na<sub>2</sub>O in samples is corrected by the factor  $\frac{\text{Na}_2\text{O interlab.}}{\text{Na}_2\text{O observed}} = 0.92 \text{ (W-1)}$   
 $\frac{\text{Na}_2\text{O interlab.}}{\text{Na}_2\text{O observed}} = 0.93 \text{ (G-1)}$   
 Mean = 0.92

Table 6. Chemical Analyses

## Biotite

Wt. %		B32		B38		B40	
		A	B	A	B	A	B
SiO <sub>2</sub>	1	36.56	36.12	35.43	35.48	36.87	35.86
	2	36.79	36.31	35.43	35.61	37.43	36.70
	3					36.16	35.88
Al <sub>2</sub> O <sub>3</sub> <sup>1*</sup>	1	20.04	20.17	21.28	21.35	20.86	21.13
	2	20.16	20.26	20.43	20.42	20.10	20.20
	3			20.64	20.55		
total Fe as Fe <sub>2</sub> O <sub>3</sub>		25.99	25.78	25.70	25.23	25.64	25.50
FeO	1	21.62	21.47	21.13	21.68	21.04	21.00
	2			20.45	20.91		
Fe <sub>2</sub> O <sub>3</sub> <sup>2</sup>		2.06	1.85	2.32	1.85	2.29	2.15
MgO		4.69	4.77	5.52	5.50	5.22	5.17
TiO <sub>2</sub>		2.73	2.73	2.71	2.64	2.66	2.67
MnO		0.095	0.091	0.068	0.071	0.069	n.d.
K <sub>2</sub> O		8.28	8.24	8.83	8.71	9.03	8.75
Na <sub>2</sub> O <sup>3</sup>		0.17	0.17	0.16	0.15	0.16	0.17
CaO		- <sup>4</sup>	-	-	-	-	-
P <sub>2</sub> O <sub>5</sub>		n.d. <sup>5</sup>	n.d.	0.13	0.03	0.02	0.02

\*  
footnotes at end of table

Table 6 -2.

Biotite		B43		B45		B56	
Wt. %		A	B	A	B	A	B
SiO <sub>2</sub>	1	35.63	35.88	34.71	35.26	37.01	36.08
	2	35.85	36.15	34.97	35.43	36.16	36.16
Al <sub>2</sub> O <sub>3</sub>	1	20.24	20.14	20.40	20.75	21.57	21.77
	2	20.30	20.19	20.49	20.77	21.05	20.71
	3					20.80	20.95
total Fe as Fe <sub>2</sub> O <sub>3</sub>		25.24	25.24	25.52	25.60	26.01	25.77
FeO	1	20.83	20.98	21.21	21.29	20.80	21.54
	2					21.07	
Fe <sub>2</sub> O <sub>3</sub>		2.02	2.02	1.91	1.99	2.52	2.28
MgO		5.60	5.68	5.79	5.82	5.15	5.15
TiO <sub>2</sub>		2.84	2.85	2.79	2.80	2.67	2.66
MnO		0.097	0.097	0.093	0.101	0.100	0.097
K <sub>2</sub> O		8.60	8.58	8.78	8.76	8.67	8.68
Na <sub>2</sub> O		0.15	0.16	0.14	0.19	0.16	0.15
CaO		—	—	—	—	—	—
P <sub>2</sub> O <sub>5</sub>		n.d.	n.d.	n.d.	n.d.	0.09	0.09

Table 6 -3.

Biotite		B57		B60		B75	
Wt. %		A	B	A	B	A	B
SiO <sub>2</sub>	1	36.32	35.99	36.71	35.71	37.96	37.89
	2	36.14	36.03	35.59	35.58	38.29	38.17
	3			35.45	35.69		
Al <sub>2</sub> O <sub>3</sub>	1	21.02	21.21	20.94	21.37	19.60	19.63
	2	19.98	19.96	19.81	20.54	19.72	19.61
	3	20.40	20.66	20.33	20.54		
total Fe as Fe <sub>2</sub> O <sub>3</sub>		25.41	25.38	25.78	25.69	24.84	24.70
FeO		21.26	20.99	20.82	20.58	20.09	20.27
Fe <sub>2</sub> O <sub>3</sub>		1.95	1.92	2.78	2.69	2.42	2.28
MgO		5.44	5.32	5.42	5.32	5.72	5.74
TiO <sub>2</sub>		2.76	2.75	2.64	2.66	1.37	1.38
MnO		0.103	0.103	0.094	0.089	0.296	0.301
K <sub>2</sub> O		8.56	8.65	8.76	8.60	7.04	7.09
Na <sub>2</sub> O		0.17	0.19	0.16	0.16	0.37	0.39
CaO		—	—	—	—	0.19	0.19
P <sub>2</sub> O <sub>5</sub>		0.03	0.02	0.03	0.03	n.d.	n.d.

Table 6 -4.

Biotite		B82		B83		B87	
Wt. %		A	B	A	B	A	B
SiO <sub>2</sub>	1	35.81	36.16	36.50	35.49	36.77	37.38
	2	35.80	36.24	36.36	35.66	37.04	37.53
	3			35.90	35.38		
Al <sub>2</sub> O <sub>3</sub>	1	20.90	21.05	21.56	21.34	20.95	20.85
	2	20.03	20.35	21.04	20.56	20.85	20.97
	3	20.23	20.46	20.46	20.53		
total Fe as Fe <sub>2</sub> O <sub>3</sub>		25.47	25.35	25.02	25.27	24.40	24.42
FeO		20.67	20.96	21.26	20.91	20.35	20.02
Fe <sub>2</sub> O <sub>3</sub>		2.34	2.22	1.60	1.85	1.98	2.00
MgO		5.73	5.69	5.54	5.59	6.30	6.34
TiO <sub>2</sub>		2.61	2.63	2.50	2.56	1.63	1.64
MnO		0.102	0.100	0.119	0.123	0.166	0.169
K <sub>2</sub> O		8.84	8.83	8.62	8.85	7.33	7.31
Na <sub>2</sub> O		0.19	0.19	0.18	0.19	0.35	0.36
CaO		—	—	—	—	—	—
P <sub>2</sub> O <sub>5</sub>		0.05	0.02	0.05	0.02	n.d.	n.d.

Table 6 -5.

## Cordierite

		C32		C38		C40	
		A	B	A	B	A	B
SiO <sub>2</sub>	1	n.d.	n.d.	49.17	50.04	51.16	50.15
	2			49.04	49.78	50.35	49.96
	3			49.00	50.02	50.34	50.24
Al <sub>2</sub> O <sub>3</sub>	1	n.d.	n.d.	31.12	32.80	32.44	32.86
	2			31.09	32.57	32.63	32.73
total Fe as Fe <sub>2</sub> O <sub>3</sub>		11.08	11.03	13.33	13.35	13.82	13.83
FeO		9.19	9.19	11.16	11.38	11.70	11.74
Fe <sub>2</sub> O <sub>3</sub>		0.87	0.82	0.81	0.83	0.80	0.81
MgO		3.67	3.69	5.02	5.04	4.77	4.75
TiO <sub>2</sub>		0.49	0.51	0.24	0.24	0.19	0.19
MnO		0.364	0.364	0.266	0.269	0.224	0.229
K <sub>2</sub> O		n.d.	n.d.	0.65	0.64	0.51	0.50
Na <sub>2</sub> O		n.d.	n.d.	0.44	0.46	0.33	0.33
CaO		n.d.	n.d.	—	—	—	—
P <sub>2</sub> O <sub>5</sub>		n.d.	n.d.	0.06	0.05	0.06	0.05



Table 6 -6.

Cordierite		C43		C45		C56	
		A	B	A	B	A	B
SiO <sub>2</sub>	1	n.d.	n.d.	49.42	49.10	50.76	50.18
	2			49.92	50.00	50.17	49.91
	3					50.31	50.30
Al <sub>2</sub> O <sub>3</sub>	1	n.d.	n.d.	31.93	32.19	31.68	31.90
	2			31.86	31.91	31.94	31.57
total Fe as Fe <sub>2</sub> O <sub>3</sub>		9.79	9.74	13.04	13.02	13.30	13.26
FeO	1	8.01	7.94	10.64	11.04	11.12	11.08
	2			10.90			
Fe <sub>2</sub> O <sub>3</sub>		0.92	0.87	0.93	0.91	0.98	0.94
MgO		3.77	3.75	5.42	5.45	4.45	4.45
TiO <sub>2</sub>		0.50	0.50	0.24	0.25	0.15	0.15
MnO		0.180	0.183	0.276	0.280	0.203	0.217
K <sub>2</sub> O		n.d.	n.d.	0.23	0.23	0.86	0.88
Na <sub>2</sub> O		n.d.	n.d.	0.31	0.31	0.52	0.53
CaO		n.d.	n.d.	—	—	0.19	0.21
P <sub>2</sub> O <sub>5</sub>		n.d.	n.d.	n.d.	n.d.	0.06	0.06

Table 6 -7.

Cordierite		C57		C60		C82	
		A	B	A	B	A	B
SiO <sub>2</sub>	1	50.53	49.10	49.42	49.80	48.80	48.85
	2	49.62	49.05	49.15	49.60	48.36	48.60
	3	49.77	49.95				
Al <sub>2</sub> O <sub>3</sub>	1	31.43	32.09	32.37	32.76	32.04	32.38
	2	31.79	32.02	32.83	31.94	31.88	32.02
total Fe as Fe <sub>2</sub> O <sub>3</sub>		13.29	13.25	13.53	13.55	12.64 <sup>6</sup>	13.11
FeO		11.31	11.19	11.07	11.17	10.72	10.68
Fe <sub>2</sub> O <sub>3</sub>		0.72	0.82	1.18	1.20	0.75 <sup>6</sup>	1.22
MgO		4.85	4.92	4.87	4.85	5.00 <sup>6</sup>	5.28
TiO <sub>2</sub>		0.26	0.25	0.12	0.11	0.25 <sup>6</sup>	0.25
MnO		0.298	0.287	0.242	0.242	0.268 <sup>6</sup>	0.271
K <sub>2</sub> O		0.73	0.74	0.48	0.48	0.36 <sup>6</sup>	0.39
Na <sub>2</sub> O		0.44	0.44	0.43	0.44	0.37 <sup>6</sup>	0.41
CaO		0.12	0.16	—	—	—	—
P <sub>2</sub> O <sub>5</sub>		0.11	0.06	0.08	0.09	0.05 <sup>6</sup>	0.07

Table 6 -8.

		Cordierite		Chlorite		Slate	
		C83		Ch65		O65	
		A	B	A	B	A	B
SiO <sub>2</sub>	1	50.36	49.49	30.00	28.86	60.06	60.30
	2	49.96	49.37	29.28	29.04	60.12	60.48
Al <sub>2</sub> O <sub>3</sub>	1	31.71	31.68	24.24	24.27	20.48	20.26
	2	31.90	31.58	24.37	24.22	20.55	20.37
total Fe as Fe <sub>2</sub> O <sub>3</sub>		13.03	12.92	30.25	30.25	7.56	7.54
FeO		11.04	10.90	25.39	24.96	5.56	5.53
Fe <sub>2</sub> O <sub>3</sub>		0.84	0.73	2.28	2.28	1.41	1.39
MgO		4.85	4.91	8.25	8.22	1.87	1.92
TiO <sub>2</sub>		0.37	0.37	0.29	0.28	0.98	0.99
MnO		0.353	0.366	0.298	0.291	0.101	0.095
K <sub>2</sub> O		0.64	0.63	1.27	1.28	3.83	3.85
Na <sub>2</sub> O		0.44	0.42	0.15	0.15	1.11	1.12
CaO		0.26	0.23	—	—	0.36	0.31
P <sub>2</sub> O <sub>5</sub>		0.08	—	n.d.	n.d.	n.d.	n.d.

## Footnotes to Table 5

- 1 - uncorrected in this table for total iron and titanium interference  
2 - Fe<sub>2</sub>O<sub>3</sub> = total Fe as Fe<sub>2</sub>O<sub>3</sub> - mean FeO as Fe<sub>2</sub>O<sub>3</sub>  
3 - corrected values on the basis of G-1 and W-1  
4 - below the limit of detection  
5 - not determined  
6 - rejected as improperly prepared solution

Table 7. Corrections to Chemical Analyses

Biotite	B32		B38		B40	
	1* Mean	2 Corrected	Mean	Corrected	Mean	Corrected
SiO <sub>2</sub>	36.45	36.47	35.49	35.60	36.48	36.54
Al <sub>2</sub> O <sub>3</sub> <sup>3</sup>	18.39	18.40	19.13	19.19	18.85	18.88
total Fe as FeO <sup>4</sup>	23.30	23.29	22.94	22.87	23.03	22.99
FeO	21.54	21.53	21.04	20.97	21.02	20.98
Fe <sub>2</sub> O <sub>3</sub>	1.96	1.96	2.08	2.09	2.22	2.22
MgO	4.73	4.73	5.51	5.53	5.20	5.21
TiO <sub>2</sub>	2.73	2.70	2.68	2.53	2.66	2.58
MnO	0.093	0.093	0.070	0.070	0.069	0.069
K <sub>2</sub> O	8.26	8.26	8.77	8.80	8.89	8.90
Na <sub>2</sub> O	0.17	0.17	0.16	0.16	0.16	0.16
CaO	—	—	—	—	—	—
P <sub>2</sub> O <sub>5</sub>	n.d.	n.d.	0.08	0.08	0.02	0.02
H <sub>2</sub> O+ <sup>5</sup>	5.68	5.69	4.99	4.98	4.43	4.44
Total	100.00	100.00	100.00	100.00	100.00	100.00
Total impurity <sup>6</sup>	0.3		1.0		0.7	
Impurity cor- rected: ilmenite <sup>7</sup>	0.05	—	0.3	—	0.15	—
Mole Ratios <sup>8</sup>						
a		0.694		0.655		0.668
b		0.713		0.677		0.691
c		0.194		0.193		0.190
d		0.184		0.183		0.179
e		-0.282		—		—
f		-0.260		—		—
g		0.77		0.59		0.59
h		0.71		0.54		0.54
i		0.926		0.918		0.913

\* footnotes at end of table

Table 7 -2.

Biotite	B43		B45		B56	
Wt. %	Mean	Corrected	Mean	Corrected	Mean	Corrected
SiO <sub>2</sub>	35.88	35.93	35.09	35.26	36.35	36.40
Al <sub>2</sub> O <sub>3</sub>	18.70	18.73	18.90	18.99	19.58	19.61
total Fe as FeO	22.72	22.68	23.00	22.89	23.30	23.27
FeO	20.90	20.86	21.25	21.14	21.14	21.10
Fe <sub>2</sub> O <sub>3</sub>	2.02	2.02	1.95	1.96	2.40	2.40
MgO	5.64	5.65	5.80	5.83	5.15	5.16
TiO <sub>2</sub>	2.84	2.76	2.80	2.57	2.66	2.58
MnO	0.097	0.097	0.097	0.097	0.098	0.099
K <sub>2</sub> O	8.59	8.60	8.77	8.81	8.68	8.69
Na <sub>2</sub> O	0.14	0.14	0.16	0.16	0.16	0.16
CaO	—	—	—	—	—	—
P <sub>2</sub> O <sub>5</sub>	n.d.	n.d.	n.d.	n.d.	0.09	0.09
H <sub>2</sub> O+	5.19	5.21	5.18	5.18	3.69	3.71
Total	100.00	100.00	100.00	100.00	100.00	100.00
Total impurity	0.3		1.2		0.4	
Impurity cor- rected: ilmenite	0.15	—	0.45	—	0.15	—
Mole Ratios						
a		0.646		0.644		0.672
b		0.667		0.664		0.695
c		0.189		0.184		0.204
d		0.179		0.176		0.192
e		-0.294		—		—
f		-0.272		—		—
g		0.83		0.82		0.84
h		0.76		0.76		0.76
i		0.918		0.925		0.907

Table 7 -3.

Biotite	B57		B60		B75	
	Mean	Corrected	Mean	Corrected	Mean	Corrected
SiO <sub>2</sub>	36.12	36.24	35.79	35.85	38.08	36.92
Al <sub>2</sub> O <sub>3</sub>	18.86	18.92	18.94	18.97	18.55	18.98
total Fe as FeO	22.86	22.79	23.17	23.14	22.30	22.75
FeO	21.12	21.05	20.70	20.66	20.18	20.58
Fe <sub>2</sub> O <sub>3</sub>	1.94	1.95	2.74	2.74	2.35	2.40
MgO	5.38	5.40	5.37	5.38	5.73	5.86
TiO <sub>2</sub>	2.76	2.61	2.65	2.57	1.37	1.32
MnO	0.103	0.103	0.092	0.092	0.298	0.305
K <sub>2</sub> O	8.60	8.63	8.68	8.69	7.06	7.23
Na <sub>2</sub> O	0.18	0.18	0.16	0.16	0.38	0.39
CaO	—	—	—	—	0.19	0.19
P <sub>2</sub> O <sub>5</sub>	0.02	0.02	0.03	0.03	n.d.	n.d.
H <sub>2</sub> O <sup>+</sup>	4.92	4.90	4.85	4.86	5.81	5.82
Total	100.00	100.00	100.00	100.00	100.00	100.00
Total impurity	1.1	—	0.6	—	3.1	—
Impurity cor- rected: ilmenite quartz	0.30	—	0.15	—	0.15	—
					2.0	—
<b>Mole Ratios</b>						
a		0.659		0.647		0.651
b		0.679		0.684		0.674
c		0.191		0.198		0.208
d		0.182		0.181		0.197
e		—		—		-0.121
f		—		—		-0.113
g		0.87		0.79		—
h		0.80		0.71		—
i		0.924		0.894		0.905

Table 7 -4.

Biotite	B82		B83		B87	
Wt. %	Mean	Corrected	Mean	Corrected	Mean	Corrected
SiO <sub>2</sub>	36.00	36.11	35.88	36.16	37.18	36.75
Al <sub>2</sub> O <sub>3</sub>	18.88	18.94	19.36	19.51	19.80	19.85
total Fe as FeO	22.87	22.80	22.63	22.46	21.97	22.24
FeO	20.82	20.74	21.08	20.89	20.18	20.41
Fe <sub>2</sub> O <sub>3</sub>	2.28	2.29	1.72	1.73	1.99	2.03
MgO	5.71	5.73	5.56	5.60	6.32	6.46
TiO <sub>2</sub>	2.62	2.47	2.53	2.15	1.64	1.43
MnO	0.101	0.101	0.121	0.121	0.166	0.169
K <sub>2</sub> O	8.84	8.87	8.74	8.81	7.32	7.48
Na <sub>2</sub> O	0.19	0.19	0.18	0.18	0.36	0.37
CaO	—	—	—	—	—	—
P <sub>2</sub> O <sub>5</sub>	0.04	0.04	0.03	0.03	n.d.	n.d.
H <sub>2</sub> O+	4.52	4.52	4.80	4.82	5.04	5.05
Total	100.00	100.00	100.00	100.00	100.00	100.00
Total impurity	0.6		1.2		1.9	
Impurity cor- rected: ilmenite	0.30	—	0.75	—	0.45	—
quartz	—	—	—	—	1.0	—
andalusite	—	—	—	—	0.6	—
<b>Mole Ratios</b>						
a		0.643		0.655		0.624
b		0.667		0.672		0.645
c		0.187		0.194		0.218
d		0.177		0.186		0.205
e		—		—		-0.109
f		—		—		-0.103
g		0.87		1.03		—
h		0.79		0.96		—
i		0.912		0.930		0.916

Table 7 -5.

Cordierite	C32		C38		C40	
	Mean	Corrected	Mean	Corrected	Mean	Corrected
Wt. %						
SiO <sub>2</sub>	n.d.	n.d.	49.51	49.22	50.37	49.77
Al <sub>2</sub> O <sub>3</sub>	n.d.	n.d.	31.67	32.14	32.46	33.07
total Fe as FeO	9.95	10.13	12.01	11.97	12.44	12.50
FeO	9.19	9.31	11.27	11.22	11.72	11.77
Fe <sub>2</sub> O <sub>3</sub>	0.84	0.90	0.82	0.83	0.80	0.82
MgO	3.68	3.96	5.03	5.10	4.76	4.85
TiO <sub>2</sub>	0.50	—	0.24	—	0.19	—
MnO	0.364	0.391	0.268	0.271	0.226	0.231
K <sub>2</sub> O	n.d.	n.d.	0.65	0.66	0.51	0.52
Na <sub>2</sub> O	n.d.	n.d.	0.45	0.46	0.33	0.34
CaO	n.d.	n.d.	—	—	—	—
P <sub>2</sub> O <sub>5</sub>	n.d.	n.d.	0.06	0.06	0.06	0.06
H <sub>2</sub> O <sup>+</sup>	n.d.	n.d.	n.d.	n.d.	n.d.	n.d.
Total	14.57	14.56	99.97	99.96	101.43	101.43
Total impurity	n.d.	n.d.	n.d.	—	n.d.	—
Impurity cor- rected: ilmenite <sup>9</sup>	0.90	—	n.d.	—	n.d.	—
quartz	n.d.	n.d.	1.0	—	1.5	—
biotite	0.36	—	—	—	—	—
<b>Mole Ratios</b>						
a		0.570		0.553		0.577
b		0.590		0.574		0.592
c		—		0.524		0.528
d		—		0.512		0.520
e		—		—		—
f		—		—		—
g		7.48		4.31		3.49
h		6.88		4.03		3.30
i		0.915		0.940		0.943



Table 7 -6.

Cordierite	C43		C45		C56	
	Mean	Corrected	Mean	Corrected	Mean	Corrected
SiO <sub>2</sub>	n.d.	n.d.	49.62	48.30	50.27	49.52
Al <sub>2</sub> O <sub>3</sub>	n.d.	n.d.	31.71	32.85	31.56	32.21
total Fe as FeO	8.79	8.91	11.73	12.15	11.95	12.06
FeO	7.98	8.02	10.90	11.06	11.10	11.20
Fe <sub>2</sub> O <sub>3</sub>	0.90	0.98	0.92	0.95	0.96	0.97
MgO	3.76	4.10	5.44	5.64	4.45	4.54
TiO <sub>2</sub>	0.50	—	0.25	—	0.15	—
MnO	0.182	0.198	0.278	0.288	0.210	0.214
K <sub>2</sub> O	n.d.	n.d.	0.23	0.24	0.87	0.89
Na <sub>2</sub> O	n.d.	n.d.	0.31	0.32	0.52	0.53
CaO	n.d.	n.d.	—	—	0.20	0.20
P <sub>2</sub> O <sub>5</sub>	n.d.	n.d.	n.d.	n.d.	0.06	0.06
H <sub>2</sub> O <sup>+</sup>	n.d.	n.d.	0.34 (by diff)	0.35 (by diff)	n.d.	n.d.
Total	13.32	13.30	100.00	100.00	100.35	100.33
Total impurity	n.d.	—	3.2	—	2.2	—
Impurity cor- rected: ilmenite	0.54	—	0.36	—	0.36	—
quartz	n.d.	n.d.	3.0	—	1.75	—
biotite	0.84	—	—	—	—	—
<b>Mole Ratios</b>						
a	—	0.523	—	0.524	—	0.580
b	—	0.549	—	0.548	—	0.598
c	—	—	—	0.521	—	0.533
d	—	—	—	0.508	—	0.522
e	—	—	—	—	—	—
f	—	—	—	—	—	—
g	—	4.40	—	4.60	—	3.40
h	—	3.96	—	4.22	—	3.15
i	—	0.903	—	0.928	—	0.929

Table 7 -7.

Cordierite	C57		C60		C82		C83	
	Mean	Corr.	Mean	Corr.	Mean	Corr.	Mean	Corr.
SiO <sub>2</sub>	49.67	49.27	49.49	49.22	48.65	48.11	49.80	48.86
Al <sub>2</sub> O <sub>3</sub>	31.51	32.06	32.30	32.62	31.83	32.48	31.41	32.45
total Fe as FeO	11.95	11.93	12.19	12.20	11.80	11.82	11.68	11.72
FeO	11.25	11.21	11.12	11.12	10.70	10.69	10.97	10.99
Fe <sub>2</sub> O <sub>3</sub>	0.77	0.78	1.19	1.20	1.22	1.24	0.78	0.81
MgO	4.88	4.97	4.86	4.91	5.28	5.39	4.88	5.04
TiO <sub>2</sub>	0.26	—	0.12	—	0.25	—	0.37	—
MnO	0.288	0.297	0.242	0.244	0.271	0.277	0.360	0.372
K <sub>2</sub> O	0.73	0.74	0.48	0.48	0.38	0.39	0.64	0.66
Na <sub>2</sub> O	0.44	0.45	0.44	0.44	0.41	0.42	0.43	0.44
CaO	0.14	0.14	—	—	—	—	0.24	0.25
P <sub>2</sub> O <sub>5</sub>	0.08	0.08	0.08	0.08	0.07	0.07	0.08	0.08
H <sub>2</sub> O <sup>+</sup>	n.d.	n.d.	n.d.	n.d.	n.d.	n.d.	n.d.	n.d.
Total	100.03	100.01	100.32	100.31	99.06	99.07	99.96	99.95
Total impurity	2.0	—	1.0	—	2.6	—	3.2	—
Impurity corrected:	0.36	—	0.18	—	0.36	—	0.54	—
ilmenite	1.25	—	0.75	—	1.5	—	2.5	—
quartz								
<b>Mole Ratios</b>								
a		0.559		0.558		0.526		0.550
b		0.574		0.582		0.546		0.566
c		0.524		0.533		0.527		0.528
d		0.515		0.519		0.516		0.519
e		—		—		—		—
f		—		—		—		—
g		4.72		3.90		4.58		6.02
h		4.44		3.56		4.15		5.65
i		0.940		0.917		0.903		0.939

## Footnotes to Table 7

- 1 - mean of A and B (Table 5)  
 2 - sample correction calculation, Table 7  
 3 - corrected for iron and titanium interference  
 4 - not included in total  
 5 - by difference from 100.00%  
 6 - volume %  
 7 - weight %  
 8 - key to mole ratios:

	<u>analyzed FeO only</u>		<u>total Fe as FeO</u>
a =	$\frac{\text{FeO} - \text{TiO}_2}{(\text{FeO}) - \text{TiO}_2 + \text{MgO}}$	b =	$\frac{\text{FeO} - \text{TiO}_2}{(\text{FeO} - \text{TiO}_2) + \text{MgO}}$
c =	$\frac{\text{Al}_2\text{O}_3 - \text{K}_2\text{O}}{(\text{Al}_2\text{O}_3 - \text{K}_2\text{O}) + (\text{FeO} - \text{TiO}_2) + \text{MgO}}$	d =	$\frac{\text{Al}_2\text{O}_3 - \text{K}_2\text{O}}{(\text{Al}_2\text{O}_3 - \text{K}_2\text{O}) + (\text{FeO} - \text{TiO}_2) + \text{MgO}}$
e =	$\frac{\text{Al}_2\text{O}_3 - 3\text{K}_2\text{O}}{(\text{Al}_2\text{O}_3 - 3\text{K}_2\text{O}) + (\text{FeO} - \text{TiO}_2) + \text{MgO}}$	f =	$\frac{\text{Al}_2\text{O}_3 - 3\text{K}_2\text{O}}{(\text{Al}_2\text{O}_3 - 3\text{K}_2\text{O}) + (\text{FeO} - \text{TiO}_2) + \text{MgO}}$
g =	$\frac{\text{MnO}}{\text{FeO}} \times 100$	h =	$\frac{\text{MnO}}{\text{FeO}} \times 100$
i =	$\frac{\text{FeO}}{\text{FeO} + 2\text{Fe}_2\text{O}_3}$		

- 9 - instead of correcting  $\text{TiO}_2$  and FeO on the basis of opaque count,  $\text{TiO}_2$  is assumed to be all in ilmenite and FeO corrected accordingly. This assumption results in a slightly larger correction than would be applied on the basis of the opaque estimate in all cases except that of C-56.

Table 8. Sample Calculation of Mean Corrected Chemical Analysis

C-83. 2.5% quartz 0.3% (vol.) ilmenite =  $0.3 \times 1.8 = 0.54\%$  (wt.)

Wt.%	A	B	Mean	Corrections	Corrected Values	Recalculated to Total
SiO <sub>2</sub>	50.16	49.43	49.80	2.5	47.30	48.86
uncorr. Al <sub>2</sub> O <sub>3</sub>	31.80	31.63	31.72			—
TiO <sub>2</sub> corr. <sup>1</sup>	—	—	0.18			—
total Fe corr. <sup>1</sup>	—	—	0.13			—
corr. Al <sub>2</sub> O <sub>3</sub>	—	—	31.41			32.45
total Fe as Fe <sub>2</sub> O <sub>3</sub>	13.03	12.92	12.98			—
total Fe as FeO <sup>2</sup>			11.68	0.33	11.35	11.72
FeO	11.04	10.90	10.97	0.33	10.64	10.99
Fe <sub>2</sub> O <sub>3</sub>	0.84	0.73	0.78			0.81
MgO	4.85	4.91	4.88			5.04
TiO <sub>2</sub>	0.37	0.37	0.37	0.37	—	—
MnO	0.353	0.366	0.360			0.372
K <sub>2</sub> O	0.64	0.63	0.64			0.66
Na <sub>2</sub> O	0.48	0.45	—			—
corr. Na <sub>2</sub> O <sup>3</sup>	0.44	0.42	0.43			0.44
CaO	0.26	0.23	0.24			0.25
P <sub>2</sub> O <sub>5</sub>	0.08	—	0.08			0.08
Total			99.96			99.95

1 - empirically determined by Shapiro and Brannock (1956, and communication to this laboratory)

$$2 - \frac{\text{Fe}_2\text{O}_3}{1.111} = \text{FeO}$$

3 - corrected Na<sub>2</sub>O =  $\frac{\text{Na}_2\text{O}}{1.08}$  on the basis of G-1 and W-1

a) Reduce TiO<sub>2</sub> arbitrarily to zero; correction to FeO assuming all TiO<sub>2</sub> in ilmenite = %TiO<sub>2</sub> x .89 = .37 x .89 = .33

b) Correction to recalculate analysis to original total: Calculated %ilmenite = %TiO<sub>2</sub> x 1.89 = .37 x 1.89 = .70 Correction factor =  $\frac{1.0004}{1.0000 - (.025 + .0070)} = 1.0330$

Table 9. Correction of Analysis of chlorite Ch-65.

oxide	wt.%	mole frac. <sup>1</sup>	cation frac. <sup>2</sup>	muscovite cation frac. <sup>3</sup>	corrected cation frac. <sup>4</sup>	oxygen frac. <sup>5</sup>		$\frac{\text{cations}}{18\text{O, OH}}^6$
SiO <sub>2</sub>	29.30	.487	.487	.096	.391	.782	Si	2.90
Al <sub>2</sub> O <sub>3</sub>	23.91	.235	.470	.096	.374	.561	Al	2.78
FeO	25.18	.350	.350		.350	.350	Fe <sup>II</sup>	2.60
Fe <sub>2</sub> O <sub>3</sub>	2.28	.014	.029		.029	.044	Fe <sup>III</sup>	.22
MgO	8.24	.204	.204		.204	.204	Mg	1.52
TiO <sub>2</sub>	0.28	.003	.003		.003	.006	Ti	0.02
MnO	0.30	.004	.004		.004	.004	Mn	0.03
K <sub>2</sub> O	1.28	.014	.028	.032	—	—	K	—
Na <sub>2</sub> O	0.15	.002	.004		—	—	Na	—
H <sub>2</sub> O+ by diff	9.08	.504	1.008	.064	.944	.472	H	7.01
Total	100.00					2.423		

1 - weight % / "molecular weight" of oxide

2 - mole fraction x no. cations in oxide

3 - muscovite =  $\text{KAl}_2(\text{AlSi}_3)\text{O}_{10}(\text{OH})_2$

4 - alkalis reduced to zero and other constituents corrected in same proportion as in muscovite

5 - cation fraction x no. O atoms in oxide

6 - cation fraction x  $18 / \sum$  oxygen fractions

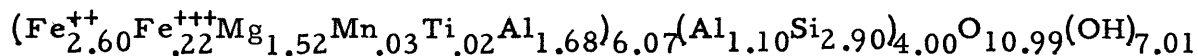
Check of calculation  $\sum(-) = 36.00$   $\sum(+) = 35.99$

Table 9 -2

oxide	corrected mole frac.	SiO <sub>2</sub> reduced so that octahedral Al = tetrahedral Al					
		wt.%	recalc. to 100%	corrected cation frac.	oxygen frac.	cations 18O, OH	recalc. to 100 wt.%
SiO <sub>2</sub>	.391	23.50	26.92	.295	.590	2.38	21.74
Al <sub>2</sub> O <sub>3</sub>	.187	19.02	21.79	.372	.558	3.01	23.38
FeO	.350	25.18	28.84	.351	.351	2.83	30.87
Fe <sub>2</sub> O <sub>3</sub>	.014	2.28	2.61	.029	.044	.23	2.80
MgO	.204	8.24	9.44	.204	.204	1.65	10.10
TiO <sub>2</sub>	.003	0.28	0.32	.003	.006	.02	.34
MnO	.004	0.30	0.34	.004	.004	.03	.37
K <sub>2</sub> O	—	—	—	—	—	—	—
Na <sub>2</sub> O	—	—	—	—	—	—	—
H <sub>2</sub> O+ by diff	.472	8.50	9.74	.944	.472	7.63	10.42
Total		87.30	100.00		2.421		100.02

Structural formulae:

a) muscovite correction only:



b) muscovite and SiO<sub>2</sub> corrections:

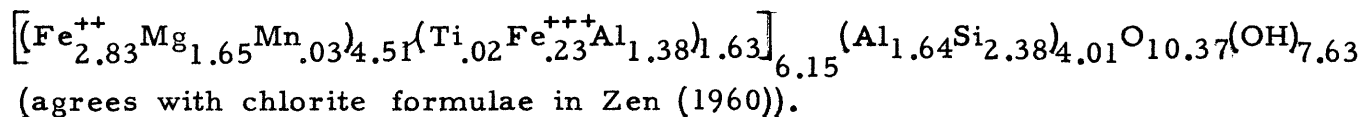


Table 10. Calculation of Mode of Slate O-65.

oxide	weight %	mole frac.	cation fraction								
			total rock	chlorite <sup>1</sup>	muscovite <sup>2</sup>	albite <sup>3</sup>	calcite <sup>4</sup>	opaque	quartz	remainder	
SiO <sub>2</sub>	60.24	1.002	1.002	.090	.282	.144			—	.486	—
corrected Al <sub>2</sub> O <sub>3</sub>	19.84	.195	.390	.086	.282	.024			—	—	-.002
FeO	5.54	.077	.077	.081	—	—	—	—	—	—	-.004
Fe <sub>2</sub> O <sub>3</sub>	1.40	.009	.018	.006	—	—	—	.012	—	—	—
MgO	1.90	.047	.047	.047	—	—	—	—	—	—	—
TiO <sub>2</sub>	0.98	.012	.012	.001	—	—	—	.011	—	—	—
MnO	0.10	.001	.001	.001	—	—	—	—	—	—	—
K <sub>2</sub> O	3.84	.041	.082	—	.082	—	—	—	—	—	—
Na <sub>2</sub> O	1.12	.018	.036	—	.012	.024	—	—	—	—	—
CaO	0.34	.006	.006	—	—	—	.006	—	—	—	—
H <sub>2</sub> O (by diff)	4.70	.261	.522	.217	.188	—	—	—	—	—	-.117
CO <sub>2</sub>							.005				
Total	100.00										

1 - all MgO assumed in chlorite

2 - muscovite assumed to have same Na/K ratio as in uncorrected chlorite analysis - all K<sub>2</sub>O assumed in muscovite

3 - remainder of Na<sub>2</sub>O assumed in albite

4 - all CaO as calcite

Mode (total for each phase of cation fraction calculated to weight %)

chlorite	20.21	Recalculated to 100.0% and rounded off	chlorite	20.1
muscovite	37.24		muscovite	37.0
albite	10.61		albite	10.5
quartz	29.20		quartz	29.0
opaque	1.84		opaque	1.8
water	1.04		water	1.0
calcite	0.56		calcite	0.6
	<u>100.70</u>		<u>100.0</u>	

## IX. DISCUSSION OF RESULTS

### A. Precision and Accuracy of Chemical Analyses

#### 1. Precision

Before the analytical data can be properly interpreted, it is necessary to have an appreciation of the precision and accuracy of these results. Since the values are all the means of replicate determinations, an estimate of precision is possible if the deviations from the mean are considered. For each element, the sample showing the largest precision error was determined by inspection, and the following statistical parameters calculated:

$$1) \text{ Standard deviation } s = \sqrt{\frac{\sum d^2}{n-1}}$$

Where:

$$x_1, x_2 \dots x_i = \text{replicate values}$$

$$n = \text{number of values}$$

$$\bar{x} = \frac{\sum_{i=1}^n x_i}{n}$$

$$d = (\bar{x} - x_1), (\bar{x} - x_2), \dots (\bar{x} - x_i)$$

$$\sum d^2 = \sum_{i=1}^n (\bar{x} - x_i)^2$$

$$2) \text{ Standard error of the mean } s_{\bar{x}} = \sqrt{\frac{\sum d^2}{n(n-1)}} = \frac{s}{\sqrt{n}}$$

$$3) \text{ Relative error of the mean } R = \frac{s_{\bar{x}}}{\bar{x}} \times 100\%$$



Table 11. Precision of Analytical Results

Constituent	Sample	No. of values	$\bar{x}$	s	$\frac{s}{\bar{x}}$	R%
SiO <sub>2</sub>	B-40	6	36.48	0.62	0.25	0.69
	C-57	6	49.67	0.56	0.23	0.46
SiO <sub>2</sub> in cordierite	C-57 combined with		quartz count: analytical error:		0.5 0.55	1.1
Al <sub>2</sub> O <sub>3</sub> (uncorrected)	B-60	6	20.59	0.53	0.22	1.0
	C-60	4	32.48	0.41	0.20	0.62
total Fe as Fe <sub>2</sub> O <sub>3</sub>	B-38	4	25.48	0.29	0.15	0.59
	C-45	4	13.03	0.13	0.062	0.48
FeO	B-38	4	21.04	0.51	0.26	1.2
	C-45	3	10.86	0.20	0.12	1.1
Fe <sub>2</sub> O <sub>3</sub> (s, $\frac{s}{\bar{x}}$ calculated from total Fe, FeO)	B-38	4	2.08	0.66	0.33	16.
	C-45	3	0.92	0.26	0.14	15.
(MgO+CaO) as MgO	B-57	4	5.44	.070	.035	0.65
	C-40	4	4.89	.039	.019	0.40
CaO (using rejected results, negative values as zero)	B-82	4	0.18	0.18	.088	49.
	C-40	3	0.10	0.17	.095	95.
MgO (s, $\frac{s}{\bar{x}}$ calculated from (CaO+MgO) as MgO, CaO, and MnO)	B-82	4	5.73	0.14	.072	1.3
	C-40	3	4.85	0.14	.071	1.5
TiO <sub>2</sub>	B-38	2	2.68	.050	.035	1.3
	C-32	2	0.496	.013	.0030	0.055
Al <sub>2</sub> O <sub>3</sub> (corrected) calculated from Al <sub>2</sub> O <sub>3</sub> , TiO <sub>2</sub> , total Fe	B-60	6	18.93	0.54	0.22	1.2
	C-60	4	32.29	0.41	0.20	0.62
MnO	B-45	2	0.097	0.0057	0.0040	4.1
	C-56	2	0.210	0.0099	0.0070	3.3
K <sub>2</sub> O	B-60	4	8.89	0.19	0.093	1.0
	C-56	4	0.87	0.026	0.013	1.5

Table 11 -2

Constituent	Sample	No. of values	$\bar{x}$	s	$\frac{s}{\bar{x}}$	R%
Na <sub>2</sub> O (uncorrected)	B-45	4	0.17	0.029	0.015	8.7
	C-83	4	0.48	0.024	0.013	2.6
P <sub>2</sub> O <sub>5</sub>	B-83	2	0.034	0.026	0.018	54.
	C-57	2	0.088	0.035	0.025	28.

## Precision of Mole Ratios

Mole Ratio	R%			
	Biotite		Cordierite	
	FeO	all Fe as FeO	FeO	all Fe as FeO
$\frac{\text{FeO} - \text{TiO}_2}{(\text{FeO} - \text{TiO}_2) - \text{MgO}}$	1.7	0.91	1.4	0.84
$\frac{\text{Al}_2\text{O}_3 - \text{K}_2\text{O}}{(\text{Al}_2\text{O}_3 - \text{K}_2\text{O}) - (\text{FeO} - \text{TiO}_2) - \text{MgO}}$	3.0	2.8	0.85	0.80
$\frac{\text{MnO}}{\text{FeO}}$	4.1	4.1	3.3	3.3
$\frac{\text{FeO}}{\text{FeO} - 2\text{Fe}_2\text{O}_3} = \frac{\text{FeO}}{\text{total Fe as FeO}}$	1.4	—	1.2	—

From the errors of the respective element determinations,  $R$  was calculated for certain of the mole ratios, by means of the relations:

- 4)  $s_{\bar{x}}$  of the sum  $(a \pm s_{\bar{x}a}) + (b \pm s_{\bar{x}b})$  or the difference  $(a \pm s_{\bar{x}a}) - (b \pm s_{\bar{x}b})$ :

$$s_{\bar{x}(a\pm b)} = \sqrt{(s_{\bar{x}a})^2 + (s_{\bar{x}b})^2}$$

- 5)  $s_{\bar{x}}$  of the product  $(a \pm s_{\bar{x}a})(b \pm s_{\bar{x}b})$  or the

$$\text{quotient } \frac{a \pm s_{\bar{x}a}}{b \pm s_{\bar{x}b}} :$$

$$\frac{s_{\bar{x}(ab)}}{ab} \quad \text{or} \quad \frac{s_{\bar{x}}\left(\frac{a}{b}\right)}{\frac{a}{b}} = \sqrt{\left(\frac{s_{\bar{x}a}}{a}\right)^2 + \left(\frac{s_{\bar{x}b}}{b}\right)^2}$$

All the above formulae are presented, or can be derived from relations in, Topping (1955).

All the errors so calculated are tabulated in Table 11. It should be emphasized that these represent the most "pessimistic" evaluation of precision possible, which in a few cases is not representative. For example, the over-all precision error of the total iron determination would appear to be about half that of the worst result.  $\text{Al}_2\text{O}_3$  in C-38, with  $s = 0.92$ ,  $s_{\bar{x}} = 0.46$ , and  $R = 1.4\%$ , shows the largest precision error of all the determinations. These values are not included in Table 11 because they are more than double those for all other cor-dierites. Instead, the next largest error is illustrated. Because all the errors have been calculated from relatively few replicate results, they have a large uncertainty. For spectrophotometric results, the

number of values represented by each error calculation is actually larger than that indicated in Table 11, because each figure is the mean of up to four instrument readings. The maximum number of values represented by an error calculation are actually those tabulated in section E above.

It is apparent from the precision data as well as from the discussion of analytical procedures that the fourth figure in the  $\text{SiO}_2$ ,  $\text{Al}_2\text{O}_3$ , total Fe and FeO percentages is not significant, being rendered so by weighing error in the first three cases. The fourth figure was retained in order to avoid round-off error in calculation, and is reproduced in the tables as a service to anyone interested in the evaluation of over-all precision of the procedures.

## 2. Accuracy

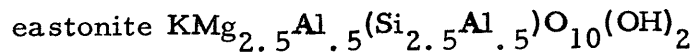
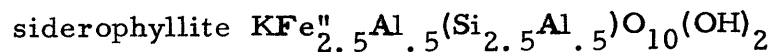
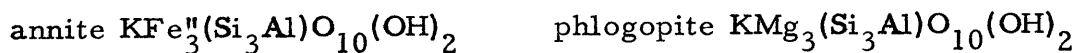
Accuracy of the analyses may be evaluated in several ways:

- a) By comparison of the analyses by the writer of W-1 and G-1 with the interlaboratory mean values as most recently compiled in Fairbairn (1953). The only significant and consistent departure from the accepted analytical values for these standards was encountered in the case of sodium. Accordingly,  $\text{Na}_2\text{O}$  values for all the analyzed samples are adjusted on the basis of the rock standards. The standard rocks were employed as monitors to guard against major procedural errors passing unnoticed; though there is a suggestion of a consistent error in  $\text{SiO}_2$ , total Fe and CaO, the data are not considered adequate to warrant correcting the sample values.
- b) The absence of values for  $\text{H}_2\text{O}$  makes impossible the usual 100% check in the case of biotite; cordierite usually contains some water

but it is not necessary to the structure (Leake, 1960). Thus it is possible that a cordierite analysis may total 100% in the absence of a water determination. Inspection of the complete cordierite analyses shows that only two fall outside the acceptable  $100.0 \pm 0.5\%$ . The departure of the totals of C-40 and C-82 from 100% correlates with variation in  $\text{SiO}_2$ , and these two samples represent the extremes of silica determined in cordierite. The errors in the totals could thus be caused by erroneous  $\text{SiO}_2$  values; however, these values are reproducible and there is no other evidence to suggest such an error. The bulk of the data show that these cordierites are essentially anhydrous.

c) In the case of mineral analyses, a further check is possible in that the proportions of the constituents are limited by the structure. Structural formulae were calculated for each sample by the usual method, the calculation in Table 8 being an example. These are presented in Table 12.

The compositions of biotites have been represented in terms of four end-members (Winchell and Winchell (1951)):



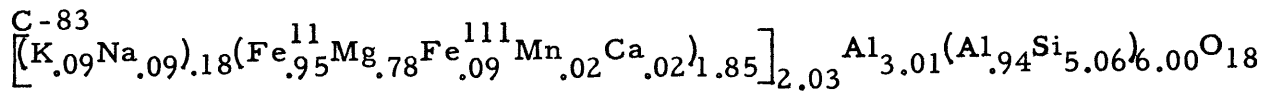
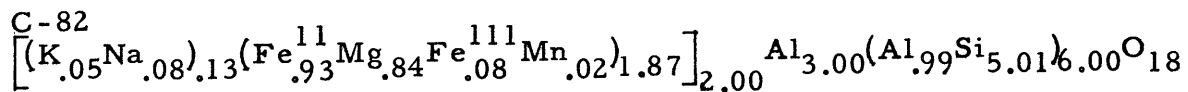
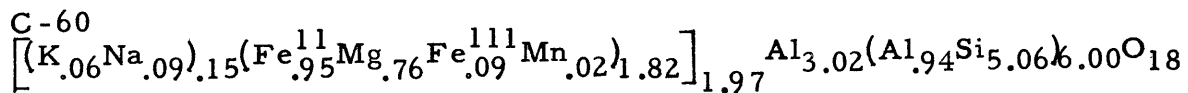
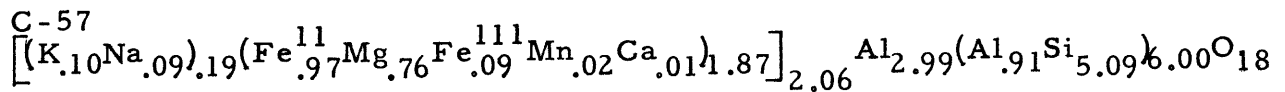
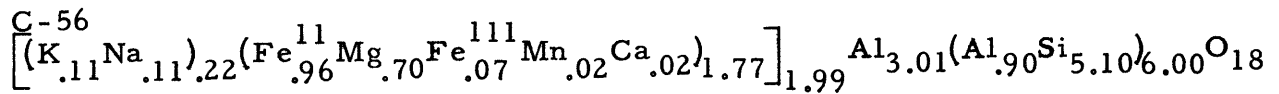
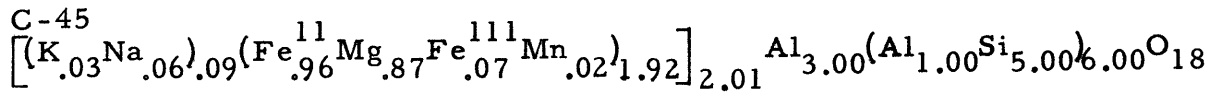
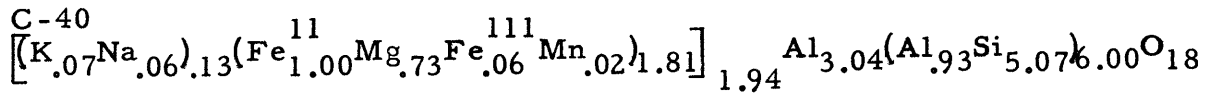
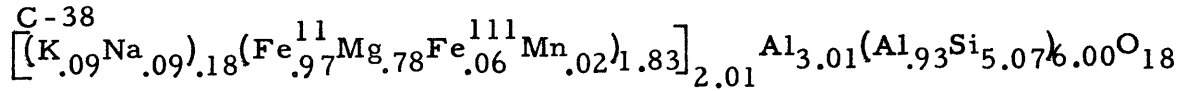
In the annite-phlogopite series an Al:Si ratio of 1:3 results in a negative charge on the tetrahedral sheets, which is neutralized by one potassium atom per 10 O, resulting in complete filling of the interlayer positions. In the siderophyllite-eastonite series, extra Al is accommodated by substitution of one Al for an octahedrally coordinated

Table 12. Structural Formulas of Biotite and Cordierite.

Biotite (to 12O,OH)	octahedral	tetrahedral
B-32	(K <sub>.79</sub> Na <sub>.03</sub> ) <sub>.82</sub> (Fe <sub>1.34</sub> <sup>11</sup> Mg <sub>.52</sub> Fe <sub>.11</sub> <sup>111</sup> Ti <sub>.15</sub> Al <sub>.32</sub> ) <sub>2.44</sub> (Al <sub>1.29</sub> Si <sub>2.71</sub> ) <sub>4.00</sub> O <sub>9.17</sub> (OH) <sub>2.83</sub>	
B-38	(K <sub>.84</sub> Na <sub>.03</sub> ) <sub>.87</sub> (Fe <sub>1.32</sub> <sup>11</sup> Mg <sub>.62</sub> Fe <sub>.12</sub> <sup>111</sup> Ti <sub>.14</sub> Al <sub>.38</sub> ) <sub>2.58</sub> (Al <sub>1.32</sub> Si <sub>2.68</sub> ) <sub>4.00</sub> O <sub>9.50</sub> (OH) <sub>2.50</sub>	
B-40	(K <sub>.85</sub> Na <sub>.03</sub> ) <sub>.88</sub> (Fe <sub>1.33</sub> <sup>11</sup> Mg <sub>.59</sub> Fe <sub>.13</sub> <sup>111</sup> Ti <sub>.15</sub> Al <sub>.44</sub> ) <sub>2.64</sub> (Al <sub>1.24</sub> Si <sub>2.76</sub> ) <sub>4.00</sub> O <sub>9.76</sub> (OH) <sub>2.24</sub>	
B-43	(K <sub>.82</sub> Na <sub>.02</sub> ) <sub>.84</sub> (Fe <sub>1.30</sub> <sup>11</sup> Mg <sub>.63</sub> Fe <sub>.12</sub> <sup>111</sup> Ti <sub>.16</sub> Al <sub>.34</sub> ) <sub>2.56</sub> (Al <sub>1.31</sub> Si <sub>2.69</sub> ) <sub>4.00</sub> O <sub>9.40</sub> (OH) <sub>2.60</sub>	
B-45	(K <sub>.85</sub> Na <sub>.03</sub> ) <sub>.88</sub> (Fe <sub>1.32</sub> <sup>11</sup> Mg <sub>.65</sub> Fe <sub>.11</sub> <sup>111</sup> Ti <sub>.14</sub> Al <sub>.33</sub> ) <sub>2.55</sub> (Al <sub>1.35</sub> Si <sub>2.65</sub> ) <sub>4.00</sub> O <sub>9.40</sub> (OH) <sub>2.60</sub>	
B-56	(K <sub>.84</sub> Na <sub>.03</sub> ) <sub>.87</sub> (Fe <sub>1.35</sub> <sup>11</sup> Mg <sub>.59</sub> Fe <sub>.14</sub> <sup>111</sup> Ti <sub>.15</sub> Al <sub>.53</sub> ) <sub>2.76</sub> (Al <sub>1.23</sub> Si <sub>2.77</sub> ) <sub>4.00</sub> O <sub>10.11</sub> (OH) <sub>1.89</sub>	
B-57	(K <sub>.83</sub> Na <sub>.03</sub> ) <sub>.86</sub> (Fe <sub>1.32</sub> <sup>11</sup> Mg <sub>.60</sub> Fe <sub>.11</sub> <sup>111</sup> Ti <sub>.15</sub> Al <sub>.39</sub> ) <sub>2.57</sub> (Al <sub>1.28</sub> Si <sub>2.72</sub> ) <sub>4.00</sub> O <sub>9.54</sub> (OH) <sub>2.46</sub>	
B-60	(K <sub>.83</sub> Na <sub>.03</sub> ) <sub>.86</sub> (Fe <sub>1.30</sub> <sup>11</sup> Mg <sub>.60</sub> Fe <sub>.15</sub> <sup>111</sup> Ti <sub>.14</sub> Al <sub>.38</sub> ) <sub>2.57</sub> (Al <sub>1.30</sub> Si <sub>2.70</sub> ) <sub>4.00</sub> O <sub>9.56</sub> (OH) <sub>2.43</sub>	
B-75	(K <sub>.68</sub> Na <sub>.06</sub> Ca <sub>.02</sub> ) <sub>.76</sub> (Fe <sub>1.27</sub> <sup>11</sup> Mg <sub>.64</sub> Fe <sub>.13</sub> <sup>111</sup> Ti <sub>.08</sub> Al <sub>.37</sub> ) <sub>2.49</sub> (Al <sub>1.28</sub> Si <sub>2.72</sub> ) <sub>4.00</sub> O <sub>9.14</sub> (OH) <sub>2.86</sub>	
B-82	(K <sub>.85</sub> Na <sub>.03</sub> ) <sub>.88</sub> (Fe <sub>1.31</sub> <sup>11</sup> Mg <sub>.65</sub> Fe <sub>.13</sub> <sup>111</sup> Ti <sub>.14</sub> Al <sub>.41</sub> ) <sub>2.64</sub> (Al <sub>1.28</sub> Si <sub>2.72</sub> ) <sub>4.00</sub> O <sub>9.72</sub> (OH) <sub>2.28</sub>	
B-83	(K <sub>.85</sub> Na <sub>.03</sub> ) <sub>.88</sub> (Fe <sub>1.31</sub> <sup>11</sup> Mg <sub>.63</sub> Fe <sub>.10</sub> <sup>111</sup> Ti <sub>.12</sub> Al <sub>.44</sub> ) <sub>2.60</sub> (Al <sub>1.28</sub> Si <sub>2.72</sub> ) <sub>4.00</sub> O <sub>9.60</sub> (OH) <sub>2.40</sub>	
B-87	(K <sub>.70</sub> Na <sub>.05</sub> ) <sub>.75</sub> (Fe <sub>1.26</sub> <sup>11</sup> Mg <sub>.71</sub> Fe <sub>.12</sub> <sup>111</sup> Ti <sub>.08</sub> Al <sub>.46</sub> ) <sub>2.63</sub> (Al <sub>1.28</sub> Si <sub>2.72</sub> ) <sub>4.00</sub> O <sub>9.50</sub> (OH) <sub>2.50</sub>	

Table 12 -2

## Cordierite (to 18O)



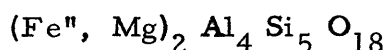
divalent cation for every tetrahedral Al in excess of the 1:3 ratio. Study by Foster (1960) of a large number of biotite analyses shows that aluminum in excess of 1Al:3Si is accommodated in this way and also by a mechanism which leads to less than full occupancy of the octahedral layer, with Si:Al near 3:1. Such substitution might be effected by random mixed-layering of phlogopite-type and muscovite-type units, as suggested by Foster, or by simple substitution of 2Al for 3(Fe, Mg) as suggested by Zen (1960, p. 136-137) for chlorite. Zen does not favour this suggestion, since it must lead to large local variations in bond energy. More than one mode of substitution is exhibited by single specimens. B-40, B-56, and B-82 show (OH) contents near the ideal and may be considered examples of this dual substitution, for octahedral occupancy is less than 3 cations/10 O and less than the ideal 3 Si/10 O are present. Not quite 1Al:3Si is required to accommodate the alkalis, since the interlayer sites are filled to only an average of 87% of capacity. This underfilling is even more obvious in the biotites coexisting with muscovite-albite (B-75, B-87), in which only about 75% of the interlayer positions are filled. This effect is clearly outside the limits of analytical error.

The hydroxyl of the analyzed biotites was calculated by assuming the difference between the total of the analysis and 100% to be H<sub>2</sub>O. The (OH) value is very sensitive to small errors in this total, thus the erratic variations in (OH) exhibited by the formulae possibly reflect error in the totals, dominantly negative, as it is unlikely that hydroxyl substitutes for other elements in the structure. The only element showing reciprocal variation is Al. In view of the analytical



difficulties with this element in biotite it is highly possible that negative error is present in the  $\text{Al}_2\text{O}_3$  values. It is evident in any case that there is considerable excess of aluminum over that required in tetrahedral coordination. It is to be expected that the content of Al in biotite coexisting with aluminosilicate should represent the maximum possible under the particular external conditions of metamorphism. If  $\text{Fe}^{\text{III}}$  is a primary constituent of the mineral, it may substitute for Al; whereas all  $\text{Fe}^{\text{III}}$  resulting from secondary oxidation must be represented as ferrous in the formula. The formula for B-56, which contains the most nearly ideal number of (OH), shows about the same approach to layer charge balance whether iron is represented as analyzed or all as  $\text{Fe}^{\text{II}}$ . The two possibilities therefore cannot be distinguished. The biotites analyzed are closer to siderophyllites than any other end-member.

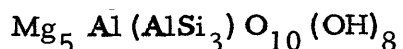
The ideal formula of cordierite is:



which may be derived from that of its analogue, beryl  $\text{Be}_3\text{Al}_2\text{Si}_6\text{O}_{18}$ , by substitution of 1Al:5Si in the hexagonal rings, each such substitution permitting a corresponding substitution of one Al for a divalent cation (Gossner and Mussgnug (1928)). The large channels parallel the c-axis are believed to accommodate  $\text{H}_2\text{O}$  molecules and alkalies (Folinsbee (1941)). Introduction of alkali requires a proportionate decrease in the number of other cations in order to maintain neutrality. Analyses of natural cordierites collected by Leake (1960) and experimental syntheses (Schreyer (1959)) show that most cordierites do not

deviate significantly from the composition  $(\text{Fe, Mg})\text{O}:\text{Al}_2\text{O}_3:\text{SiO}_2 = 2:2:5$ . Inspection of the cordierite formulae in Table 12 reveals that best agreement with the ideal structure is obtained if alkalis are considered to substitute for divalent cations, charge balance being maintained by a slight excess of Si over the ideal ratio and by  $\text{Fe}^{\text{III}}$  in divalent cation sites. This relationship consistently provides better agreement with the analyses than the hypothesis that alkalis are "stuffed" into the structure, which requires that some divalent cation sites be vacant. For example, if the Si:Al ratio is 4:5, the number of vacant divalent cation sites must equal exactly one-half the number of stuffed alkali atoms. Unless alkalis actually substitute for divalent cations, there is no reason why the number of vacant cation sites should exactly equal the number of alkali atoms. Whether such substitution of large cations for tetrahedrally-coordinated atoms could be accomplished in a stable structure is a matter for further investigation.

The chlorite formulae calculated in Table 8 may be compared with the Pauling (1930) formula:



Agreement with this model is obtained by correcting for muscovite. Aluminum is present in excess of that in the above formula, half the excess (with  $\text{Fe}^{\text{III}}$ ) being accommodated by replacement of divalent cations in octahedral coordination, half by replacement of tetrahedral Si, the content of the octahedral sites remaining constant. The structural formula so obtained is very similar to those published by Zen (1960), from low-grade regionally metamorphosed pelites in Vermont.

The large excess of aluminum shows that Al-for-Si is an important compositional variable which must be taken into account in paragenetic studies of chlorite-bearing rocks.

In summary, structural formula calculations show that no serious errors exist in the mineral analyses, except that Al may be low in most of the biotites. It will be apparent from the discussion to follow that such an error, if present, does not effect the major conclusions from the data.

## B. Graphical Presentation of Data

### 1. A-F-M plots

Figures 14(a) and 14(b) are A-F-M plots similar to those developed earlier in the thesis. Projection through quartz, K feldspar and ilmenite is employed. In each case, the projected points are calculated by subtracting the compositions of the projection points from the compositions of the plotted phases in an amount sufficient to bring them into the plane of projection. For example, in projecting through K feldspar,  $\text{Al}_2\text{O}_3$  and  $\text{K}_2\text{O}$  are subtracted in the ratio 1:1 until  $\text{K}_2\text{O} = 0$ . The projected  $\text{Al}_2\text{O}_3$  value is then  $\text{Al}_2\text{O}_3 - \text{K}_2\text{O}$ . The coordinates of the plots have been made orthogonal for simplicity, hence the "A corner" is at infinity, and the three-phase triangle Al-silicate-biotite-cordierite is not completed. "A" values for C 32 and C 43 are arbitrary. The plots are "compound" phase diagrams, as each tie line represents a different specimen formed under different values of the external variables. Each is the limiting tie line of a three (plus three)-field, shown schematically for a single assemblage in the corner of

Figure 14. Biotite-cordierite tie lines in the A-F-M triangle, projected through quartz, K-feldspar, and ilmenite. (a) All iron plotted as FeO.

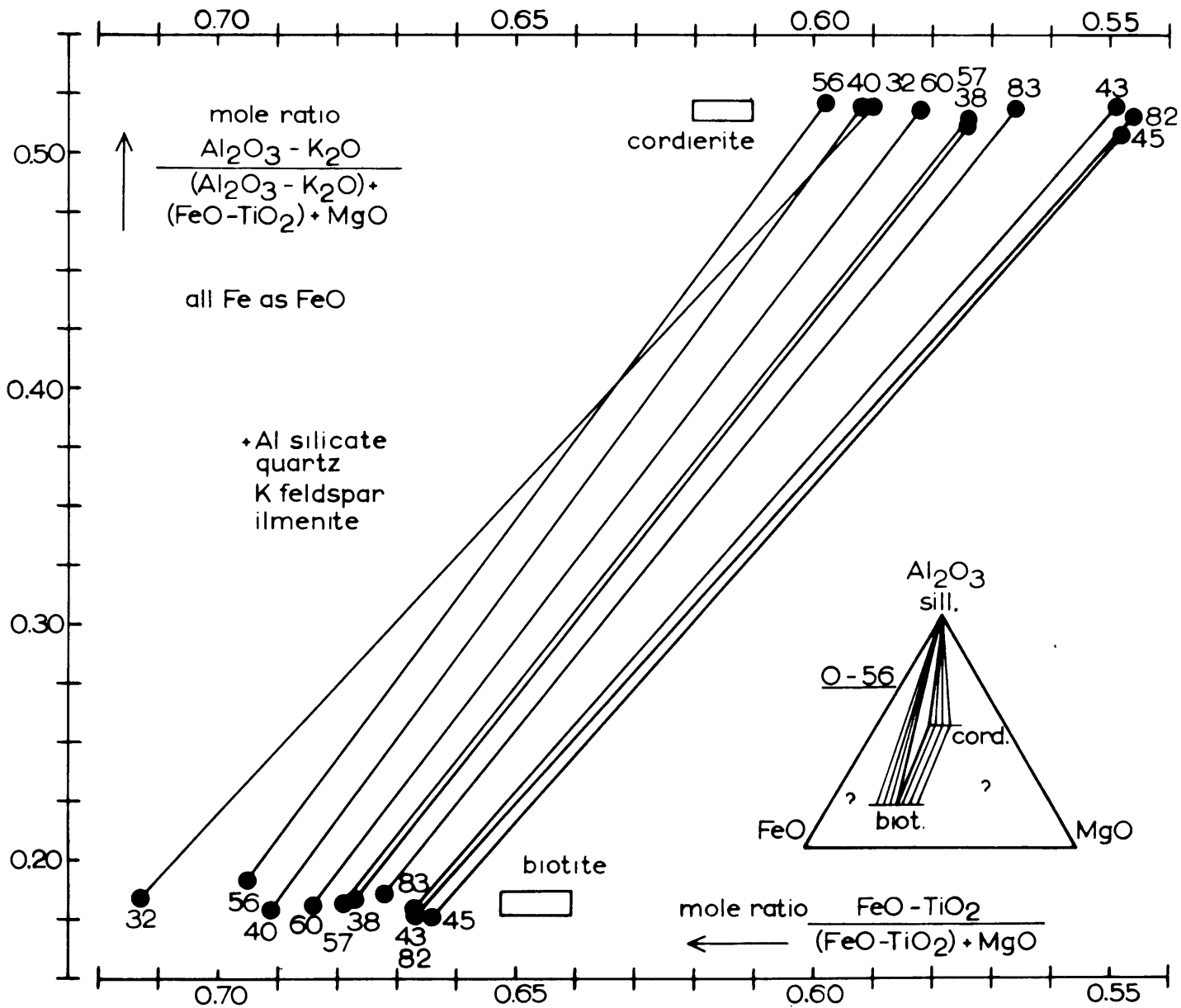


Figure 14(b). Analyzed FeO only plotted.

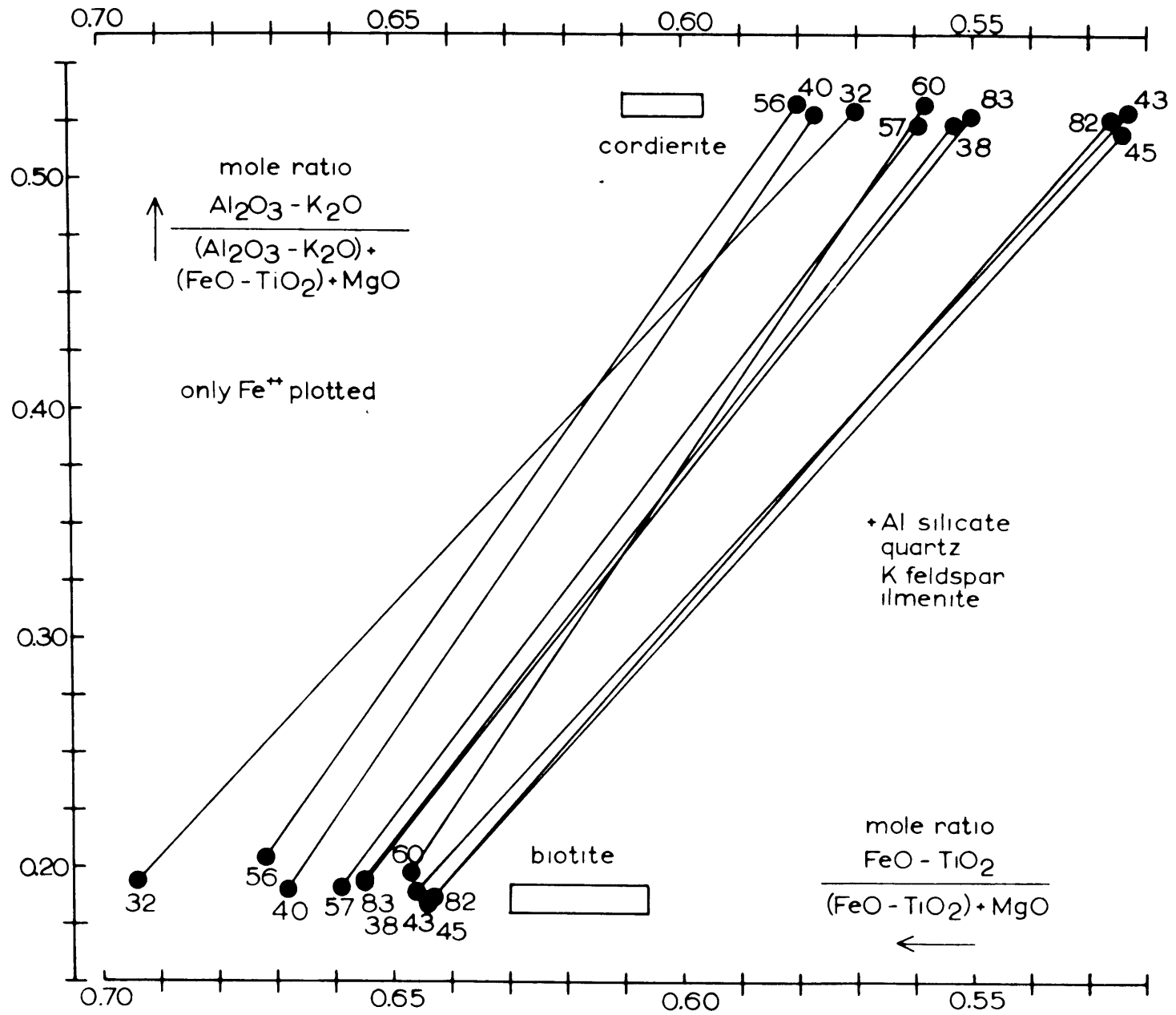


Figure 14a, hence the position of the tie lines is a function of external variables only. The boxes represent the maximum standard errors of the plotted ratios. Whether iron is plotted as all divalent or the FeO content only is represented, no tie lines are discordant within the limits of error except that for sample 0-32. The absence of crossing joins in Figure 14(a) seems to be highly coincidental if the indicated error is representative. A better explanation is that the error is overestimated. Two possible contributing factors are:

- a) The average precision of the total iron determination is much better than the worst estimate.
- b) No significant calcium is present in any of the phases plotted, hence the CaO precision error does not affect the MgO determination and should not be included in the error calculations.

All tie lines have sufficiently steep slopes that the small scatter in the points for each phase with respect to the aluminum variable is insufficient to induce discordant relations. Since the magnitude of the possible Al error is similar, such an error cannot significantly affect the array.

The general absence of crossing tie lines shows that equilibrium has been closely approached with respect to all significant compositional variables, at least at metamorphic grade above the K feldspar isograd. These variables are the substitution of iron and magnesium in cordierite, and iron, magnesium, and aluminum in biotite. Minor irregularities in the "A" coordinate value may be due to imprecision in the Al determination and/or to small variations in the position of the point of projection, as the mineral compositions are not controlled

with respect to bulk Na/K variations in the absence of a sodic phase. Na/K ratios are very consistent in the biotites, but less so in cordierite, so that the information is not conclusive in this respect.

The discordance exhibited by the 0-32 tie line cannot be a function of the external variables, since these will not result in the join crossing the rest of the array, as pointed out in section VI. Since no compositional variables exist in these phases which could induce the discordance, it is ascribed simply to disequilibrium in the assemblage. Since no other data are available from the Barren Mountain locality, no general conclusions can be drawn regarding the geographic extent of such a disequilibrium effect. The evidence of equilibrium throughout the Boarstone-Onawa area suggests that the conclusions drawn there should be applicable to the rest of the high grade part of the aureole.

If Figure 14 represents a group of equilibrium limiting tie lines, variations in external conditions should be reflected in shifts of these lines. As external variables are related to the intrusive contact, movement of the field Al-silicate-biotite-cordierite should also be so related. That this is so in a general way is shown by Figure 14(a). The order of decreasing temperature of formation of the plotted pairs, as nearly as can be deduced from geographic relation to the contact and from textural features, is (beginning at the contact): 0-40, 60, 38, 56, 57, 82, 83, 45, (43 and 32) (ending on the K feldspar isograd). It may be that this sequence is incorrect, in that the true distance to the contact may be less than the horizontal distance, or recrystallization favoured by high  $\mu_{\text{H}_2\text{O}}$  rather than high temperature. If the dis-

equilibrium tie line 0-32 is disregarded, the first five occupy the left (iron-rich) side of the diagram, and the last four are more magnesian. This distribution is not so well-defined in Figure 14(b). The conclusion is that the stability field shifts to the iron-rich side toward the contact, but that complications are present. Pairs of assemblages collected in fairly close proximity each show significant differences one from another, as between 0-38 and 0-40, 0-56 and 0-57, and 0-82 and 0-83. These differences are not consistent with the proposal of smooth gradients in the external variables. Possible explanations of this irregular shifting of the stability field will be presented in the discussion of metamorphic reactions to follow.

The distribution of ferrous and ferric iron between coexisting biotite and cordierite is illustrated in Figure 15. The large standard error with respect to the scale of the plot indicates that the differences in oxidation state amongst the pairs are barely significant; the nearly-uniform trend of the points in the diagram is more evidence that the precision error of the iron determinations has been overestimated, for data show that the iron in cordierite becomes more reduced with respect to that in biotite as the contact is approached. That there is no over-all oxidation or reduction in the ferromagnesian minerals relative to the intrusive is shown by the random scatter of ratios along the line representing zero fractionation of ferric iron. Trivalent iron in the analyzed minerals could be either a primary feature or a result of oxidation subsequent to equilibration of the assemblage during metamorphism. The systematic distribution shown by Figure 15, together with the near uniformity of ferrous/ferric ratio among the



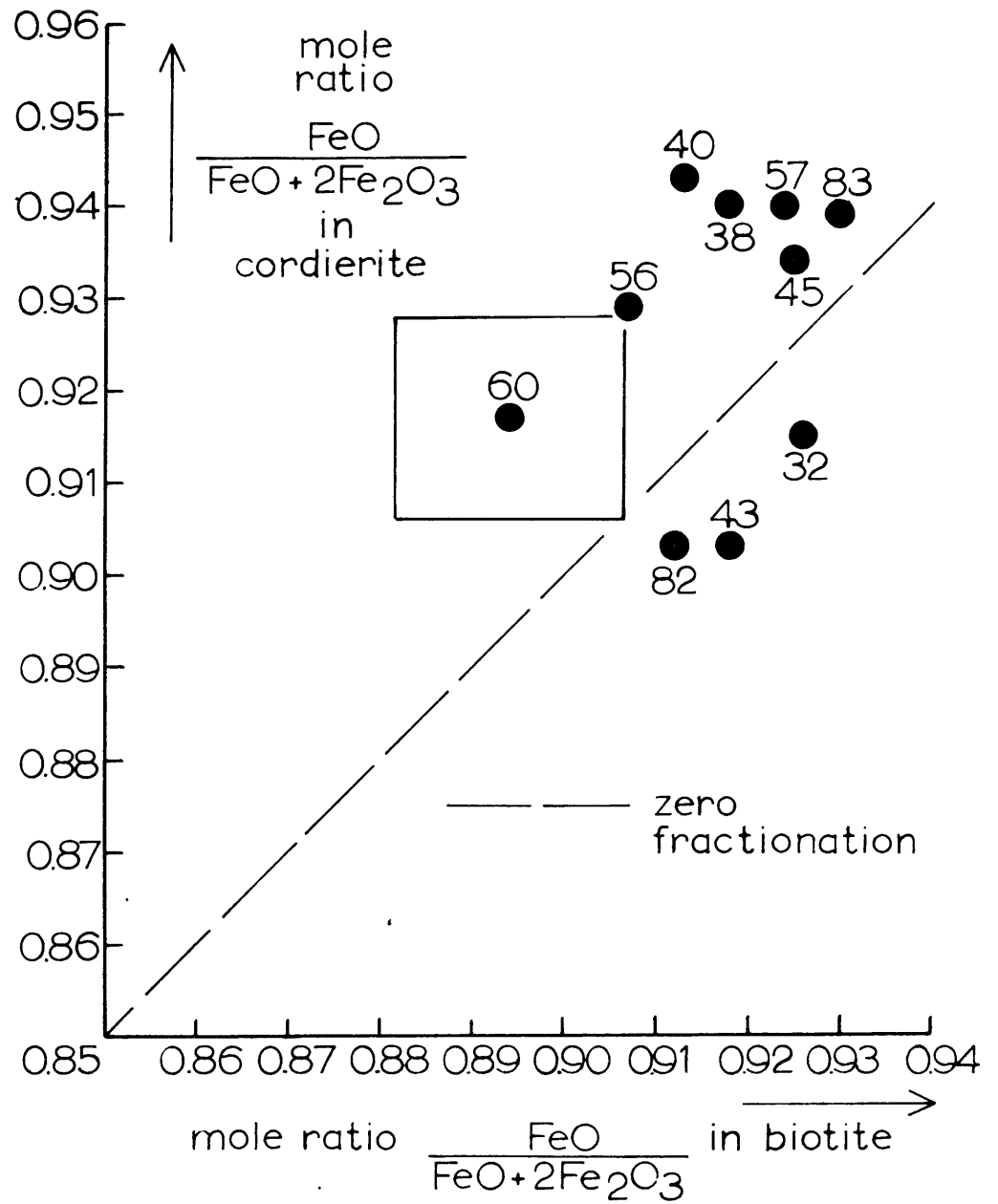


Figure 15. Oxidation state of iron in coexisting biotite and cordierite.

assemblages, suggests that the ferric iron is original.

If the system were open to oxygen during metamorphism, the over-all oxidation state of iron in the rocks is a result of an externally imposed  $\mu_{\text{O}_2}$ , whereas if oxygen were an inert component, bulk oxygen content determined the net oxidation state of iron. Small variations in  $\text{Fe}^{\text{II}}/\text{Fe}^{\text{III}}$  indicated by the mineral analyses may result from an approximate equilibrium with respect to an external  $\mu_{\text{O}_2}$  which does not change appreciably, or from small bulk variations with oxygen an inert component. Two other pieces of information bear on the role of oxygen:

- a) The nature of the oxide mineral assemblage: treatment of  $\text{Fe}_2\text{O}_3$  as an independent component (system closed to oxygen) permits two oxide minerals in the hornfels, for example magnetite and ilmenite. The presence of only one oxide, ilmenite, in the hornfels could thus be caused either by oxygen being mobile or by the solubility limit of ferric iron in the silicates not being exceeded.
- b) The most consistent graphical treatment: the plot of Figure 14(a), by treating all Fe as  $\text{Fe}^{\text{II}}$ , assumes either that all the iron was reduced at the time of equilibration of the minerals, or that the system was open to oxygen. Evidence has been presented to show that the  $\text{Fe}^{\text{III}}$  is primary, thus the more consistent relations of the joins in 14(a) with respect to 14(b) might be interpreted as supporting the thesis that  $\mu_{\text{O}_2}$  is externally controlled. However, since the plot of 14(b) is not proven to be significantly less consistent, such a conclusion is not firmly based.

In summary, several small points of evidence support the conclusion

that oxygen must be treated as a mobile component in the assemblages plotted in Figure 14, whereas no evidence contradicts this proposal.

Eugster (1959) points out that diffusion of hydrogen is possibly the most important process governing both hydration-dehydration and oxidation-reduction reactions in metamorphism. If the oxygen content of the system is not free to change, but hydrogen is mobile,  $\mu_{\text{H}_2\text{O}}$  and  $\mu_{\text{O}_2}$  will both be defined by  $\mu_{\text{H}_2}$ ,  $p$ , and  $T$ . If oxygen is also mobile, then  $\mu_{\text{O}_2}$ ,  $\mu_{\text{H}_2}$ ,  $p$ , and  $T$  define  $\mu_{\text{H}_2\text{O}}$ . Should a vapor phase be present, unless it has exactly the composition  $\text{H}_2\text{O}$  reactions involving change in the water content of the assemblage must also be redox reactions.

In Figure 16, a number of compositions are plotted on the A-F-M projection through quartz, muscovite, and ilmenite, expressing all iron as FeO.

The position of the slate in the plot is misleading, as sodium is not taken into account. The calculation of Table 9 shows that all the Al of the slate is accommodated in chlorite, muscovite, and albite. Thus the slate composition, projected through the opaque phase, is essentially coincident with the chlorite composition in the A-F-M plot. If chlorite in the slate was capable of only restricted compositional variation, such coincidence would be unlikely; the more valid interpretation is that chlorite occupies a large field in the plot throughout which its composition is entirely dependent on the bulk composition. No coexisting Al-silicate such as pyrophyllite or andalusite is thus permitted in the analyzed slate, although with increasing bulk Al the solubility limit in chlorite will eventually be exceeded and some more

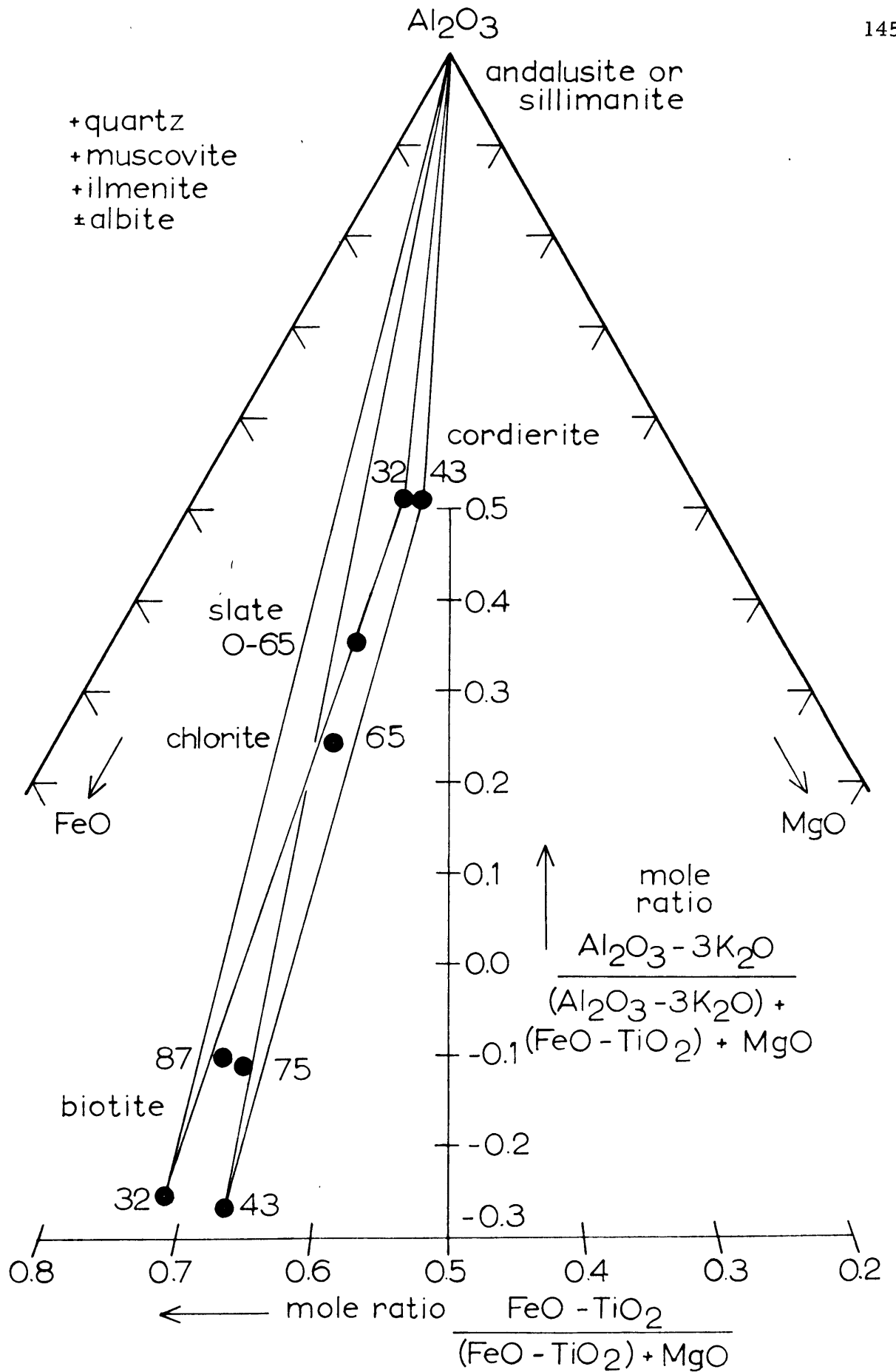


Figure 16. Compositions of biotite, cordierite, chlorite, and slate in the A-F-M triangle, projected through quartz, muscovite, and ilmenite, all iron plotted as FeO.

aluminous mineral must appear in the assemblage.

The presence of relict andalusite in the slate shows that the solubility limit of Al in chlorite was exceeded. Either local variations in composition toward higher Al than the bulk value promoted formation of andalusite, or the retrograde reaction which destroyed the andalusite involved the total rock. In the latter event, the Al content of the analyzed chlorite is higher than the prograde equilibrium value.

The tie lines from 0-32 and 0-43 may be plotted also on the A-F-M projection through quartz, muscovite, and ilmenite, since both muscovite and K feldspar are members of the assemblage. These joins represent the approximate limits of compositional variation of all the pairs analyzed. If equilibrium was attained, the bulk composition of the assemblage must fall within the stability field of the coexisting phases. It is thus of interest to note that the bulk composition of slate 0-65 in Figure 16 (best indicated by the position of the chlorite composition) is nearly within all the three-phase triangles determined. As a consequence, no significant compositional changes are required to produce the potassic feldspar-bearing hornfelses from slate of the same composition as that one analyzed.

The compositions of the biotites from below the K feldspar isograd plot nearer the A apex because of lower potassium, rather than higher aluminum, contents. These lower-grade biotites are lower in  $\text{TiO}_2$  and in Fe, so that the points of projection are not significantly different from those above the isograd. These compositional changes are coincident with the change in biotite color and opaque habit observed petrographically.

## 2. Distribution of manganese

Figure 17 is a distribution diagram illustrating the substitution of manganese for total iron as FeO in coexisting biotite and cordierite. Mn undoubtedly substitutes for Fe<sup>2+</sup> and Mg, because of similar size and valence; since the composition of the host mineral with respect to these elements varies over only a small range, the diagram has the same appearance whether Mn only, Mn/FeO, or Mn/(FeO+MgO) is plotted. The Mn content of the phases is a function of the bulk Mn composition of the rock, since the system is not controlled with respect to Mn variations. Unfortunately, the range of concentrations is not sufficient to indicate to what extent the solution is ideal; variations of the distribution are significant, as indicated by the size of the error box, but are small except in the case of 0-32. This variation is related neither to grade nor concentration, nor does it correlate with the position of the tie lines of Figure 14. The conclusion is that a significant, but small departure from an equilibrium distribution is present, reflected in a relative error in the average distribution coefficient (not including 0-32) of about  $5\frac{1}{2}\%$ . This deviation from equilibrium is much larger than that of the Fe/Mg distribution. The marked anomaly in the case of 0-32 is more evidence that this assemblage was never close to chemical equilibrium.

## C. Metamorphic Reactions in the Onawa Aureole

### 1. Prograde reactions

Having discussed the features of the sequence of assemblages constituting the aureole, it is now possible to deduce some of the relations

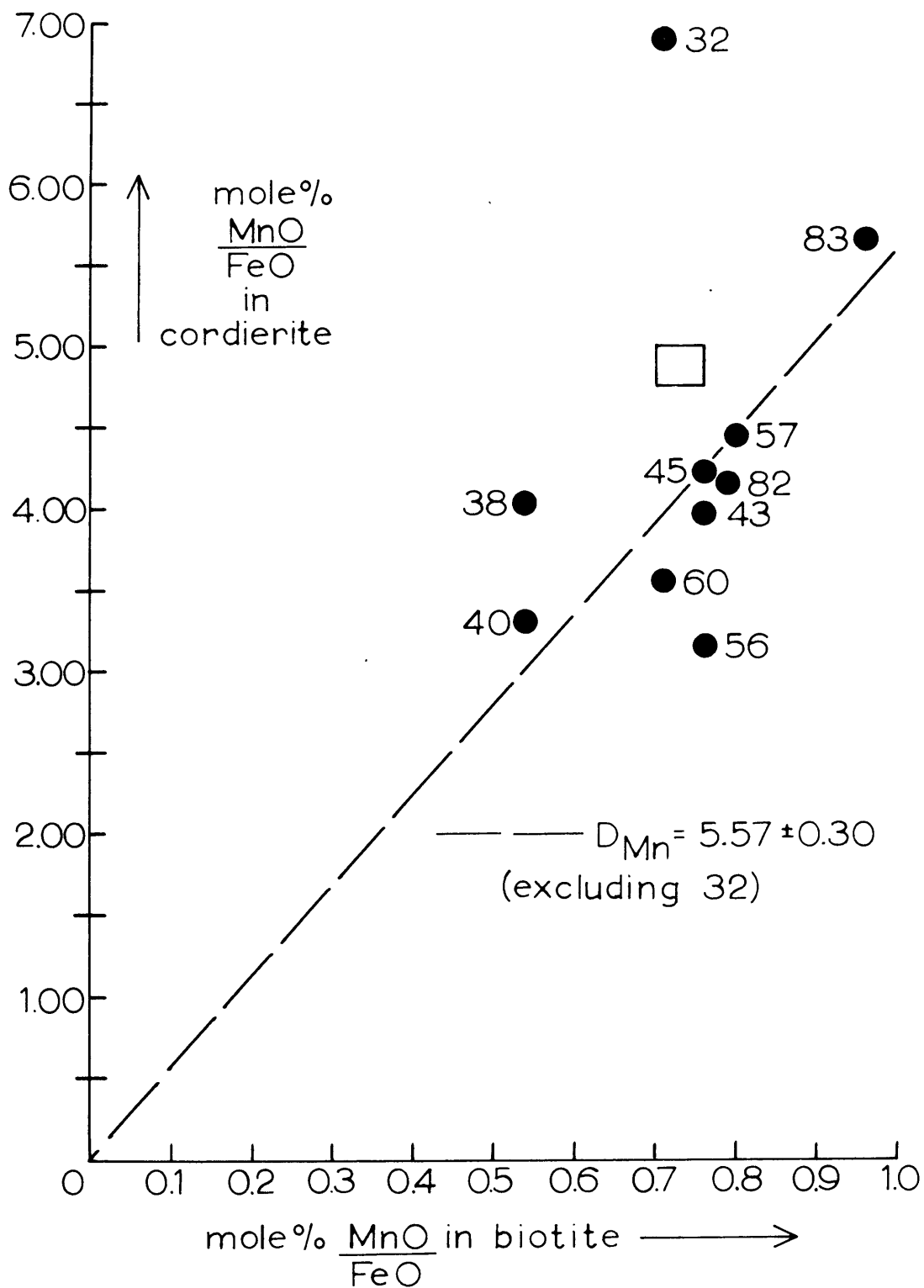


Figure 17. Distribution of manganese between coexisting biotite and cordierite.

between them, that is, the sequence of reactions with increasing metamorphic grade, i. e., toward the contact. Since little chemical data is available for the lower grades, the proposals for these rocks must rest mostly on petrographic observation. The prograde reactions are most easily illustrated on A-F-M plots as developed above, considered as projections through quartz and muscovite (Figure 18). As previously explained, these plots assume either that water is present as the pure phase or that  $H_2O$  is a mobile component, and that either all the iron is divalent or that oxygen is a mobile component. Each mobile component involved in a reaction increases the degrees of freedom of the system by one, so the terms "univariant" and "divariant" used in the discussion to follow actually refer to the internal or compositional variables plus  $p$  and  $T$ , and thus mean " $(1 + c_m)$  variant" and " $(2 + c_m)$  variant" respectively. Alternatively, these terms can be stated with the qualification: "at constant chemical potentials of the mobile components."

The slate assemblage:

quartz-chlorite-muscovite-albite (e. g., 0.3, 0.66)

is illustrated in Figure 18(a). The limits of the chlorite field cannot be determined in the Onawa area, since bulk composition variations are not so great that other assemblages appear in the slates. This compositional uniformity is a hindrance to "filling in" the composition triangle at all metamorphic grades of the aureole. The plot 18(b), taken from Zen (1960, p. 160) illustrates the range of assemblages possible in slates and phyllites with greater variations in composition. The first contact metamorphic reaction observed results



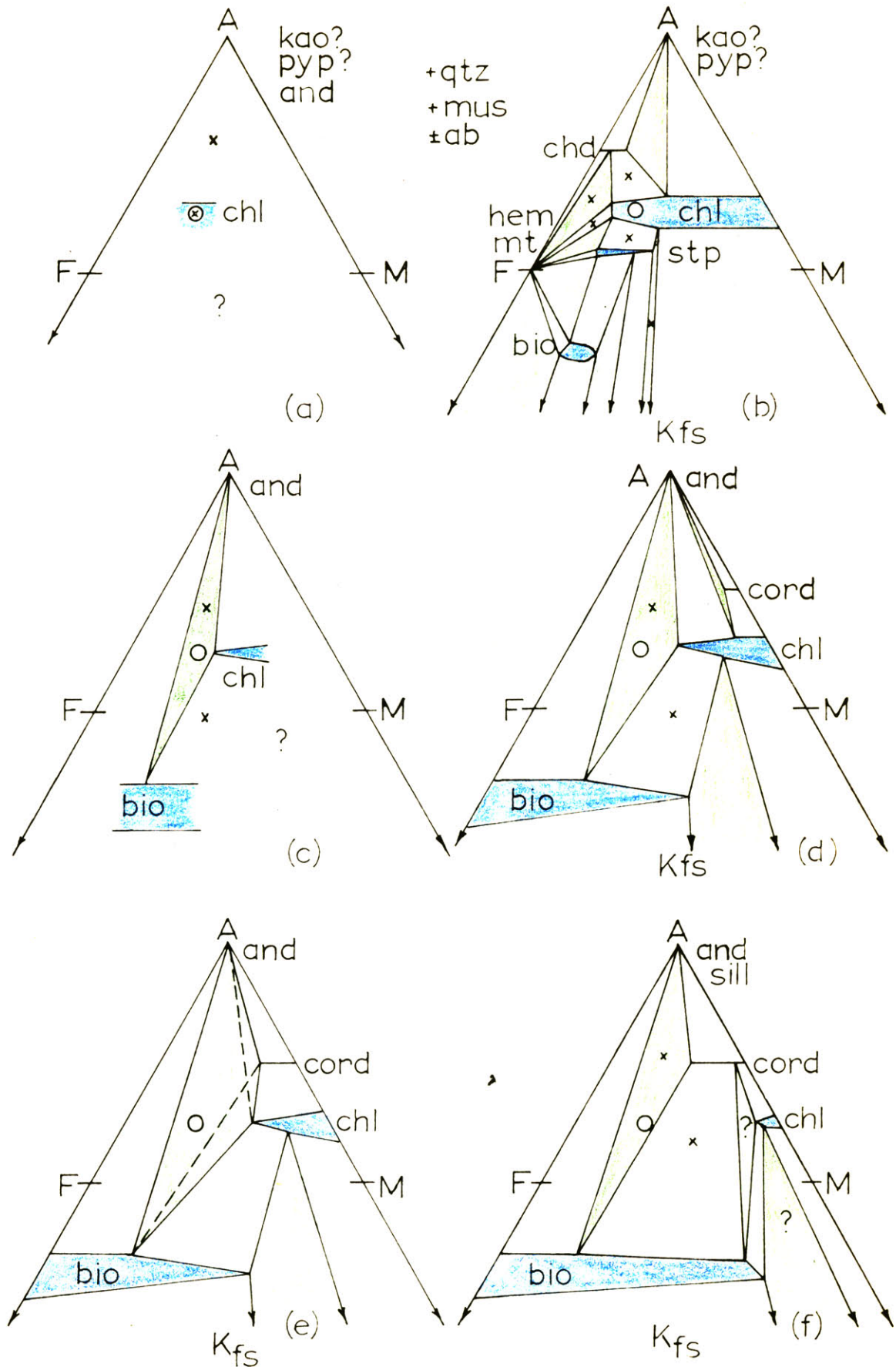
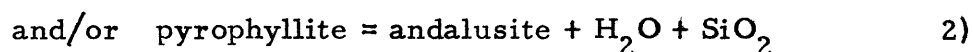
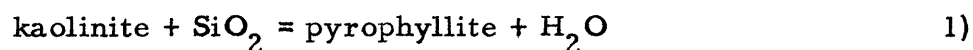
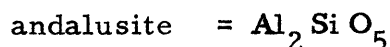
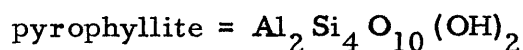
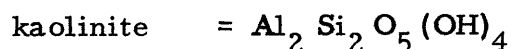


Figure 18. Suggested prograde assemblages in pelitic hornfels  $A = Al_2O_3$ ,  $F = FeO$ ,  $M = MgO$ . Open Circle: composition of 0-65. x: observed assemblage. Blue: one phase. White: two phases. Green: three phases.

in the appearance of andalusite in 0-65, represented by a single relict chiastolite. Since the analyses show that no excess of aluminum is present in this slate, a local compositional anomaly may be present such that a small volume of the slate falls in the field chlorite-andalusite 18(a). The reactions:



where

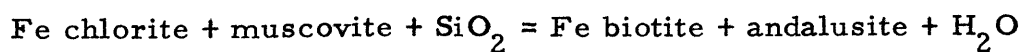


take place at the "A" apex with increasing grade from slate to chiastolite slate; the stability limits of the chlorite may change continuously.

The assemblage:

quartz-biotite-andalusite-chlorite-muscovite-albite (0-69)

requires a configuration similar to 18(c), if biotite is assumed to be more iron-rich than the coexisting chlorite. The distinct red-brown color of the earliest-formed biotite could be due to either extremely high iron content or to high Ti (Hall, 1941). Since Ti in the biotite is seen to increase with metamorphic grade, and higher-grade biotite than that coexisting with chlorite is not red, the color is more likely due to high Fe content. The first appearance of biotite in the diagram, if the simple configuration of 18(c) is correct, must be on the left-hand (pure Fe) edge, as a result of the reaction:



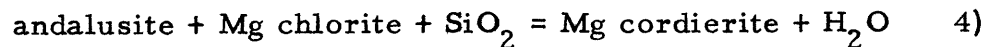
3)

This reaction is univariant (five phases and four inert components if  $H_2O$  is mobile. Note that quartz and muscovite are "in excess" and may participate in all reactions). However, the first appearance of biotite in the system under consideration results from a decrease of the solubility limits of iron in biotite and chlorite so that the bulk composition falls within the triangle andalusite-chlorite-biotite of 18(c). The reaction resulting in the shift of this stability field is the same as that given above except that it involves Mg, hence must be divariant. The first appearance of biotite in the system is thus dependent upon the bulk composition, as is apparent from the diagram.

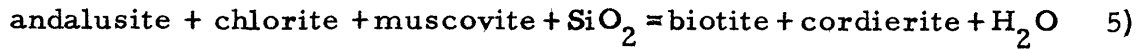
The next higher grade assemblage is:

quartz-andalusite-biotite-cordierite-muscovite-albite (e. g., 0-52, 0-87) (cordierite represented by "spots" in low-grade specimens)

There is no petrographic evidence of the stable coexistence of cordierite and chlorite, although such assemblages must exist at appropriate bulk compositions, and a chlorite-biotite-cordierite isograd must intervene between parageneses of 0-69 and 0-52. Observation of these reactions is prevented by lack of sufficiently magnesian specimens and by retrograde reactions, but one probable scheme, in which the cordierite is more magnesian than the coexisting chlorite, is illustrated in 18(d) to (f). Cordierite appears on the magnesian side of the diagram by the reaction:

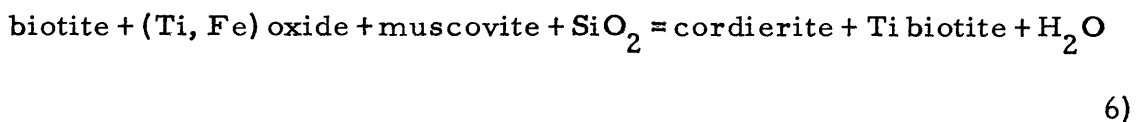


Thereafter, the assemblage cordierite-andalusite-chlorite is visible in sufficiently magnesian rocks (18(d)). The appearance of cordierite in andalusite-bearing pelites comes about as a result of the reaction:



represented by the shift of the join andalusite-chlorite to biotite-cordierite. Compositions so low in Al or high in Mg as to be below the new join will produce the new assemblage cordierite-biotite-chlorite. At the reaction point (isograd) three ferromagnesian coexist; the joins must be lines rather than fields because all compositions are unique. Since  $c_i + 1$  phases coexist, the position of this reaction is independent of bulk composition; it is univariant. If water is mobile then the reaction takes place at a given T for given values of p and  $\mu_{\text{H}_2\text{O}}$ . The diagram has the configuration on the upgrade side of all higher-grade assemblages in the aureole, provided that the chlorite field shrinks toward Mg so that chlorite-bearing assemblages are no longer observed. 18(f) illustrates this result.

The following reactions, none of which affect the mutual arrangement of the stability fields, may take place with increasing grade:



This reaction is an approximation and cannot be illustrated on the A-F-M plot. It describes the increase in Ti, Fe and K observed in comparing the analyses of B-75 and B-87 with those of the higher grade biotites. It is certain that the increase in redness is primarily a result of increased Ti, and the correlation of the color change with the change in opaque habit indicates that the opaque mineral is participating in the reaction. As the opaques on each side of the reaction are identical in X-ray powder pattern, it is most logical to assume that

the reaction is a divariant one representing the extension of the solubility limits of Ti and Fe in biotite. Consequently it is necessary that cordierite become more iron-rich and that muscovite and oxide mineral decrease in quantity. If the identity of the opaque actually changes across the reaction, a redox reaction is likely, suggested by the following megascopic observation: coincident with the change from platy to rounded opaque is a change from cordierite which forms black spots on the weathered surface to cordierite which weathers to rusty pits. Cordierite free of inclusions does not weather appreciably, for spots are not apparent on the weathered surface of hornfelses with inclusion-free cordierite (0-82 and higher-grade). The color of the weathering product shows that the iron is dominantly oxidized. As opaque inclusions are prominent in cordierite at low grade, the difference between rusty and dark spots possibly reflects a difference in the original oxidation state of iron in the opaque, the lower-grade assemblage being dominantly ferric and thus stable at atmospheric conditions. A qualitative test showed that both higher- and lower-grade opaques contain some ferric iron, so no definite conclusion can be made. The reduction of ferric titanium oxide to ilmenite is a possibility. If oxygen is mobile, it is not necessary that the reaction balance, but the oxidation of graphite may be concomitant, as fine opaque material is not generally visible in higher-grade assemblages. It is not clear whether or not the change in potassium content of the biotite is related to the above reaction or to the appearance of potassic feldspar (see below). The change in habit of andalusite which takes place at about the same grade as reaction 6) appears to be an adjustment

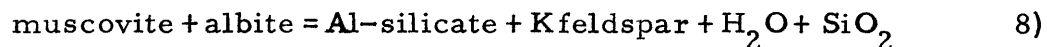
to the higher grade (changing surface energies of the minerals with respect to one another). The pink tinge in this mineral is probably an indication of increasing ferric iron content at higher temperature. (Macdonald and Merriam (1938) found that pleochroic andalusite color variation from almost clear to deep pink parallel to X correlated with variation in  $\text{Fe}_2\text{O}_3$  from 0.51 to 2.44%.)

The reaction:



follows with increasing grade. The first fibrolite observed is in a sample not containing K feldspar (0-79). Though this reaction never goes to completion in the aureole (andalusite persists to the intrusive contact), sillimanite is undoubtedly the stable aluminosilicate from its first appearance up to the contact. The inversion is dependent only on p and T, since none of the possible mobile components are involved.

The K feldspar isograd is represented by the reaction:



The K feldspar is microcline microperthite, interpreted as an originally homogeneous phase. There is no guarantee that the stable feldspar was microcline, for an inversion of orthoclase to microcline may have occurred with falling temperature in the late stages of metamorphism. The albite of the intergrowth is assumed to result from exsolution of Na with falling temperature. If no Na were present, the reaction would be written without albite. This reaction may be illustrated in an A-K-N plot, in which the compositions of aluminosilicate, micas and feldspars (without Ca) are represented, projected through quartz and

water (Figure 19). The compositions of the coexisting muscovite and albite were determined from the analytical and X-ray data on the slate; the bulk composition of the microcline microperthite is not known, but is illustrated schematically according to the findings of J. B. Thompson, Jr. (lectures, 1959). The approximate composition of the Onawa pelites with respect to the phases in the projection is also plotted. Since the isograd must be at higher temperature than that of the slate assemblage, the limits of solubility of Na and K in muscovite and albite are probably somewhat higher than illustrated. It is possible that a very narrow field of paragonite, the Na analogue of muscovite, could be present on the right hand side, separated from the observed assemblage by the join Al silicate-albite. In no samples studied is the alternative join muscovite-paragonite represented. It must be concluded that the stability limit of all but very pure paragonite is definitely exceeded in the area. At the reaction point, two feldspars plus muscovite are coexistent; this assemblage is not positively detected because untwinned albite is difficult to distinguish petrographically, and because the albite intergrown with microcline obscures the X-ray pattern of any prograde albite coexisting with K feldspar. Depending upon the position of the two-phase field Al silicate-microcline relative to the bulk composition, K feldspar-bearing assemblages above the isograd may be:

Al silicate-muscovite-microcline

Al silicate-microcline

Al silicate-microcline-albite

Only the second assemblage is verified by observation except near

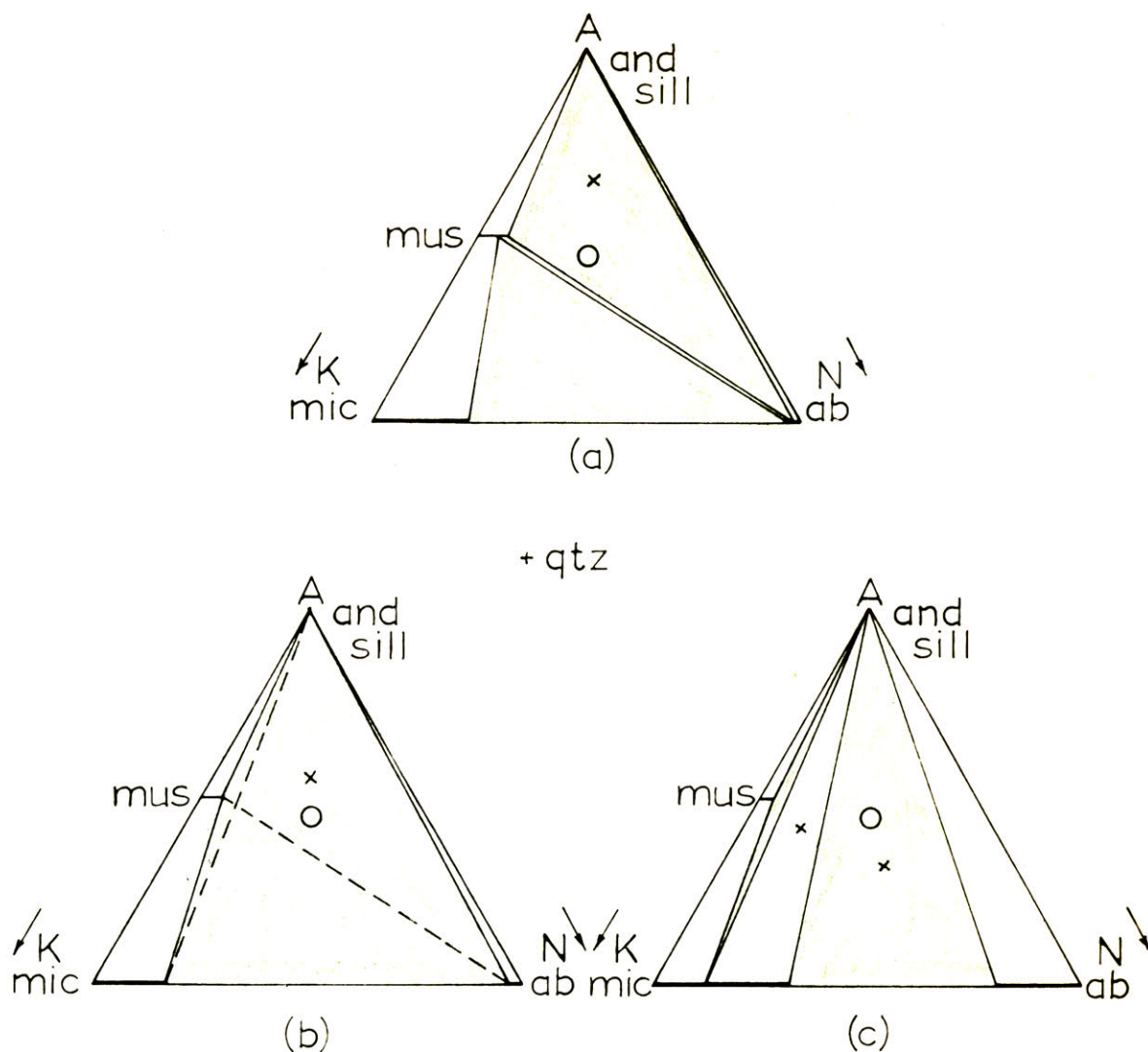


Figure 19. Mica-feldspar assemblages across the K feldspar isograd  
 $K = K_2O$   $N = Na_2O$  mic = Microcline ab = albite.

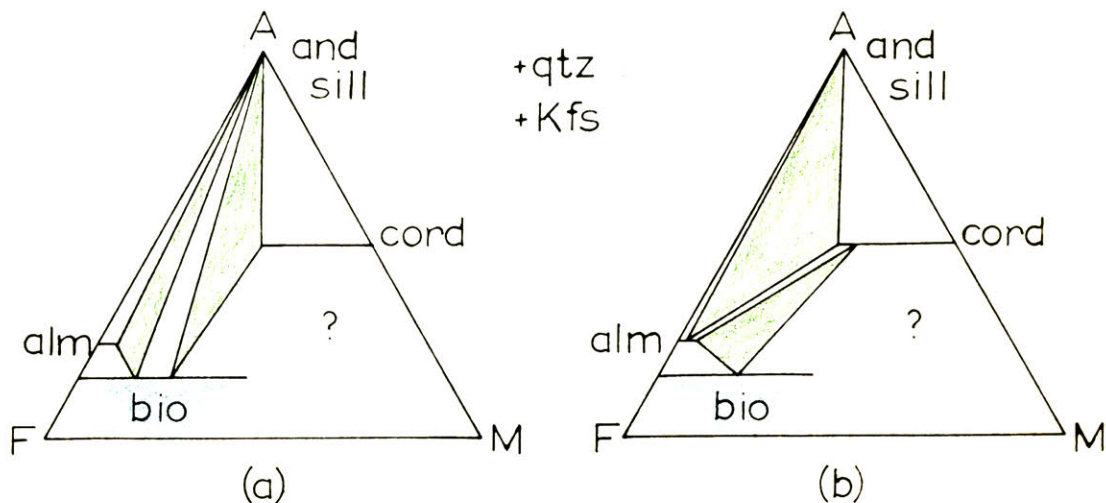


Figure 20. Reactions involving almandite garnet (=alm) in hornfels.



the contact, where zoned and twinned albite appears with the K feldspar. Due to the reasons mentioned above, albite may pass unnoticed in some assemblages. As the reaction 19(b) illustrates the K feldspar isograd, this isograd represents a lower temperature (at given  $\mu_{\text{H}_2\text{O}}$ ) than the maximum stability limit of muscovite with quartz (disappearance of the muscovite field on the left-hand side of the diagram).

The position of the bulk composition point suggests that the two-feldspar assemblage should be the dominant one, but solid solution of Na in the potassic feldspar may be more extensive than illustrated, and progressive destruction of biotite with increasing grade (see below) renders the bulk feldspar composition progressively more potassic.

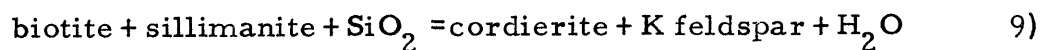
The aluminosilicate resulting from the proposed reaction is not obvious in thin section, but is represented in part by the retrograde muscovite. If the change in K content of the biotite is part of the reaction, it is more complex than illustrated.

The position of reaction 8) with respect to reaction 7) is subject to reversal with decrease in  $\mu_{\text{H}_2\text{O}}$ , since the temperature of dehydration will be decreased, while that of the aluminosilicate inversion remains constant. Thus a good petrographic indicator of  $\mu_{\text{H}_2\text{O}}$  variations is suggested; this is unfortunately rendered largely useless by the sporadic occurrence of fibrolite, a reflection of the very slow rate of reaction 7).

Above the isograd, the projection through K feldspar must be employed. The arrangement of the stability fields on the A-F-M plane and the observed ferromagnesian-aluminosilicate assemblages remain the same as in Figure 18(f), but the appearance of the diagram is

changed as a result of the new projection point, so that the plot is as shown in the schematic diagram of Figure 14(a). The A-K-N diagrams show schematically the actual points of projection through muscovite and K feldspar; though they depart significantly from the A-K line, they must move continuously with changes in the external variables provided that they represent the limiting Na content. Points of projection in the two-phase fields will introduce no inconsistencies only if bulk Na/K does not vary significantly among the assemblages compared.

Movement of the three-phase field cordierite-biotite-sillimanite necessitates the divariant reaction:



which must go to the right with increasing grade. Because biotite is more iron-rich than the coexisting cordierite, the cordierite must become more iron-rich with increasing grade. The restrictions on the movement of the limiting tie line further necessitate that the biotite become more iron-rich also. Thus the shift of the tie lines toward more iron-rich compositions as the contact is approached is in accord with the theory, and only the irregularities in this shift require special consideration.

As previously stated, metamorphic grade as defined by dehydration reactions increases with increasing temperature and decreases with increasing  $\mu_{\text{H}_2\text{O}}$ . Further, the above reaction involves a change in oxidation state, the left hand side being favoured by increasing oxygen pressure (or  $\mu_{\text{O}_2}$ ). Increasing total pressure strongly favours the

left hand side also because the reactants are much denser than the products. It has been suggested above that  $T$ ,  $\mu_{\text{H}_2\text{O}}$ , and  $\mu_{\text{O}_2}$  may all be related to the intrusive contact. Whether or not water and oxygen are perfectly mobile components, reversals of reaction 9) may be expected in the presence of a continuous temperature gradient. For example, if  $\text{H}_2\text{O}$  and  $\text{O}_2$  were mobile and all gradients were negative away from the contact, the temperature effect is counteracted by the effects of  $\mu_{\text{O}_2}$  and  $\mu_{\text{H}_2\text{O}}$ , thus local changes in the gradients may drive the reaction to the left or right. If the system were closed to all components, such shifts would occur with bulk variations in  $\text{O}_2$  and  $\text{H}_2\text{O}$  in the "intergranular phase." The dominant shift toward more iron-rich compositions ("cordierite forming at the expense of biotite") shows that the effect of the temperature gradient is not annulled by other variables.

This reaction illustrates the importance of taking into account the mineral assemblage when interpreting compositional changes in minerals in terms of metamorphic grade. Biotite coexisting with magnetite and potassic feldspar becomes more magnesian with increasing temperature at constant total pressure =  $p_{\text{H}_2\text{O}}$ . (Wones and Eugster (1959)).

An alternative explanation of the irregularities in the movement of the biotite-cordierite joins is patterned after that of Phinney (1959) to explain apparent disequilibrium in regionally metamorphosed pelites. It is possible that the two ferromagnesian are in mutual equilibrium in each assemblage, but are not in equilibrium with the aluminosilicate. This suggestion is supported by petrographic evidence of lack of

equilibrium between the ferromagnesian and fibrolite; the metastability of andalusite will not affect the other equilibria, but its presence testifies to the extreme sluggishness of reactions involving aluminosilicates. If the radius of diffusion of the inert components is very small, the low abundance of Al-silicate could also account for its not being a member of the stable assemblage. The consequence would be that the compositions of biotite and cordierite are not controlled in the assemblage, and would vary throughout the sample with bulk variations. The most iron-rich composition would be observed very close to the Al-silicate grains, and would represent the true limiting tie line, whereas many small volumes would contain an assemblage without Al-silicate, in which the position of the join would be displaced toward more magnesian compositions according to the bulk composition of the volume. The tie lines of Figure 14 would then each represent average values. To obtain a consistent configuration such as Figure 14 in such a situation would require that the slope of the tie lines in the two-phase field biotite-cordierite not change significantly over the range of grade represented by the samples, otherwise joins close together on the diagram, i. e., of similar average composition, but of different grade, would cross. Variation in the position of the tie lines would be correlated with average bulk composition as well as with grade, the most iron-rich tie lines tending to occur in the samples with the most Al-silicate and having the highest iron contents. Proof of this suggestion would require bulk composition data for all the samples. It may apply to 0-40

and 0-60, both of which have less Al silicate than the other samples and are more magnesian than would be expected from their location relative to the pluton. Reactions leading to higher-grade assemblages than those of Figure 14 are not proposed, since such parageneses were not observed in the aureole. The only higher-grade assemblage:

plagioclase-hypersthene-spinel-cordierite-biotite-microcline was observed in a xenolith. It cannot be compared with the others since it represents a quartz-free, highly calcic system. Probably the bulk compositional differences between this xenolith and the rocks of the aureole are due to metasomatic exchange with the melt.

The aplitic veinlets which are common in the inner hornfels of the aureole contain the same phases as the hornfels, but with a preponderance of quartz and microcline microperthite. The reason for these concentrations is not obvious. They were termed "injection veinlets" by Philbrick, but their discontinuous nature and wide distribution suggest that they were derived from the host rock. This suggestion is supported by the petrographic evidence of mafic enrichment in the walls of the veinlets, but could only be proven by statistical sampling and chemical analysis of hornfels with and without injection veinlets. It is possible that the veinlets are the result of partial fusion of the hornfels. If so, the veinlets represent nearly the minimum melting fraction in the system. This liquid would be of approximately the same composition as the minimum in the "granite" system studied by Tuttle and Bowen (1958). Thus modal analysis of the veinlets, together with determination of the bulk

composition of the feldspar, might be sufficient to shed light on their origin.

The apparent replacement of biotite by fibrolite is not explained by any of the proposed reactions. However, biotite is destroyed with increasing temperature, and sillimanite is forming by inversion of andalusite. It may be that biotite forms a favourable host for the formation of new sillimanite. Reaction along grain boundaries would be facilitated by the presence of water, well known to increase the rate of many silicate reactions (Tuttle and Bowen (1958)).

## 2. Retrograde reactions

Retrograde metamorphic reactions are the reverse of the prograde reactions in that they proceed with falling temperature or rising  $\mu_{\text{H}_2\text{O}}$  and involve hydration in most instances. The products may not be identical to the reactants of the prograde reactions because the retrograde reactions often do not go to completion and because the final state may be different than the premetamorphic state. In the case of the Onawa pluton the initial prograde reactions proceeded in a relatively "wet" environment, and the retrograde reactions took place in the less hydrous hornfelses. Only where water was available did excessive hydration take place with falling temperature, as evidenced by the formation of chlorite and white mica in three environments:

a) Adjacent to the contact, where water expelled upon crystallization of the intrusive was available. All minerals of the hornfels except quartz and opaque show evidence of replacement by chlorite and sericite.

b) In the fissile rocks of the outer part of the aureole. The inner limit of chlorite-muscovite replacement of cordierite coincides with the outer limit of the hornfels texture. It is apparent that the hornfels was dehydrated and rendered sufficiently impermeable by recrystallization that the relatively anhydrous assemblage was preserved, even though lower grade assemblages must have become stable as temperature decreased. The andalusite slates, with a high degree of preferred orientation and much greater grain boundary surface, permitted diffusion of water from the country rock. The extent of retrograde reaction becomes greater as the outer edge of the aureole is approached, an observation in accord with the theory that the slates were the source of water. Reaction of andalusite to form chlorite plus muscovite shows that the radii of diffusion of the inert components are about as great in the retrograde process as in the prograde metamorphism. The extensive hydration of the outer part of the aureole suggests that water expelled from the hornfels was concentrated in the immediate country rock, and thus argues for a chemical potential gradient of water away from the intrusive.

c) Locally throughout the hornfels, probably near fracture systems carrying volatiles from the intrusive. Replacement of cordierite by muscovite is prominent in these areas. The common minor replacement of biotite by muscovite need not involve hydration.

It is obvious that all the retrograde reactions are complex, involving most or all of the components of the system, although the only bulk chemical change definitely required is in the water content. The retrograde reaction of cordierite may merely be the reverse of prograde

reaction 5). Comparison of the analyses of biotites 0-75 and 0-87 shows that no radical change in biotite composition accompanies this retrograde transition. To determine the extent of equilibrium in the retrograde processes and to properly represent the parageneses would require a more detailed compositional study such as was applied to the higher-grade hornfelses.

### 3. Comparison with other localities

Metamorphism of pelitic sediments at intrusive contacts has been studied in many localities and numerous petrographic accounts are available. The classic work is Rosenbusch's (1877) study of the metamorphism of the Steiger Schiefer around the Barr-Andlau granite. Subsequent treatments of well-known aureoles involving pelitic rocks include those of Rastall (1910) on the Skiddaw slates; Goldschmidt (1911) on the Kristiania area; and Tilley (1924) on the diorite aureole at Comrie in the Perthshire Highlands. Harker (1950, pp. 25-26) lists a number of descriptions of British localities. All the assemblages characteristic of the Onawa aureole have been observed elsewhere, and numerous reactions have proposed to explain them.

Descriptions of "spotted slates" are common, but this term has been applied to a multitude of different mineralogical and textural features. The term "Knotenschiefer" was coined by Rosenbusch (1877) to describe slates in the outermost part of the aureole, which contain ill-defined dark spots containing a concentration of very fine opaque. He applied the term "Knotenglimmerschiefer" to higher-grade spotted

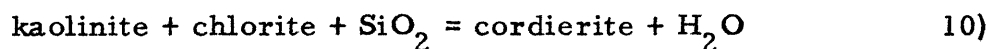


slates in which the mica is less fine. Subsequent writers have used the term "spotted" to describe slates with the following types of textural feature:

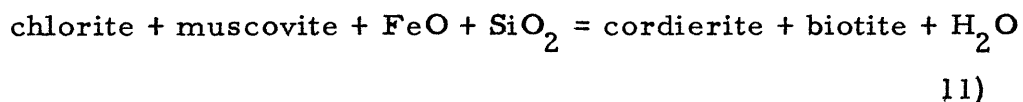
- a) Rounded masses containing a concentration of opaque, or an "amorphous, isotropic substance of a pale yellow color" (Harker (1950, p. 15)).
- b) Metacrysts of a single mineral with poorly developed crystal outline, such as micas (Ussher et al (1909)), andalusite, or cordierite (Harker (1950, p. 51)).
- c) Fine micaceous aggregates usually consisting of chlorite and muscovite (Tilley (1924), Ussher et al (1909)).

It seems highly possible that, as at Onawa, spots of types a) and c) are alteration products of cordierite and in some cases andalusite. Cordierite metacrysts observed by the writer in low grade contact slate at Squaw Mountain are so crowded with inclusions as to be barely distinguishable from the matrix, and resemble some of the "Knoten" of Rosenbusch as illustrated in Harker (1950, p. 24). An isotropic yellow retrograde product often forms after cordierite, having been observed by the writer at Onawa and described elsewhere (Williams, Turner and Gilbert (1954, p. 183)). The pair chlorite-muscovite is a common retrograde product after cordierite (Harker (1954), Schreyer and Goder (1959, p. 100)). Tilley (1924) considered that cordierite forms with rising grade on the sites of chlorite-muscovite spots. Rastall (1910, p. 128) made the same suggestion. Ussher et al (1909, p. 97) write: "It is conceivable that such spots might be secondary

after cordierite, but that mineral is restricted to the inner parts of the aureole, while spotted slates of this type occur at a considerable distance from the edge of the granite." The evidence at Onawa shows that cordierite was stable at distances of over a mile from the contact. Small amounts of cordierite associated with the spots are more likely to be in process of destruction than formation, for the spots have the form of cordierite metacrysts. It is therefore probable that cordierite is stable at the lowest grades of contact metamorphism of normal pelites. The reaction suggested by Tilley (1924):



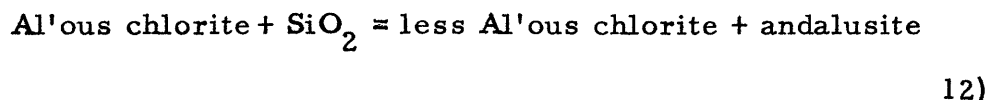
is identical with reaction 4) proposed above except that andalusite rather than kaolinite is observed to be stable at the first appearance of cordierite at Onawa. Probably this reaction with Fe involved is important where cordierite does not coexist with biotite, cordierite-biotite assemblages arising from reaction 5), which is similar to the reaction:



suggested also by Tilley on the basis of the appearance of cordierite on the sites of spots. Even the spots be retrograde, the reverse, prograde reaction may still be valid. It is unfortunate these reactions are generally obscured by the retrograde alteration.

Harker suggests the simple dehydration of kaolinite to produce andalusite at low grade (1950, p. 49). At Onawa andalusite is produced at the lowest grade of contact metamorphism from a slate containing

no aluminosilicate, most likely by the reaction representing the shrinking of the chlorite field in Figure 18(a):



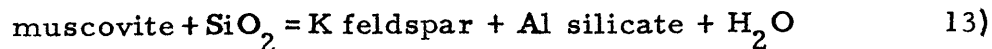
The high Al content of low-grade chlorite (this study and Zen (1960)) must be appreciated in order to understand the contact reactions. It is undoubtedly true, however, that slates containing Al in excess of that soluble in chlorite would exhibit the dehydration sequence in the aluminosilicates as suggested in the section on prograde reactions.

Biotite may arise simply by reaction 3); it is observed associated with opaque minerals when first formed in some localities; these must be involved in the reaction if they occupy the "F" corner of the A-F-M projection as shown in Figure 18(b). The association of chlorite and biotite at the lowest grade as at Onawa (chlorite is observed with biotite in the outer parts of most aureoles, but may be retrograde in many cases) requires that the stability limit of stilpnomelane (Figure 18(b)) be exceeded. The reddening of biotite toward the contact was noted by Tilley (1926) and others and generally ascribed to increasing iron content. Subsequent analytical work (Hall (1941) and this study) shows that increasing titanium content has the most profound effect upon the color. G. A. Chinner (personal communication) suggested that reactions involving the opaque phases might account for the change in the solubility limit of titanium in biotite. Harker (1950, p. 52) describes the reaction of rutile and magnetite to form ilmenite, and states that "most of the original rutile has gone into biotite."

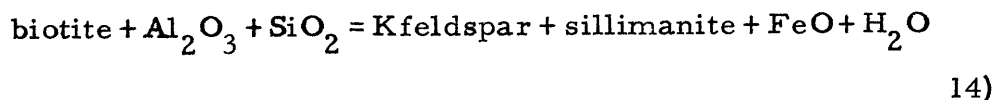
The appearance of potassic feldspar in place of muscovite as the

contact is approached is observed in a number of aureoles, for example those of Comrie (Tilley (1924)) and Belhelvie (Stewart (1947)).

The reaction proposed is always:



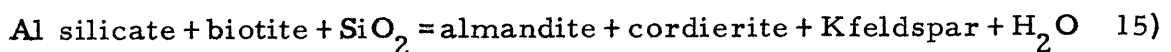
although this reaction is not observed in process. The "second generation of andalusite" resulting from this reaction should be apparent petrographically, unless other reactions are operative. At Onawa, concomitant changes in the composition of biotite and cordierite which lead to the formation of more cordierite may take up most of the excess Al resulting from the decomposition of muscovite. Sillimanite (as fibrolite) is not generally recognized below the stability limit of muscovite, but is prominent with potassic feldspar, often in replacement relation to the biotite (Harker (1950, p. 58)). Francis (1956) suggests the reaction:



but the source of the Al is not obvious.

Minerals not observed at Onawa are found in other areas at comparable grades. Phillips (1928) describes the contact metamorphism of chloritoid-chlorite phyllites by the Bodmin Moor granite, and reports the association chloritoid-andalusite. Such a paragenesis is possible at Onawa in slates of higher iron content than those studied, although the association chloritoid-chlorite with quartz and muscovite is ruled out by the join biotite-andalusite (Figure 18(b) and (c)). Red garnet is often observed, though less commonly than the members of the Onawa assemblages. Sometimes this phase is high in manganese

(Tilley (1926)), so that MnO must be included with the other determining inert components and the extra phase garnet is permitted. As the solubility limits of manganese in biotite and cordierite may be quite low (the Mn contents of biotite and cordierite determined by the writer are as high as any he has seen reported for these minerals in similar assemblages), only slightly higher than normal bulk Mn content may stabilize a garnet with biotite, cordierite and Al silicate. In the event that almandite may be stable in a system in which Mn is an isomorphous component, two possible configurations of the stability relations are shown in Figure 20(a) and (b). These were constructed on the basis of a number of reported assemblages from different areas, and are identical to the tetrahedra proposed by Harker (1954), projected through K feldspar. All four three-phase assemblages are reported by Harker, coexistent with muscovite, on the basis of interpretation of retrograde-altered assemblages in the Carn Chuinneag aureole. Assemblages of 20(a) are observed in the southwest part of the complex, whereas those permitted in 20(b) occur in the northeast part. The three ferromagnesian are not all found together with andalusite in the same assemblage, indicating that the garnet is not stabilized by excess Mn. The configuration of 20(a) is compatible with the Onawa assemblages, as the field almandite-Al silicate-biotite might occur on the iron-rich side of the triangle of Figure 14(a). The arrangement of Figure 20(b) is not possible at Onawa. The alternative joins are related by the reaction:



so that 20(b) is the higher-grade diagram. The right hand side of the reaction is also favoured by increased total pressure because of the very high density of almandite garnet relative to the other phases.

Figure 21 permits comparison of the stability relations in the high-grade part of the Onawa aureole with those determined elsewhere.

The range of equilibrium tie lines at Onawa is plotted along with data from the following assemblages:

01 – Onawa, Maine. Specimen 0-56

quartz-sillimanite-biotite-cordierite-K-feldspar hornfels

02 – Onawa, Maine. Specimen 0-43

quartz-sillimanite-biotite-cordierite-muscovite-potassic feldspar hornfels

C-Chinner (1959, p. 113) Glen Doll, Scotland. garnet-cordierite-biotite-feldspar-quartz(?) hornfels

T1-Tsuboi (1938) Kaziyabara, Japan. sillimanite-biotite-cordierite-orthoclase-plagioclase-quartz hornfels

T2-Tsuboi (1938) Tenryukyo, Japan. biotite-cordierite-orthoclase-plagioclase-quartz hornfels

M-Mathias (1952) Upington, South Africa. sillimanite-biotite-cordierite-K feldspar-plagioclase-quartz rock

F-Folinsbee (1941a) Great Slave Lake, Canada. sillimanite-garnet-biotite-cordierite-spinel-microcline-plagioclase-quartz gneiss (biotite composition estimated from optics, not reliable)

Hi-Hietanen (1956) Idaho, U. S. A. kyanite-sillimanite-andalusite-biotite-cordierite-corundum-plagioclase-quartz schist

He-Heald (1950) New Hampshire, U. S. A. garnet-biotite-cordierite-microcline-quartz "quartz monzonite" (analyzed phases not all from same location, but all three, with same optics as those analyzed, coexist)

The presence of crossing joins on the plot is not necessarily evidence

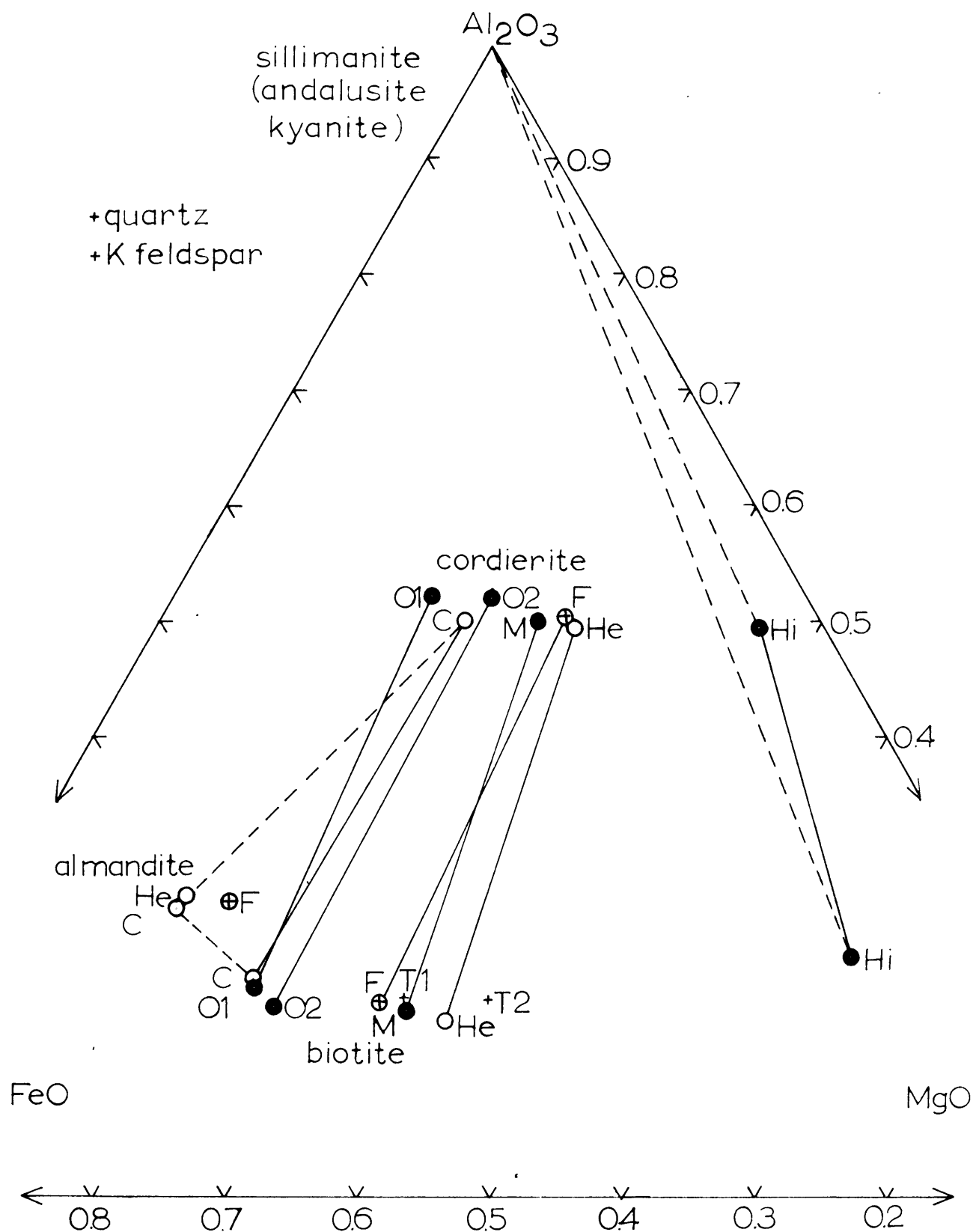


Figure 21. Comparison of Onawa assemblages with those of other localities. Open circles: biot.-cord.-alm. Solid circles: biot.-cord.-sill. Circles with cross: biot.-cord.-alm.-sill. Crosses: biot.-cord.-sill (T1); biot.-cord. (T2). Hi lacks K feldspar.

of disequilibrium, as the composition of biotite F is uncertain and biotite C may coexist with a different oxide assemblage than the Onawa biotites.

The plot shows that no significant difference exists between the compositions of biotite-cordierite joins whether they limit three-phase fields with garnet or with sillimanite, but that definite variations occur from one locality to another, much greater than the variations at Onawa. The Hi and T2 data are not strictly comparable with the others, as the Idaho rock lacks a potassic feldspar and the T2 biotite does not coexist with an aluminosilicate. The more magnesian compositions of these phases may be in part a result of these differences. Several other available compositions were not plotted because the assemblages lacked phases required in the projection, but these do not fall outside the limits of the data presented. It is apparent that the joins definitely from contact aureoles (C, 01, 02) are the most iron-rich; indeed, of 62 complete analyses of cordierite collected by Leake (1960) only three are more iron-rich than those from Onawa and Glen Doll, and all those come from pegmatites. Joins from regional metamorphic assemblages are displaced toward the MgO side of the diagram. In accord with reaction 9), lower temperature and/or higher total pressure is suggested for the regional environment. In particular, the presence of kyanite in the Idaho assemblage and associated rocks, with evidence of all mutual reactions among the three aluminosilicates except andalusite  $\rightarrow$  kyanite, suggests p and T near the triple point where all three coexist. The pressure of this point must be higher than in contact aureoles, for kyanite has never been proven



to be stable in the latter environment, and is favoured by high pressure on account of its relatively low molar volume. Chinner (1959) has observed the same shift in a set of garnet-cordierite tie lines and proposes that pressure is the most important variable. This conclusion is applicable to the biotite-cordierite joins also, because the relatively small variation across the aureole indicates that temperature has a relatively small effect, unless the temperature effect is opposed by chemical potential gradients. With regard to the role of garnet, it must be concluded that garnet-cordierite parageneses may be stabilized in several ways:

- 1) By bulk Mn content high enough to permit an extra phase. This situation apparently applies in the case of the F assemblage of Figure 21, where sillimanite, almandite, cordierite and biotite all coexist.
- 2) By high enough pressure and/or temperature or low enough  $\mu_{\text{H}_2\text{O}}$  to result in the configuration of Figure 20(b), with bulk composition falling in a field in which cordierite-garnet are stable. Reaction 15) is univariant only at constant  $\mu_{\text{H}_2\text{O}}$  if K feldspar is stable (but independent of  $\mu_{\text{H}_2\text{O}}$  if muscovite instead is present, as the mica content of the system must remain constant as a result of fixed  $\text{K}_2\text{O}$  content, and micas are the only hydrous minerals). Increasing pressure drives the reaction to the right, and favours magnesian compositions, whereas increasing  $\mu_{\text{H}_2\text{O}}$  also favours magnesian compositions, but drives the reaction to the left. Therefore it is impossible to predict a consistent displacement of the limiting biotite-cordierite join in Figure 20(a) with respect to 20(b). In the case of the Glen Doll aureole, higher

pressure and lower  $\mu_{\text{H}_2\text{O}}$  with respect to temperature than at Onawa would stabilize the parageneses of 20(b) at compositions comparable to Onawa.

Other phases which may occur outside the compositional stability limits of the assemblages at Onawa are staurolite (not common in aureoles, perhaps unstable at the pressures extant or restricted to iron-rich extremes of composition) and hypersthene or anthophyllite. The latter two probably occupy the more magnesian side of the projection, hypersthene being favoured by low  $\mu_{\text{H}_2\text{O}}$  but are not compatible with aluminosilicate. At the lowest grade of occurrence, hypersthene is not stable with K feldspar (Harker (1950, p. 53)) but shrinking of the biotite stability field with increasing grade permits this association. It is possible that hypersthene and sillimanite may be compatible at the highest grades of contact metamorphism; Niggli (1950) reports the assemblage:

quartz-cordierite-hypersthene-sillimanite-K feldspar

All prograde reactions above the lowest grades require subtraction of water and addition of  $\text{SiO}_2$ . The latter necessitates a progressive reduction in quartz content, so that if initial quartz is low the hornfels may become "undersaturated" with increasing grade. This effect is exhibited at Comrie (Tilley, 1924) where initially quartz-bearing pelites bear spinel instead at the highest grades.

Of all the reactions discussed which are independent of bulk composition a few are megascopically apparent in some hornfels and thus suitable for the establishment of isograds in the field. Reaction 5), which probably marks the first appearance of cordierite in normal

pelites, is dependent only on external conditions, and cordierite or retrograde spots are easily recognized in the hand specimen. Reaction 7) marks the first appearance of potassic feldspar, is similarly dependent, and might be approximately located by observing the development of a less micaceous appearance of the hornfels, though this is not obvious. Sillimanite is megascopically apparent as milky "veinlets" at Onawa, so that its appearance could be used as a rough index of grade, but it is seen microscopically to appear further from the contact than the veinlets. If the "injection zone" boundary is the onset of partial melting, it is also dependent in position upon external variables, but must also move with changes in bulk composition. The appearance of garnet and hypersthene, if in such an assemblage as to be controlled by physical conditions only, would be useful isograds in other aureoles than Onawa.

In the metamorphic facies classification of Fyfe, Turner, and Verhoogen (1958), the outermost edge of the aureole belongs to the albite-epidote hornfels facies, which is separated by reaction 5) from the hornblende hornfels facies, which occupies most of the outer half of the aureole. Reaction 7) separates the hornblende hornfels facies from the pyroxene hornfels facies, which obtains to the contact. The immediate country rock falls in the low green-schist (quartz-albite-muscovite-chlorite) facies or chlorite zone of regional metamorphism, although the biotite zone is represented elsewhere in the area.

#### D. Correlation with Experimental Data

One of the ultimate aims of the metamorphic petrologist is to know

quantitatively the physical conditions of metamorphism. Temperature and pressure stability limits of mineral assemblages can only be obtained directly, or by extrapolation, from experimental syntheses and physical measurements on natural minerals. In general, these studies involve systems much less complex than those observed in the field, but the data may often lead to limiting values for the external variables. Syntheses of hydrous minerals have mostly been performed in the presence of a vapor of nearly pure  $H_2O$ , hence the temperatures of dehydration reactions so studied are a maximum at a given pressure, and are reduced if  $\mu_{H_2O}$  is less than the maximum value.

The stability relations of Mg and Fe cordierite are being investigated by Schreyer (1959). The reaction:

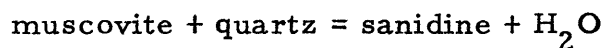
Pyrophyllite + amesite (Mg chlorite) = Mg cordierite ( $\rightarrow$  T increasing)

has been located to  $\pm 50^\circ$  C. at 2000 and 5000 bars water pressure and rises from about  $475^\circ$  to  $500^\circ$  C. in this range. Andalusite forms as a metastable reaction product on the high temperature side, and thus may be the stable form of aluminosilicate with cordierite under these conditions. This reaction thus approximately marks the appearance of cordierite in Figure 18(d), but its appearance in the observed assemblages must occur at a higher temperature than the reaction above. The temperature required would be decreased by decreased  $\mu_{H_2O}$ ; subsequent reactions involving cordierite and biotite must be studied in systems containing  $K_2O$  and  $FeO$ . Mg cordierite breaks down at 10,000 bars  $H_2O$  and  $600^\circ$  C. to chlorite, quartz and probably sillimanite; it is probable that Fe cordierite is restricted to lower

pressures than this at comparable temperatures (Schreyer, lecture, 1960). Preliminary experimental data indicates that the high-pressure limit of cordierite does not change rapidly with temperature, thus the mineral is diagnostic of relatively low pressures at all temperatures, particularly if rich in iron as at Onawa.

Because of the extremely sluggish nature of reactions among the aluminosilicates, no reaction curves have been established to limit the stability of andalusite. Sillimanite or mullite is obviously the stable form at high temperatures, from the relation of these phases to igneous contacts, and kyanite is the high pressure form. Experimental data limit andalusite to less than about 15 kilobars and 700° C. but do not better define its stable range (Clark et al (1957)).

The reaction:



was studied by Yoder and Eugster (1955), and takes place at about 600° C. at 2000 bars H<sub>2</sub>O. Undoubtedly the K feldspar isograd represents a lower temperature at a given pressure, as already explained, and in addition the temperature will be further lowered by  $\mu_{\text{H}_2\text{O}}$  being less than the maximum.

The maximum possible temperature in the aureole is determined by the temperature of the intrusion. The work of Tuttle and Bowen (1958) has shown that granitic melts may exist at temperatures as low as 640° C. at 4000 bars if water is present. In the vicinity of Boarstone Mountain, the composition of the pluton is close to granite, and two feldspars coexist in the igneous rock. Unless these exsolved

from a single phase subsequent to crystallization, the temperature of crystallization must have been no more than 660° C., and the partial pressure of H<sub>2</sub>O at least about 4000 bars; these conditions obtain when the ternary minimum in the system NaAlSi<sub>3</sub>O<sub>8</sub>-KAlSi<sub>3</sub>O<sub>8</sub>-SiO<sub>2</sub>-H<sub>2</sub>O just intersects the solvus separating the alkali feldspars (Tuttle and Bowen (1958, p. 71)). Temperature of crystallization would be increased by more mafic composition (as at Onawa Station), total pressure less than 4000 bars, or total pressure 4000 bars or more with p<sub>H<sub>2</sub>O</sub> less than 4000 bars (melt undersaturated with water). All these alternatives result in crystallization of an initially homogeneous feldspar. Subsequent exsolution would take place under "wet" conditions (Tuttle and Bowen (1958, p. 129)), ample evidence of which is furnished by extensive hydration reactions in both the intrusion and the immediate wallrock. The presence of a single feldspar in the hornfels shows that they were formed above the solvus. However, the bulk compositions of microcline microperthites in the hornfels must be much more potassic than in the intrusive, and the solvus temperature drops off rapidly toward K feldspar (Tuttle and Bowen (1958, p. 27)), so that temperatures of formation of hornfels K feldspar could be as low as about 500° C. (on the basis of the experimentally determined solvus, which applies strictly only to high temperature modifications of the feldspars). The great width of the aureole (shallow metamorphic gradient) implies a shallow temperature gradient, perhaps a result of rapid heat transfer by water expelled during metamorphism. It is possible that the Onawa pluton is truly "subsolvus"; if so, the occurrence of the K feldspar isograd at some distance from

the contact probably requires a  $\mu_{\text{H}_2\text{O}}$  gradient falling away from the contact. The temperature of first appearance of cordierite would be lowered also as required. If the "injection veinlets" arose from partial melting and thus approximate the ternary minimum in composition, then the intrusive must have been hotter than  $660^\circ \text{C.}$ , because the veinlets are distinctly "hypersolvus." Partial  $\text{H}_2\text{O}$  pressures in the intrusive after crystallization would be required to be higher with respect to the total pressure than in the wallrocks in order for nearly complete exsolution of feldspar and chloritization of biotite to progress there and not in the hornfels. If, as recrystallization of the inner hornfels progressed, the system became isolated from the intrusive, the maximum  $\mu_{\text{H}_2\text{O}}$  of metamorphism was considerably less than that of the intrusive in the late stages of crystallization. As water became concentrated in the remaining melt the temperature of crystallization decreased and the intrusive developed subsolvus features characteristic of lower temperature and higher  $p_{\text{H}_2\text{O}}$  than were extant at the height of metamorphism. Such isolation (impermeability to water) is necessary in view of the anhydrous nature of the cordierite and the paucity of retrograde reaction in the inner hornfels.

#### E. Suggestions for Further Research

In the field, further work is desirable to determine whether any exceptions exist to the sequence of reactions proposed, and to seek specimens showing extremes of composition which will enable the plotting of more paragenetic data. An investigation of the retrograde parageneses from an equilibrium standpoint would be of interest,

particularly in that it might place their identification on a firmer basis. The whole matter of opaque mineral equilibria demands attention, as it is obvious that the significance of these phases has been too often neglected. A systematic study would necessitate separation of the opaques in quantity sufficient for chemical analysis, the content of  $\text{FeO}$ ,  $\text{Fe}_2\text{O}_3$  and  $\text{TiO}_2$  being of particular interest in the Onawa locality. Suggestions for investigation into the problems of cordierite, and of the aplitic veinlets, have already been made. As more experimental data on feldspars and cordierite becomes available, a knowledge of their structural variations across an aureole may be very valuable in deducing the slope of the temperature gradient.

Improved analytical methods for aluminum in the presence of high iron and titanium concentrations, for low calcium concentrations, and a rapid method for water would be desirable. The ultimate analytical tool for very fine-grained rocks would permit determining the compositions of the phases without physical separation. Toward this end, better correlation of optics with composition and development of the "electron probe" X-ray spectrograph would permit analyses from a single thin section.

It is the writer's intent to pursue the problems of contact metamorphism, and his hope that further investigations will shed light on the many uncertainties brought to light by his present study.



## BIOGRAPHY

The author was born to Mr. and Mrs. J. M. Moore in Winnipeg, Manitoba, Canada on August 14, 1935, and he has one sister, Susan Gail.

He attended junior and high schools in Winnipeg and was awarded the degree of B.Sc. (Geological Engineering) in 1956 from the University of Manitoba. From September, 1956, to September, 1960, he was a student in the Department of Geology and Geophysics at Massachusetts Institute of Technology, Cambridge, Massachusetts.

He was married in 1958 to Margaret Anne Bastick of Winnipeg.

Honors granted him include the Engineering Institute of Canada prize, 1955; Mobil Oil Scholarship, 1955-56; University Gold Medal, 1956; Whitney Fellowship, 1956-57; and Sigma Xi Fraternity, 1959. He is a member of the Mineralogical Society of America and the Delta Kappa Epsilon fraternity.

He has spent seven summers in the field with government and private surveys in the Canadian Precambrian. For three years at Massachusetts Institute of Technology he held research and teaching assistantships.

He contributed to the following publication: Moore, J. M., et al, Potassium-argon ages in Northern Manitoba, Bull. G.S.A. 71, 225-230 (1960).

He has recently been awarded the Queen Elizabeth II Fellowship by the International Nickel Company for two years of research at Carleton University, Ottawa, Ontario.

## BIBLIOGRAPHY

- Agrell, S. O. and J. V. Smith (1960), Cell dimensions, solid solution, polymorphism and identification of mullite and sillimanite, *J. Am. Ceram. Soc.* 43, 69-76, 1960.
- Balsley, J. R. and E. P. Kaiser (1954), Aeromagnetic survey and geological reconnaissance of part of Piscataquis County, Maine; U. S. G. S. Geophysical Investigations, Map GP116, 1954.
- Bradley, W. F. (1953), X-ray diffraction criteria for the characterization of chloritic material in sediments, *Proc. 2nd National Conference on Clays and Clay Minerals*, pp. 324-334.
- Brownlow, A. H. (1960), Serpentine and associated rocks and contact minerals near Westfield, Mass., Ph. D. Thesis, M. I. T.
- Chayes, F. (1952), The staining of potash feldspar in sodium cobaltinitrate in thin section, *Am. Mineral.* 3, 337-340.
- Chinner, G. A. (1959), Garnet - cordierite parageneses, *Carnegie Inst. Wash. Yearbook* 58, 112-114.
- Clark, S. P., E. C. Robertson, and F. Birch (1957), Experimental determination of kyanite-sillimanite equilibrium relations at high temperatures and pressures, *Am. J. Sci.* 255, 628-640.
- Dale, T. N. (1906), Slate deposits and slate industry of the United States, *U. S. G. S. Bull.* 275, 154 p.
- Eskola, P. (1915), On the relation between chemical and mineralogical composition in the rocks of the Orijarvi region, *Bull. Comm. geol. Finland*, no. 44.
- Eugster, H. P. (1959), Reduction and oxidation in metamorphism, *Researches in Geochemistry*, P. Abelson, ed. Wiley, N. Y., 511 pp.
- Fairbairn, H. W. (1953), Precision and accuracy of chemical analysis of silicate rocks, *Geochim. Cos. Acta* 4, 143-156.
- Fairbairn, H. W., P. M. Hurley, W. H. Pinson, Jr., and R. F. Cormier (1960), Age of the granitic rocks of Nova Scotia, *Bull. G. S. A.* 71, 399-414.
- Faul, H. and G. L. Davis (1959), Mineral separation with asymmetric vibrators, *Am. Mineral.* 44, 1076-1082.
- Folinsbee, R. E. (1941)a, The chemical composition of garnet associated with cordierite, *Am. Mineral.* 26, 50-53.
- Folinsbee, R. E. (1941)b, Optic properties of cordierite in relation to alkalis in the cordierite-beryl structure, *Am. Mineral.* 26, 485-500.
- Foster, Margaret D. (1960), Layer charge relations in the dioctahedral and trioctahedral micas, *Am. Mineral.* 45, 383-398.
- Francis, G. H. (1956), Facies boundaries in pelites at the middle grades of regional metamorphism, *Geol. Mag.* 93, 353-368.

- Fyfe, W. S., F. J. Turner, and J. Verhoogen (1958), Metamorphic reactions and metamorphic facies, G.S.A. Mem. 73, 259 pp.
- Gibbs, J. W. (1948), The Collected Works of J. Willard Gibbs, Vol. 1, Yale University Press, 462 pp.
- Goldschmidt, V. M. (1911), Die kontaktmetamorphose im kristianiagebiet, Kristiania Vidensk. Skr., I Math-Naturv. Kl. 11, 123.
- Gossner, B. and F. Mussnug (1928), Vergleichende rontgenographische untersuchung von magnesium silikaten. Cordierit, Neues Jahrb. fur Min., Beilage B and 58A, 216-226.
- Groves, A. W. (1951), Silicate Analysis, Geo. Allen and Unwin Ltd., London (95-104) 336 pp.
- Guppy, E. M. (1956), Chemical analyses of igneous rocks, metamorphic rocks and minerals, with petrographical descriptions by P. A. Sabine, (1931-1954) Mem. Geol. Surv. Great Britain, 5+78 pp.
- Hall, A. J. (1941), The relation between color and chemical composition in the biotites, Am. Mineral. 26, 29-41.
- Harker, A. (1950), Metamorphism, 3rd Ed., Methuen, London, 362 pp.
- Harker, R. I. (1954), Further data on the petrology of the pelitic hornfelses of the Carn Chuinneag - Inchbae region, Ross-shire, with special reference to the status of almandine, Geol. Mag. 91, 445-462.
- Heald, M. T. (1950), Structure and petrology of the Lovewell Mountain quadrangle, New Hampshire, Bull. G.S.A. 61, 43-89.
- Hietanen, A. (1956), Kyanite, andalusite and sillimanite in the schist in Boehls Butte quadrangle, Idaho, Am. Mineral. 41, 1-27.
- Hitchcock, C. H. (1886), The Geology of Northern New England 5: 16 pp., 3 maps, folio.
- Hurley, P. M. and J. B. Thompson (1950), Airborne magnetic and geological reconnaissance survey in northwestern Maine, G.S.A. Bull. 61, 835-842.
- Hurley, P. M. et al (1957, 1958), 1957-NYO3937 4th Ann. Prog. Rept. for 1956-1957, U.S. Atom. Energy Comm., Dec. 1, 1957. 1958-NYO3939 6th Ann. Prog. Rept. for 1958, U.S. Atom. Energy Comm., Dec. 1, 1958.
- Hurley, P. M., A. J. Boucot, A. L. Albee, H. Faul, W. H. Pinson, and H. W. Fairbairn (1959), Minimum age of the Lower Devonian slate near Jackman, Maine, Short note, G.S.A. Bull. 70, 947-950.
- Iiyama, T. (1958), Optical properties and unit cell dimensions of cordierite and indialite, Japanese Mineral. Jour. 1, 372-394.
- Keith, A. (1933), Preliminary geologic map of Maine, Maine Geological Survey.
- Korzhinskii, D. S. (1936a), Mobility and inertness of components in metasomatism, Acad. Sci. U.S.S.R. Bull. Ser. Geol. 1, 35-60.

- Korzhinskii, D. S. (1936b), Paragenetic analysis of quartz-containing, almost calciumless crystalline schists of the Archaean complex to the south of Baikal-Sea, Mem. Soc. Russe de Mineral., 2nd Ser., 65, book 2, 247-280 (Russian, with English summary).
- Korzhinskii, D. S. (1959), Physiochemical basis of the analysis of the paragenesis of minerals, Consultants Bureau, N. Y. (translated from Russian), 142 pp.
- Kranck, S. H. (1959), Chemical petrology of metamorphic iron formations and associated rocks in the Mount Reed area in northern Quebec, Ph.D. Thesis, M.I. T.
- Leake, B. E. (1960), Compilation of chemical analyses and physical constants of natural cordierites, Am. Mineral. 45, 282-298.
- MacDonald, G. A. and R. Merriam (1938), Andalusite in pegmatite from Fresno County, California, Am. Mineral. 23, 588-594.
- Mathias, Morna (1952), An unusual cordierite rock from Uppington, Cape Province, Mineral. Mag. 29, 936-945.
- McIntyre, W. L. (1958), A thermodynamic treatment of trace element distribution in geologic systems with applications to geologic thermometry, Ph.D. Thesis, M.I. T., 207 pp.
- Miller, R. L. (1945), Geology of the Katahdin pyrrhotite deposit and vicinity, Piscataquis County, Maine, Maine Geological Survey Bull. 2, 21 pp.
- Miyashiro, A. (1957), Cordierite-indialite relations, Am. J. Sci., 5th ser: 255, 43-62.
- Miyashiro, A., T. Iiyama, M. Yamasaki, T. Miyashiro (1955), The polymorphism of cordierite and indialite, Am. J. Sci., 5th Ser: 253, 185-208.
- Niggli, P. (1950), Some hornfelses from Saxony and the problem of metamorphic facies, Am. Mineral. 35, 869-876.
- Parker, C. A. and A. P. Goddard (1950), The reaction of aluminum ions with alizarin-3-sulphonate, with particular reference to the effect of calcium ions, Annal. Chem. Acta 4, 517-524.
- Pauling, L. (1930), Structure of chlorites, Proc. Natl. Acad. Sci. 16, 578-582.
- Perkins, E. H. (1925), Contributions to the geology of Maine, no. 2, pt. 1, The Moose River sandstone and its associated formations, Am. J. Sci., 5th Ser: 10, 368-375.
- Philbrick, S. S. (1933), The contact metamorphism of the Onawa pluton, Piscataquis County, Maine, Ph.D. Thesis, The Johns Hopkins University.
- Philbrick, S. S. (1936), The contact metamorphism of the Onawa pluton, Piscataquis County, Maine, Am. J. Sci., 5th Ser: 31, 1-40.

- Philbrick, S. S. (1940), Reconnaissance of the contact metamorphism of the Katahdin and Squaw Mountain intrusives, Maine, *Am. J. Sci.*, 5th Ser.: 238, 710-716.
- Phillips, F. C. (1928), Metamorphism in the Upper Devonian of North Cornwall, *Geol. Mag.* 65, 541-556.
- Phinney, W. C. (1959), Phase equilibrium in the metamorphic rocks of St. Paul Island and Cape North, Nova Scotia, Ph.D. Thesis, M.I.T.
- Pierce, W. C. and E. L. Haenisch (1958), *Quantitative Analysis*, 4th ed., Wiley, N. Y., 497 pp.
- Pitcher, W. S. and Sinha, R. C. (1958), The petrochemistry of the Ardara aureole, *Geol. Soc. London Quart. Jour.* 113, 393-408.
- Ramberg, Hans (1952), *The Origin of Metamorphic and Metasomatic Rocks*, U. of Chicago Press, 317 pp.
- Rastall, R. H. (1910), The Skiddaw granite and its metamorphism, *Geol. Soc. London Quart. Jour.* 66, 116-141.
- Rosenbusch, H. (1877), Die Steiger Schiefer und ihre Contactzone an den Granititen von Barr-Andlau und Hohwald, *Abh. Geol. Specialkarte Elsass. Lothringen* 1, 79-393.
- Schreyer, W. and Yoder, H. S., Jr. (1959), Cordierite-water system, *Carnegie Inst. Wash. Year Book* 58, 100-104.
- Shapiro, L and W. W. Brannock (1956), Rapid analysis of silicate rocks, *U.S.G.S. Bull.* 1036-C, 56 pp.
- Smith, E. S. C. (1929), New fossils from Maine, *Science* 70, 168-169.
- Smith, J. V. (1956), The powder patterns and lattice parameters of plagioclase feldspars I. The soda-rich plagioclases, *Mineral Mag.* 31, 47-68.
- Stewart, F. H. (1947), The gabbroic complex of Belhelvie in Aberdeenshire, *Geol. Soc. London Quart. Jour.* 102, 465-495.
- Thompson, J. B. Jr. (1955), The thermodynamic basis for the mineral facies concept, *Am. J. Sci.*, 5th Ser.: 253, 65-103.
- Thompson, J. B. Jr. (1957), The graphical analysis of mineral assemblages in pelitic schists, *Am. Mineral.* 42, 842-858.
- Tilley, C. E. (1924), Contact metamorphism in the Comrie area of the Perthshire Highlands, *Geol. Soc. London Quart. Jour.* 80, 22-71.
- Tilley, C. E. (1926), Some mineralogical transformations in crystalline schists, *Mineral. Mag.* 21, 34-46.
- Topping, J. (1955), *Errors of observation and their treatment*, Institute of Physics Monograph for Students, Unwin Bros, Woking and London, 119 pp.
- Tsuboi, S. (1938), Petrological notes 19-32, *Japan. Jour. Geol. Geogr.* 15, 127-128.

- Tuttle, O. F. and N. L. Bowen (1958), Origin of granite in the light of experimental studies in the system  $\text{NaAlSi}_3\text{O}_8$ - $\text{KAlSi}_3\text{O}_8$ - $\text{SiO}_2$ - $\text{H}_2\text{O}$ , G.S.A. Mem. 74, 153 pp.
- Ussher, W. A. E., G. Barrow and D. A. MacAlister, (1909), The Geology of the Country around Bodmin and St. Austell, Mem. Geol. Surv. England and Wales, explan. of sheet 347, 80-104.
- Williams, H., F. J. Turner, and C. M. Gilbert (1954), Petrography, Freeman, San Francisco.
- Winchell, A. N. and H. Winchell (1951), Elements of optical mineralogy, 4th ed., part 2, Wiley, N. Y., 567 pp.
- Wones, D. R. and H. P. Eugster (1959), Biotites on the join phlogopite-annite, Carnegie Inst. Wash. Yearbook 58, 127-132.
- Yoder, H. S. and H. P. Eugster (1955), Synthetic and natural muscovite, Geochim. Cos. Acta 8, 225-280.
- Zen, E-An (1960), Metamorphism of lower Paleozoic rocks in the vicinity of the Taconic Range in West-Central Vermont, Am. Mineral. 45, 129-175.